The fractionation of copper isotopes in granitic and mafic intrusions: mafic enclaves in the Mannum granite, a case study

Thesis submitted in accordance with the requirements of the University of Adelaide for an Honours Degree in Geology

Oliver Thomas Pring

November 2021

THE FRACTIONATION OF COPPER ISOTOPES IN GRANITIC AND MAFIC INTRUSIONS: MAFIC ENCLAVES IN THE MANNUM GRANITE, A CASE STUDY

COPPER ISOTOPES IN THE MANNUM GRANITE

ABSTRACT

The transfer of material between mantle-sourced magma and evolved magmatic rocks may provide a mechanism for the transportation of metals such as copper, Cu, to the crust. The Mannum granite provides a case study as the A-type granite is synchronously accompanied by mafic enclaves, providing a mafic-felsic interface with differing degrees of mixing/mingling. This mafic-felsic interface shows different mechanisms of transportation such as transport of xenocrysts, compositional rimming (rapakivi feldspars) and change in overall bulk chemistry. Samples of both the granite and mafic enclaves were taken, with a focus on Cu isotope analysis which characterises Cu behaviour between the mafic enclaves and granite and shows whether any copper has been assimilated from a highly fractionated source. This study used petrography, whole rock and mineral major and trace element chemistry and whole rock Cu isotope analysis. Processes such as fractional crystallisation and magma mixing/mingling provide mechanisms for the transfer of material between the granite and the intruding mafic enclaves. There is evidence of the transfer of material in the hybridised zones, particularly the formation of rapakivi feldspars and xenocrysts from both phases. Rare earth element signatures show mineral growth has occurred prior and post injection of mafic magma into the Mannum granite and that magmatic transfer is most applicable to lithophile elements. Cu isotope results show that δ^{65}Cu values generally increase with decreasing copper concentrations and range from -0.12 to 2.34‰. The range of δ^{65}Cu values is in line with those reported in mantle derived rocks and follow Rayleigh fractionation curves. Cu isotope analyses further our understanding of Cu isotope behaviour and can be applied to ore-forming environments. Other stable transition metal isotopes could be paired with Cu isotopes, such as Zn and Fe, to further examine the role of any redox reactions.

KEYWORDS

Copper isotopes, Mannum granite, mafic enclaves, rare earth elements, Rayleigh fractionation, rapakivi feldspars

TABLE OF CONTENTS

LIST OF FIGURES AND TABLES

INTRODUCTION

Understanding the transfer of material through magmatic processes furthers our understanding of the transport of metals to the crust from the Earth's mantle. The transport of metals is key in understanding the concentration of desired metals, such as copper (Cu), and the formation of deposits. Magmatic Cu deposits such as iron-oxide-copper-gold and porphyry copper, form as a result of interaction between the mixing/mingling with other magma and fluids. Sun et al. (2017) proposed that partial melting for subducting slabs mixing and transferring material with the partial melts of mantle peridotites may lead to the formation of porphyry deposits. Zheng et al. (2018) showed that porphyries with associated mafic enclaves have elevated δ^{65}Cu values compared to average felsic rocks. This elevation of δ^{65}Cu values is inconsistent with the formation of sulphides, which often present a negative δ^{65}Cu value (Brzozowski et al., 2020). This indicates that the mixing/mingling between these two phases has caused the enrichment of ^{65}Cu (Zheng et al., 2018).

In this study, the transfer of material between two magmatic phases and its relation to the transport of transition metals from mantle to crust is investigated. The transfer of material in mantle-derived rocks occurs though fractional crystallisation, magma mixing/mingling, and the transfer by magmatic fluids. Fractional crystallisation is the process by which minerals crystallise out of a melt, removing their composition from the melt, and partitioning it into separate compositional mineral phases (Raymond, 1995). Magma mixing/mingling occurs when two melts or partial melts interact; once the two phases reach compositional and thermal equilibrium, they are deemed to have mixed. When two phases interact but remain compositionally separate, with possible mixing along the boundary between the two phases, they are deemed to have mingled (Turner and Foden, 1996; Vernon, 2016; Barnes et al., 2021).

Copper isotope systematics

Copper (Cu) is a reddish transition metal with a density of 8920 kgm^{-3} and it exists in three oxidation states: Cu(0) such as native copper, Cu(I) which commonly occurs in sulphides, and Cu(II) in oxysalts (Moynier et al., 2017; Liu et al., 2021). Cu isotope fractionation occurs during oxidation and to some extent during reduction; fractionation most readily occurs at low temperatures and through fluid interactions (Larson et al., 2003). Cu fractionation can also occur between silicates and sulphides at high temperatures (Liu et al., 2021). Copper has two stable isotopes ^{63}Cu at 69.174% and ^{65}Cu at 30.826% abundance (Shields et al., 1964); the isotopic ratio is expressed as $\delta^{65}Cu$ (relative to a standard reference material – NIST 976) (Liu et al., 2013).

Multi-collector inductively coupled mass spectrometry (MC-ICP-MS) allows precise and accurate measurements of Cu isotope ratios. Solutions of copper prepared through direct digestion and chromatographic purification yield Cu isotope ratios of the whole rock sample (Larson et al., 2003). Copper isotopes are fractionated through both abiotic and biotic processes. Mass-dependent isotopic fractionation predicts the heavier isotope ^{65}Cu will partition into more tightly bonded sites in aqueous species or solids (Bigeleisen and Mayer, 1947; Urey, 1947). The higher atomic mass of ^{65}Cu over ^{63}Cu marginally slows the kinetics of cation exchange for the heavier isotope, thus leading to isotopic fractionation. Cu isotope fractionation occurs most readily in the formation of secondary minerals at low temperature with a $\delta^{65}Cu$ range of 7 to 9 ‰ (Maréchal et al., 1999; Maréchal and Albarede, 2002) In these relatively low energy settings, fractionation is favoured, as the activation energy for exchange is relatively large compared to the thermal energy in the system (Moynier et al., 2017).

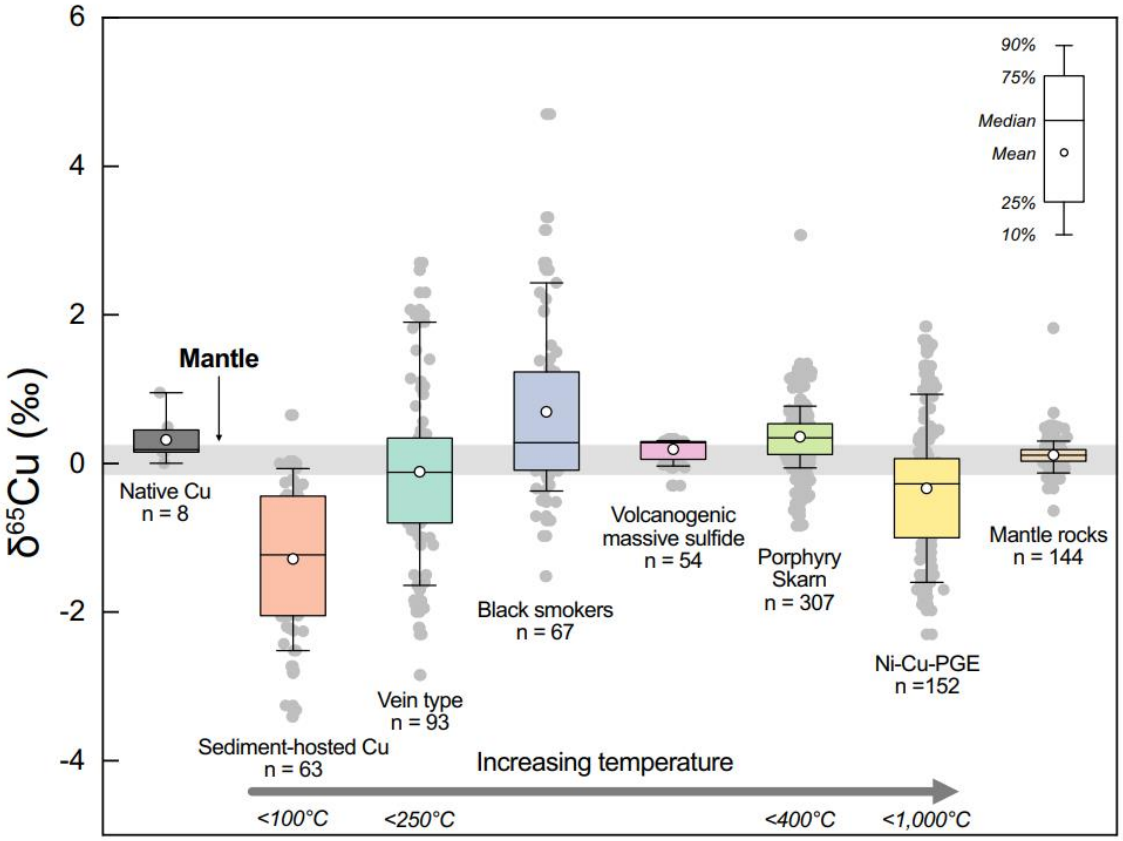

Figure 1: Schematic diagram illustrating the range δ^{65}Cu values for a range of different ore and rock types. Note the relatively narrow spread of values found in mantle-derived rocks. See Brzozowski et al. (2020) for sources of data used in this diagram (after Brzozowski et al., 2020).

The mantle displays a narrow range of copper isotope ratios while hydrothermal systems tend to display much wider ranges of isotopic ratios. Mantle-derived magma typically exhibits δ^{65}Cu values of -0.15 ‰ to 0.18 ‰ while hydrothermally altered mantle-derived rocks exhibit values from –0.64 to +1.82‰ (Liu et al., 2015). As the Mannum granite is a mantle-derived intrusion it is predicted to show a narrow range of δ^{65}Cu values, however if a wide range is found then it can be assumed the Cu content of the Mannum granite is derived from a highly fractionated source such as hydrothermal fluids, assimilation of country rock or a highly fractionated magma system (Liu et al., 2002). Homogenous magmatic-sourced Cu will present a Cu isotope ratio trend, becoming isotopically heavier with decreasing copper concentration following Rayleigh fractionation (Mathur et al., 2012). Rayleigh fractionation

is the evolution of a system as one phase; in this case, the Cu concentration is lowered, resulting in isotopic enrichment (Kendall and Caldwell, 1998).

The Mannum granite

The Mannum granite provides a case study, as it is a mantle-derived A-type granite accompanied by synchronous mafic enclaves, displaying varying degrees of mixing/mingling (Turner and Foden, 1996; Pankhurst et al., 2011). The interactions between the two phases are used as a proxy for large-scale processes involving mantle-derived magma and the crust. The investigation of processes such as fractional crystallisation, assimilation and magma mingling may reveal mechanisms of transfer of metals such as Cu. The degree to which these processes have occurred can be observed through the use of petrography, whole rock major and trace element analysis and rare earth element signature observations (Bea et al., 1994). The Cu isotope fractionation values for the host granite, the mafic enclaves and the intermediate hybridised zones, will be used to understand the degree to which these processes have transferred material from one phase to another, or if the Cu within these rocks has been sourced through assimilation of the upper crust or through interaction with magmatic or hydrothermal fluids.

GEOLOGICAL SETTING

The Mannum granite is located in the eastern Adelaide fold belt, within the Padthaway Suite. It intruded into Late Neoprotozoic early Cambrian meta sediments in the early Ordovician (482.3 ± 4.5 Ma Foden et al., 2006; Pankhurst et al., 2011).

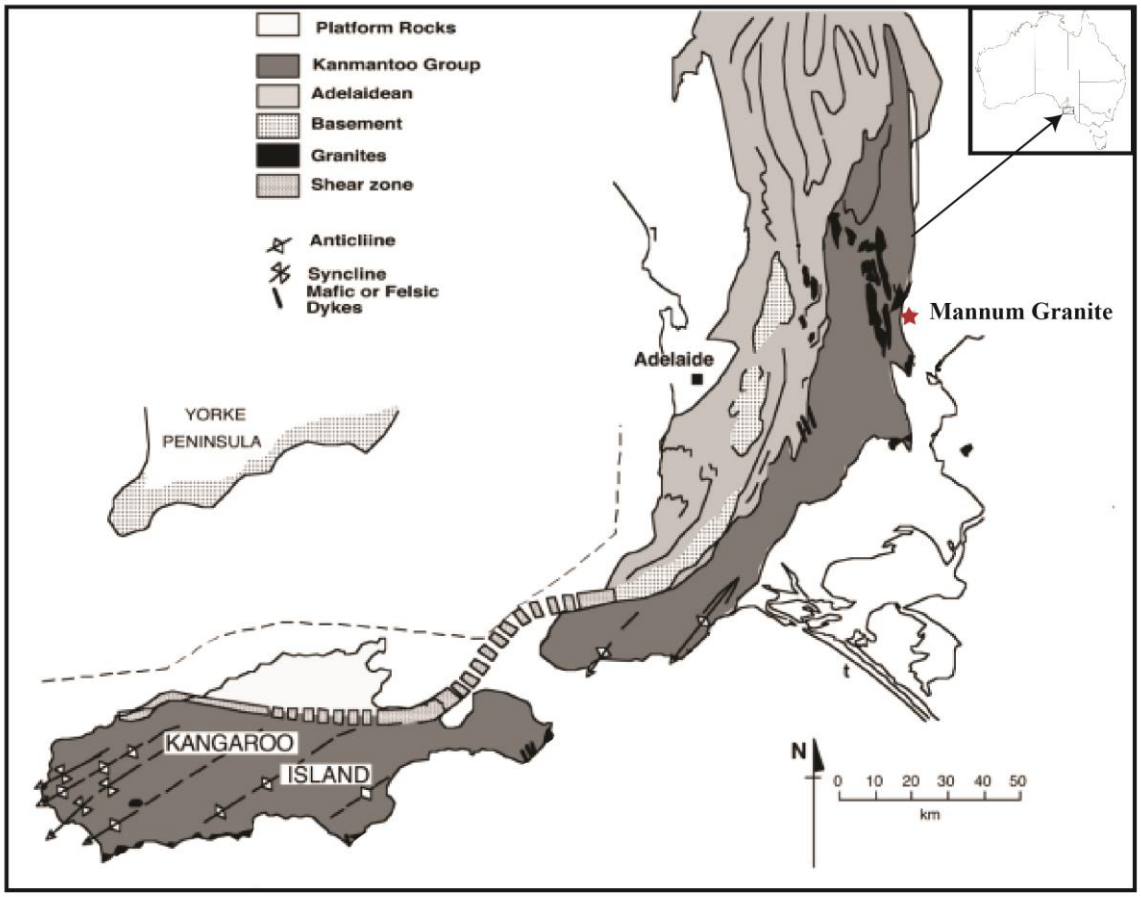

Figure 2: Geological map of Adelaide fold and thrust belt, with the location of the Mannum granite, modified from Foden et al. (2006)

The Padthaway Suite is a series of post-Delamerian granites, volcanics and associated mafic dykes and enclaves (Foden et al., 2006). The Delamerian Orogenic event occurred during the final stages of Gondwana's assembly (Foden et al., 2006). The Padthaway Suite formed due to delamination of a dense moho underplate causing thinning of the lithosphere which allowed mantle upwelling and the formation of 490-470 Ma A-type granites and associated mafic enclaves, intrusions and dykes (Foden et al., 2020). The Mannum granite pluton is

undeformed, roughly circular and 11 km in diameter, and the most prominent outcrop is at the Mannum Quarry on the eastern bank of the River Murray (Turner and Foden, 1996). The Mannum granite originates from an anhydrous magma, indicating a high magma temperature in excess of 930 ºC (Turner and Foden, 1996). The Black Hill gabbro is also a constituent of the Padthaway Suite and represents a mafic melt with similar genetics, and geothermometry reported by Turner (1996) shows a temperature of 1200-1000 ºC. The shape and physical relationship between the enclaves and host Mannum granite indicates the mafic enclaves were an almost liquid magma when injected into the crystal mush of the host granite (Turner and Foden, 1996).

Figure 3: Mannum granite quarry, showing mafic enclaves (dark grey) within host granite (pink-brown).

Turner and Foden (1996) demonstrated that the Mannum granite, and associated enclaves, show initial Sr-isotopic equilibrium indicating fractionation and subsequent mingling from the same parental magma. The Mannum granite is crosscut by a younger basalt dyke, inferred to be closer in composition to the original parental magma (Turner and Foden, 1996). The granite is composed of a medium-coarse syenite-granite and blocks of fine-grained microgranite interpreted by Turner and Foden (1996) to be contaminated margin facies. The

mafic enclaves are tear-drop shaped and range in size from 50 - 5 cm (Turner and Foden, 1996; Frost et al 2001).

The Mannum granite has been extensively studied (e.g., Turner and Foden, 1996; Foden et al., 2002; Foden et al., 2006; Pankhurst et al., 2011; Gibson et al., 2015 Foden et al., 2020) in relation to the timing and cessation of the Delamerian orogeny. As the Mannum granite is a post-tectonic A-type granite, its age (482.3 $\pm$ 4.5 Ma Turner and Foden (1996), 482 $\pm$ 8 Ma Pankhurst et al. (2011), both collected with Rb-Sr isochrons) is interpreted to provide a minimum age for the cessation of the Delamerian orogeny (Foden et al., 2020). Whole rock chemical analyses reported by Turner and Foden (1996) showed a distinct chemical difference between the host granite and the enclaves, and the transition metal composition including Ni, Cr, Sc and V showed enrichment within enclaves compared to the host granite; however, Cu was not reported, in their analysis. Turner and Foden (1996) showed, through decoupling Sr-Nd, that the mafic enclaves are a representation of the parental magma of the Mannum granite.

METHODS

Samples

Samples were collected to represent a full spectrum of phases.

Table 1: Sample names, sample sets, type of sample, use of sample.

Sample	Original no.	Geochemistry sample sets	Sample type	Use
BOUNDARY-ENCLAVE001	OPMG_001		mafic enclave-granite	petrography
BOUNDARY-ENCLAVE002	OPMG_002	2A, 2B, 2C	mafic enclave-granite	petrography and geochemistry
HYBRID/GRANITE006	OPMG_006	6A, 6B, 6C	granite-hybridised zone	petrography and geochemistry
ENCLAVE009	OPMG_009		mafic enclaves	petrography and geochemistry
BOUNDARY-GRANITE012	OPMG_012	12A, 12G	granite-mafic boundary	petrography and geochemistry
GRANITE013	OPMG_013		granite	geochemistry
BOUNDARY-GRANITE-ENCLAVE016	OPMG_016	16A, 16B, 16C, 16D, 16E, 16F	granite-mafic enclave boundary	petrography and geochemistry
ENCLAVE017	OPMG_017		mafic enclave	geochemistry
SOUTHERN DYKE001	OPMGB_001	1A, 1B	Southern mafic enclave/dyke	petrography and geochemistry
MG7 (basalt dyke)	-		dyke	geochemistry

Four enclave boundary (ts = thin section: BOUNDARYts001, BOUNDARYts002, BOUNDARYts012 and BOUNDARYts016), three hybrid (HYBIRDts006A HYBRIDts006B and HYBRIDts006C), one granite (GRANITEts006A), one mafic enclave (ENCLAVEts009) and one southern dyke (SDts001) samples were thin-sectioned by Adelaide Petrographic Inc. The sections were selected for both transmitted and reflected light petrographic analysis. These samples were used as they represent the boundary between the mafic enclaves and the host granite and the differing degrees of hybridisation between them. The mafic enclaves, the granite and the southern mafic dyke were petrographically characterised as they represent each of the phases (or lithologies) without the effects of mixing or mingling.

Whole rock major element analysis

Whole rock major element analysis was conducted by Peter Reiner Wieland at Macquarie University using the following procedure.

For XRF analysis approximately 100 mg of sample was weighed into clean 15 ml Teflon beakers and the mass recorded to four decimal places. Samples were digested using a 1:1 mixture of HF and Teflon distilled HNO_3 at 120°C for 24 hours, then dried down and repeated. Samples were then digested in a mix of 2 ml HF and 10 drops $HClO_4$ overnight and dried down gradually to remove fluoride complexes. A further digest in 6 Mol L^{-1} HCl and then 6 Mol L^{-1} HNO_3 was performed before samples were dissolved in a 2% HNO3/ 0.5% HF solution for analysis.

1:1000 dilutions of each sample were then individually spiked with a 20 µl aliquot of a solution of ^{6}Li, As, Rh, In and Bi in 2% HNO_3. Samples and standards were analysed on an

Agilent 7500cs ICPMS. BCR-2 was used as a calibration standard. Standards BIR-1 and BHVO-2 were also analysed in a 1:1000, 1:2000, and 1:5000 dilution.

A blank was subtracted using the 2% HNO_3 0.5% HF rinse.

Whole rock trace element analysis and initially Cu isotope analysis involved the digestion of samples of the various lithologies using the following bomb digestion procedure. Approximately 300 mg of powdered sample were placed into Teflon bombs, with 4 ml of 28 Mol L^{-1} HF and placed on a 140 ^oC hotplate, allowed to dry down, adding 1ml of 7 Mol L^{-1} NHO_3 just before the samples dried. After samples had dried 2 ml of 7 Mol L^{-1} NHO_3 was added and allowed to cool. 4 ml of 28 Mol L^{-1} HF was added to the samples and they were capped and sealed in bomb jackets and placed in an oven at 190^oC for 94 hours. Bombs were uncapped and allowed to dry down; 1 ml of 7 Mol L^{-1} NHO_3 was added just before the samples dried. Solid residue was taken up in 5 ml of 2% NHO_3.

For trace element solution ICP-MS analysis the following dilution procedure was used. 1:1000 dilutions were performed; aliquots were taken up into 5 ml of 2% NHO_3. Nineteen samples and two standards (USGS BHVO-2, USGS GSP-2) were analysed using Solution ICP-MS - Agilent 8900x QQQ-ICP-MS at The University of Adelaide (Adelaide Microscopy).

Electron Probe Micro Analyses (EPMA)

Chemical compositions of feldspars, titanite, biotite, magnetite, hornblende and pyrite were determined using a Cameca SXFive Electron Microprobe under standard operating conditions as detailed in Table 2. The standards used for EPMA analysis of silicate and oxide minerals were: Ca and Na (Astimex plagioclase), K (Astimex Sanidine), Mg (Astimex almandine),

Ti (P and H block rutile), Si and Al (Astimex albite), Fe (P and H block specularite), Mn (P and H block rhodonite). The standards used for EPMA analysis of sulphides were: S (pyrite), Fe (pyrite), Cu (chalcopyrite), Zn (sphalerite), Co (cobalt), Ni (nickel olivine) and As (arsenopyrite)

Table 2: EPMA operating conditions.

Analysis type	Beam current (nA)	Accelerating voltage (15kV)	Spot size
Silicate composition element analysis	20	15	5
Sulphide composition element analysis	20	13	5

LA–ICP–MS: Trace elements

Trace element analysis of feldspars, titanite, biotite, magnetite, hornblende, pyrite and matrix minerals were undertaken using an Agilent 7900x with attached RESOlution LR 193nm Excimer laser system at Adelaide Microscopy.

Standards used: GSD30, NIST612, STDGL3.

Ion Exchange Chromatography

Digested samples were taken up in 1.5 ml 6 Mol L^{-1} HCl and centrifuged for 5 minutes to separate the solid residue. Samples were passed through a pre-cleaned column with anion exchange resin (Bio-Rad AG® 1-X8 200–400 mesh), using the steps outlined in Table 3.

Table 3: Column chromatography procedure for a column with 1 ml AG1-X8 (200-400 mesh) resin.

Step	Solvent	Eluent
Cleaning	3 mol L-1 HNO3	10ml new resin, 15 ml reusing resin, into waste beaker
Cleaning	Milli-Q H2O	10ml new resin, 15 ml reusing resin, into waste beaker
Cleaning/ equilibration	6 mol L-1 HCl	10ml new resin, 15 ml reusing resin, into waste beaker

Sample load	6 mol L-1 HCl	1.5 ml into waste beaker
Elute matrix	6 mol L-1 HCl	7.5 ml into waste beaker
Collect sample into previous digestion vessel	6 mol L-1 HCl	18ml into collecting vial

On subsequent runs, samples were put through the columns twice to achieve higher purity, removing elements such as Ti and Fe which may interfere with the recorded Cu isotopic ratios. The first run was performed with a widened collection volume outlined in Table 4, eluting the matrix with 6 ml of 6 Mol L^{-1} HCl, followed by 22 ml 6 Mol L^{-1} HCl for collection. The second run was performed with 7.5 ml of 6 Mol L^{-1} HCl followed by 18 ml 6 Mol L^{-1} HCl (Table 3). Standard BCR-2 was run through columns a third time to remove any possible transition metals causing interference in Cu isotope analysis.

Table 4: Column chromatography expanded collection run.

Step	Solvent	Eluent
Cleaning	3 mol L-1 HNO3	10ml new resin, 15 ml reusing resin, into waste beaker
Cleaning	Milli-Q H2O	10ml new resin, 15 ml reusing resin, into waste beaker
Cleaning/ equilibration	6 mol L-1 HCl	10ml new resin, 15 ml reusing resin, into waste beaker
Sample load	6 mol L-1 HCl	1.5 ml into waste beaker
Elute matrix	6 mol L-1 HCl	6 ml into waste beaker
Collect sample into previous digestion vessel	6 mol L-1 HCl	22ml into collecting vial

Multi-Collector Inductively Coupled Plasma Mass Spectrometry (MC-ICP-MS)

Copper isotopic determination was performed using a ThermoFinnigan Neptune Multi-Collector (MC-ICP-MS) at CSIRO/The University of Adelaide Waite campus. Sample solutions were introduced by auto sampler under 'dry' plasma using a spray chamber. Samples and standards were diluted to 200 ppb and measured for three blocks of 60 cycles. Samples were analysed in low-resolution mode with the Faraday cup configuration in Table 5. Cu isotopic data are reported in standard δ-notation (per mil ‰) relative to a standard reference material:

$$\text{NIST 976 } \delta^{65}\text{Cu} = 65Cu/63\text{Cu sample}/\ 65\text{Cu}/63\text{Cu NIST 976} - 1 \times 1000.$$

Standard sample bracketing was used to account for machine drift and a 200 ppb Ga spike was used to correct for mass bias.

Table 5: Configuration of Faraday cup with 1011 Ω resistors for Cu isotope analysis on the ThermoFinnigan Neptune MC-ICP-MS.

Cup	L4	L3	L2	L1	C	H1	H2	H3	H4
Isotope	^{63}Cu	^{64}Zn	^{65}Cu	^{66}Zn	^{67}Zn	^{68}Zn	^{69}Ga	^{70}Zn	^{71}Ga

RESULTS

Petrography

The Mannum granite can be subdivided into six seemingly distinct phases: the host granite, intermediate hybridised zone, the mafic enclaves and southern dyke, the basalt dyke and microgranite. Examples of the spatial distribution of these lithologies are shown in Figure 4 (A and B).

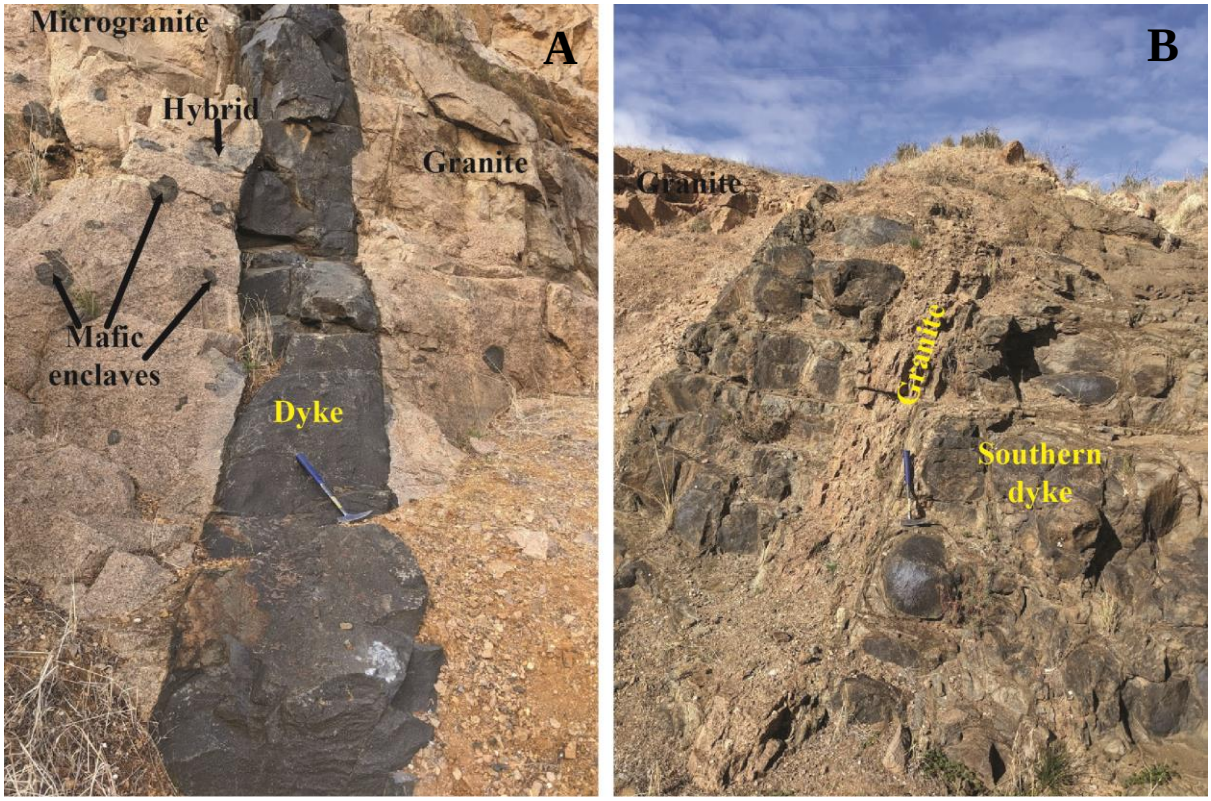

Figure 4: Different phases of the Mannum granite. (A) The Mannum dyke, fine-grained intrusive dark basalt, mafic enclaves dark grey to grey, the hybridised phase grey to light grey, granite and micro granite in beige. (B) shows the southern dyke which is contemporaneous with the mafic enclaves and shares the same mineral composition and displays mingling textures with the host granite.

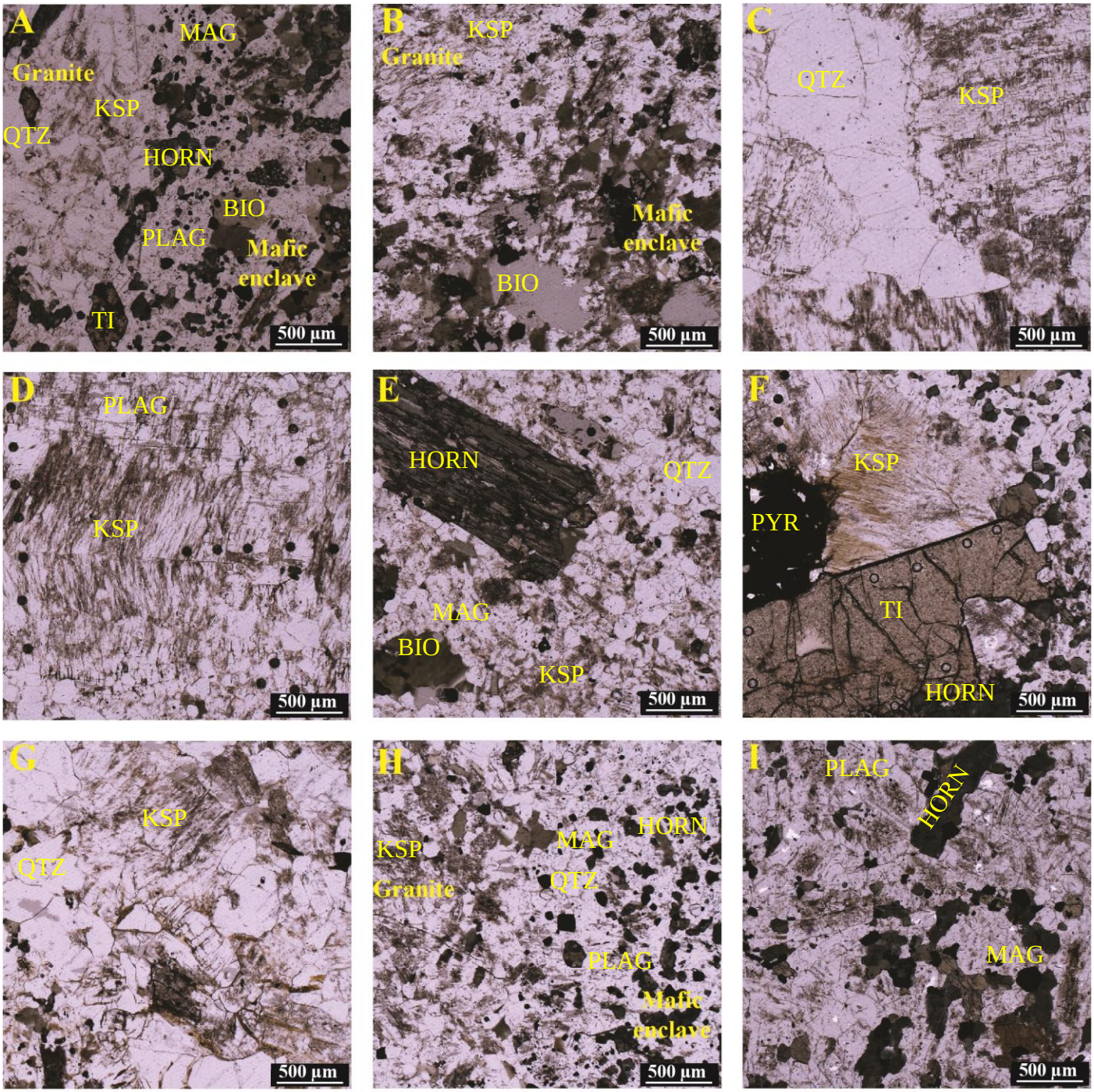

Figure 5: Photomicrographs of Mannum granite samples in plane-polarised light. (A) BOUNDARYts001 mafic enclave bounding host granite with phenocrysts of alkali feldspar and quartz, with minor biotite and titanite. The mafic enclave is dominated by plagioclase, biotite and hornblende with minor magnetite. (B) BOUNDARYts002 mafic enclaves bounding host granite, with the same mineral composition to BOUNDARYts001. (C) HYBRIDts006A host granite near to a hybrid zone, comprising quartz and alkali feldspar. (D) HYBRIDts006B intermediate hybrid zone, rapakivi texture. (E) HYBRIDts006C intermediate hybrid zone, with large xenocryst hornblende crystals, rapakivi texture, quartz and biotite. (F) ENCLAVEts009: mafic enclave, comprising hornblende and plagioclase with large titanite crystals often associated with KSP. (G) BOUNDARYts012 granite mafic enclave boundary, focused on the felsic phase, showing a lack of mixing/mingling. (H) BOUNDARYts0016, enclave-granite boundary, displaying anhedral alkali feldspar, quartz and biotite, bounding hornblende, plagioclase, magnetite. (I) SDts001, southern dyke thought to be contemporaneous with the host granite, comprising plagioclase, magnetite and horwnblende.

The mafic enclaves (Figures 5 A, B, F, H, I) are dominated by small anhedral to subhedral 100 µm scale plagioclase feldspar and hornblende crystals. Larger crystals (up to 2 mm) of plagioclase and hornblende are also present with subhedral edges and show a more degraded texture, often showing zonal rims of differing composition. Biotite is also prevalent ranging from 0.2-1 mm. The mafic enclaves also have minor magnetite and pyrite. Figure 5F shows a large anhedral pyrite crystal between the titanite and alkali feldspar. This occurrence of large 1-5 mm titanite, alkali feldspar and smaller pyrite crystals is prevalent throughout sample ENCLAVEts009, however it was not observed in other enclave samples. These titanite, alkali feldspar occurrences possess internal euhedral edges, an internal anhedral edge with pyrite, and external anhedral edges, shown in Figure 5F.

The host granite (Figure 5C, G) comprises phenocrysts of euhedral alkali feldspar (5-10 mm), with a cloudy appearance due to exsolution, euhedral quartz (1-5 mm) and anhedral biotite (1-3 mm), with minor magnetite and titanite (<0.5 mm) and very rare pyrite (<0.5 mm). In samples bounding mafic enclaves some pyrite is present, often as small anhedral crystals, however in BOUNDARYts016 there is a large subhedral pyrite crystal (1mm). Rapakivi feldspars are also found in the host granite and their frequency is dependent on proximity to mafic enclaves.

The hybrid phase is composed of alkali/rapakivi feldspar (5-10 mm), and quartz phenocrysts (1-3 mm) and anhedral biotite crystals (1-3 mm). Minor magnetite and pyrite (<0.5 mm) are also present, along with hornblende xenocrysts (Figure 5E). The width of the plagioclase rims on alkali feldspar varies greatly even within a single sample from 10 – 100 µm, and the rims are less cloudy compared to the alkali feldspar core indicating less exsolution.

Major elements

Whole rock major element data are summarised in Table 6, and Harker plots of major elements compared to SiO_2 are given in Figure 6. The orange circle in the plots in Figure 6 represents the mafic dyke, which generally lies off the trend line (K_2O, Fe_2O_3 and Al_2O_3 being exceptions). Oxides: TiO_2, Fe_2O_3 (Fe is present as Fe^{3+} and Fe^{2+}), MgO, CaO and MnO all display decreasing trends with increasing SiO_2. Al_2O_3 decreases slightly in felsic samples, Na_2O initially increases with SiO_2, peaks at 57-58% SiO_2, then decreases. The amount of Al_2O_3 decreases from a high of 15 wt% in mafic enclaves to a low of 13 wt% in felsic samples. Table 7 compares data reported by Turner and Foden (1996) specifically for MG7 which were reanalysed for this study and show only an average percent difference of 0.16% between the two analyses.

Table 6: Whole rock major element results for sample sets.

Sample	SiO_2	Al_2O_3	Na_2O	MgO	P_2O_5	TiO_2	CaO	K_2O	Fe_2O_3	MnO	Total
MG7	46.9	16.0	3.61	7.13	0.37	1.97	9.65	0.71	12.15	0.24	98.8
HYBRID006B	69.4	13.3	4.03	0.65	0.11	0.45	1.32	4.74	2.62	0.08	96.8
HYBRID0016B	66.9	13.7	4.78	1.33	0.36	0.85	2.38	3.28	4.90	0.14	98.6
HYBRID0002A	62.6	13.8	4.10	2.20	0.35	1.28	3.06	4.00	6.24	0.18	97.8
ENCLAVE016D	58.3	15.1	6.13	2.57	0.76	1.52	4.31	1.40	8.42	0.25	98.8
ENCLAVE016E	57.9	15.0	6.20	2.68	0.75	1.57	4.34	1.36	8.52	0.25	98.6
ENCLAVE016F	56.7	15.2	6.22	2.86	0.82	1.63	4.50	1.41	9.16	0.27	98.7
ENCLAVE017A	48.3	14.3	4.73	5.02	0.66	2.47	6.88	1.72	12.90	0.30	97.3
ENCLAVE016C	57.2	14.9	6.06	2.64	0.74	1.52	4.26	1.36	8.49	0.25	97.4
ENCLAVE002B	57.4	14.4	4.62	3.18	0.49	1.73	4.62	3.05	8.50	0.36	98.4
ENCLAVE002C	57.3	14.4	4.50	3.16	0.47	1.72	4.70	3.31	8.60	0.46	98.6
ENCALAVE 009	55.3	14.8	5.02	3.68	0.42	1.67	5.80	3.11	8.70	0.29	98.8
SOUTHERN DYKE/ENCLAVE001A	56.5	14.9	4.84	3.06	0.76	1.76	5.56	1.83	9.55	0.15	98.9
SOUTHERN DYKE/ENCLAVE001B	56.7	14.9	4.72	3.02	0.74	1.77	5.46	1.90	9.29	0.15	98.6
BOUNDARY012A	69.6	13.0	4.46	1.29	0.16	0.77	1.77	3.26	4.48	0.10	98.9
GRANITE013A	70.4	14.0	4.13	0.62	0.10	0.45	1.23	5.21	2.42	0.07	98.6
GRANITE016A	72.2	13.8	3.92	0.40	0.06	0.32	0.98	5.59	1.75	0.06	99.1
HYBRID006A	69.0	13.6	4.02	0.77	0.13	0.53	1.44	4.88	3.13	0.09	97.6
GRANITE012G	72.0	13.8	3.96	0.41	0.07	0.36	0.77	5.39	2.15	0.03	99.0

Table 7: Major element data sample MG7: comparison of current data to Turner and Foden (1996).

	SiO_2	Al_2O_3	Na_2O	MgO	P_2O_5	TiO_2	CaO	K_2O	Fe_2O_3	MnO	Total
2021	46.938	16.046	3.614	7.134	0.37	1.968	9.648	0.71	12.152	0.242	98.822
Turner and Foden 1996	46.61	15.93	3.47	7.37	0.37	2.03	9.62	0.75	12.33	0.23	98.71

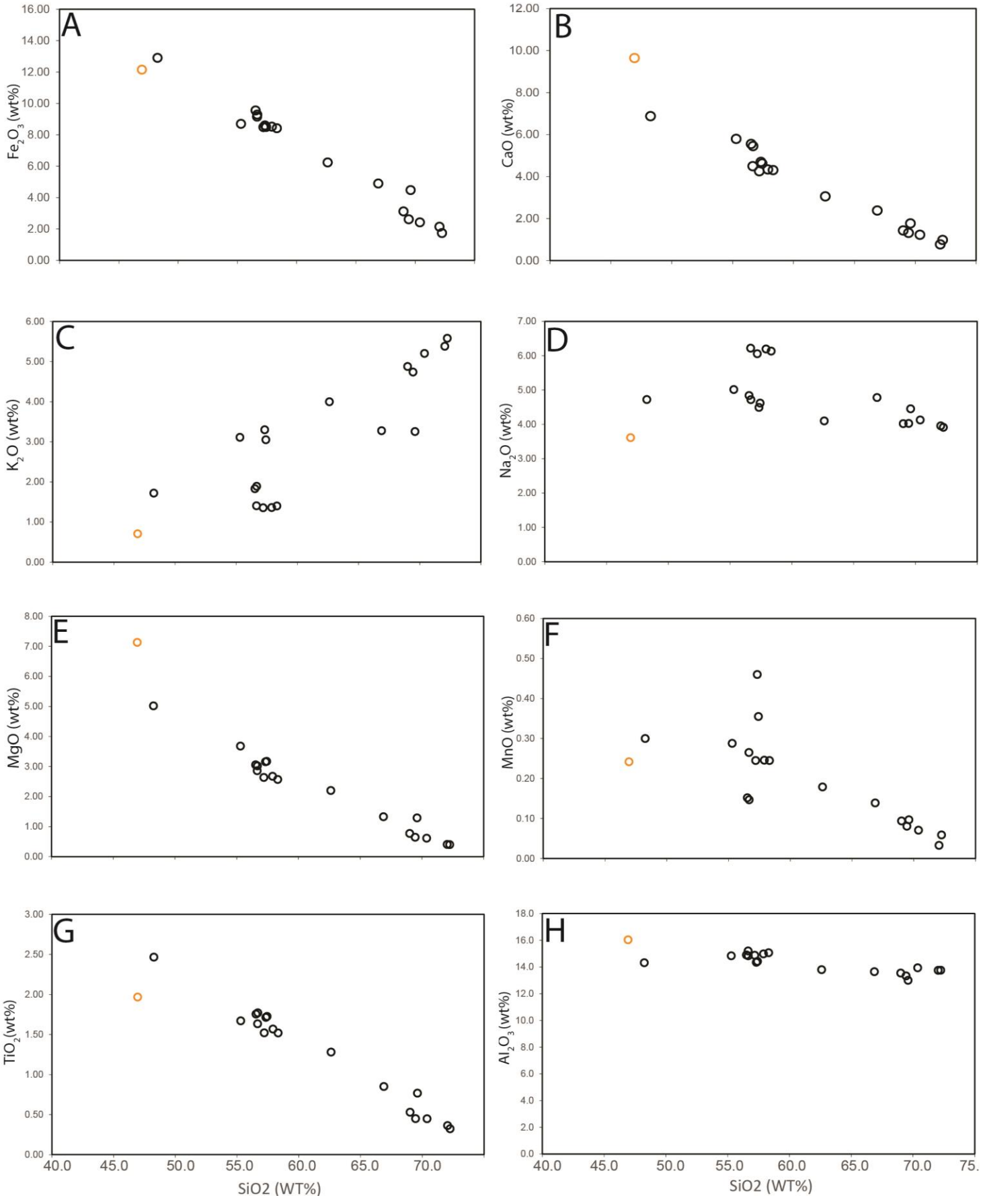

Figure 6: Harker plots of whole rock major elements. (A) Fe_2O_3 and SiO_2, (B) CaO and SiO_2, (C) K_2O and SiO_2, (D) Na_2 and SiO_2, (E) MgO and SiO_2, (F) MnO and SiO_2, (G) TiO_2 and SiO_2, (H) Al_2O_3 and SiO_2.

Electron probe micro analysis

EPMA analysis shows major element composition of individual crystals, and the changes in mineral composition due to the introduction of magma of a different composition. Figure 7A shows a rapakivi feldspar in sample HYBRID006B. Rims of the crystal show a plagioclase composition while the core has an alkali feldspar composition; the change of composition is abrupt, indicating a distinct change in local magma chemistry. An inclusion of plagioclase feldspar is also present within the crystal, possibly a former xenocryst from a less evolved magma. Figure 7B shows an alkali feldspar xenocryst within a mafic enclave, contacting titanite and pyrite. This crystal lacks a rapakivi rim; the alkali feldspar crystal is anhedral and much larger than the surrounding hornblende and plagioclase crystals, suggesting that this crystal formed before the mafic magma mingled within the host granite. EPMA analysis of titanites shows no chemical zoning of titanite in all phases titanite.

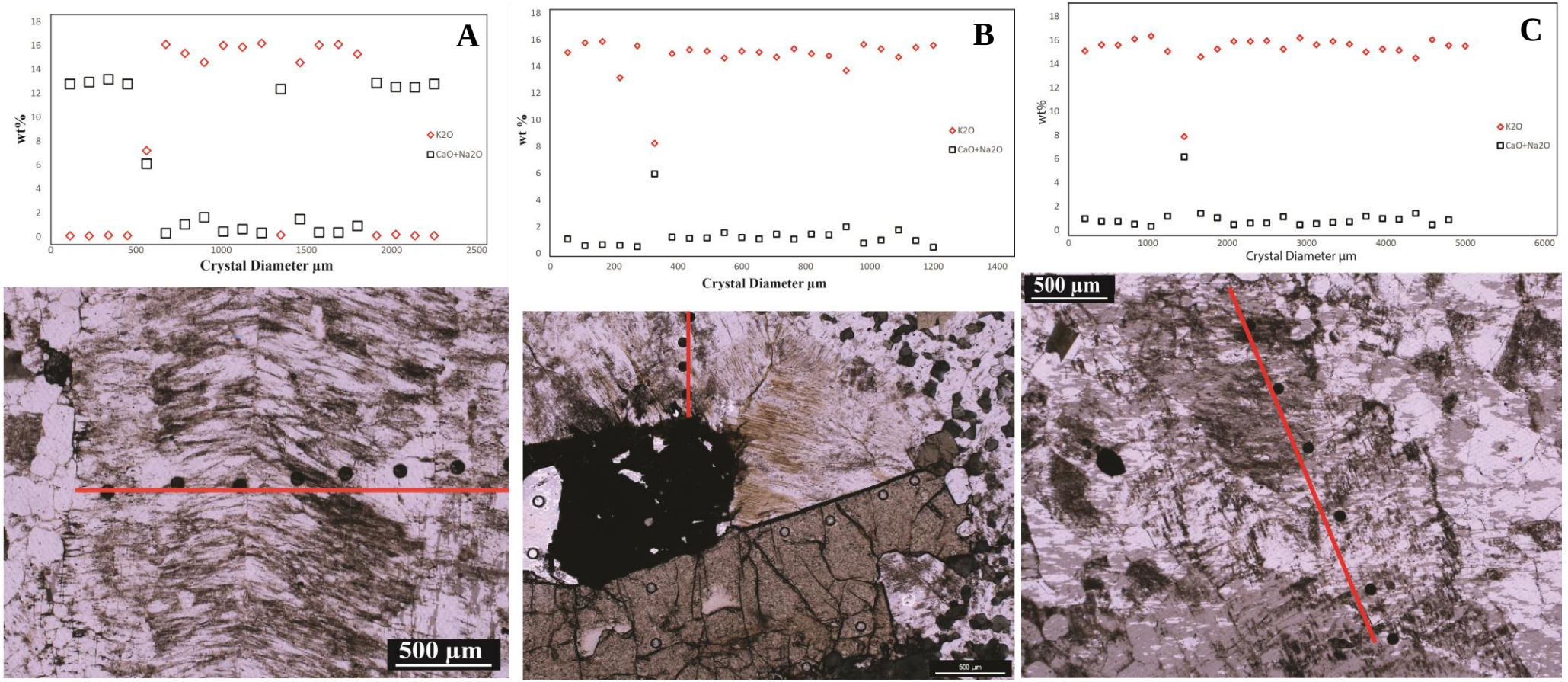

Figure 7: EPMA traverses of individual crystals in the Mannum granite. (A) rapakivi feldspar crystal in HYBRIDts006B, crystal composition change with diameter is modelled, K_2O WT% and Na_2O+CaO WT% are shown. The red line shows the extent of the traverse analysis. (B) alkali feldspar crystal in ENCLAVEts009, crystal composition change with diameter is modelled, K_2O WT% and Na_2O+CaO WT% are shown. The red line shows the extent of the traverse analysis. (C) alkali feldspar crystal in BOUNDARYts016, crystal composition change with diameter is modelled, K_2O WT% and Na_2O+CaO WT% are shown. The red line shows the extent of the traverse analysis.

Whole rock and mineral rare earth element signatures

Figure 8 shows whole rock REE signatures from trace element data from Solution ICP-MS. Figures 9 and 10 respectively show titanite and hornblende REE signatures of individual minerals from LA-ICP-MS analysis.

Figure 8 displays REE signatures and shows all samples following the same general trend. Figure 8A shows that the three most enriched in REEs are all from sample series 16, BOUNDARY016F, BOUNDARY016E and BOUNDARY016C, which are all from the mafic enclave section of the sample, near the boundary with the host granite. The mafic dyke sample, MG7, presents a very different pattern from all other samples, showing an almost straight trend depleting towards the HREEs; other samples show an initial depleting trend to Eu then a consistent trend for HREEs. Granite samples in Figure 8B show a consistent pattern with a significant negative Eu anomaly, with small variation in overall REE enrichment. Hybrid samples (Figure 8C) show a slight variation in pattern with LREEs and a small variation in overall REEs. The Eu anomaly becomes less pronounced as samples become more mafic in composition, with samples ENCLAVE009, ENCLAVE017 and ENCLAVE016D showing little to no negative Eu anomaly (Figure 8D). Sample set 016 (Figure 8E) shows a wide range in REE signatures with 16E and F presenting the highest La and Lu concentrations, while sample 16A is generally low in all REEs compared to other samples.

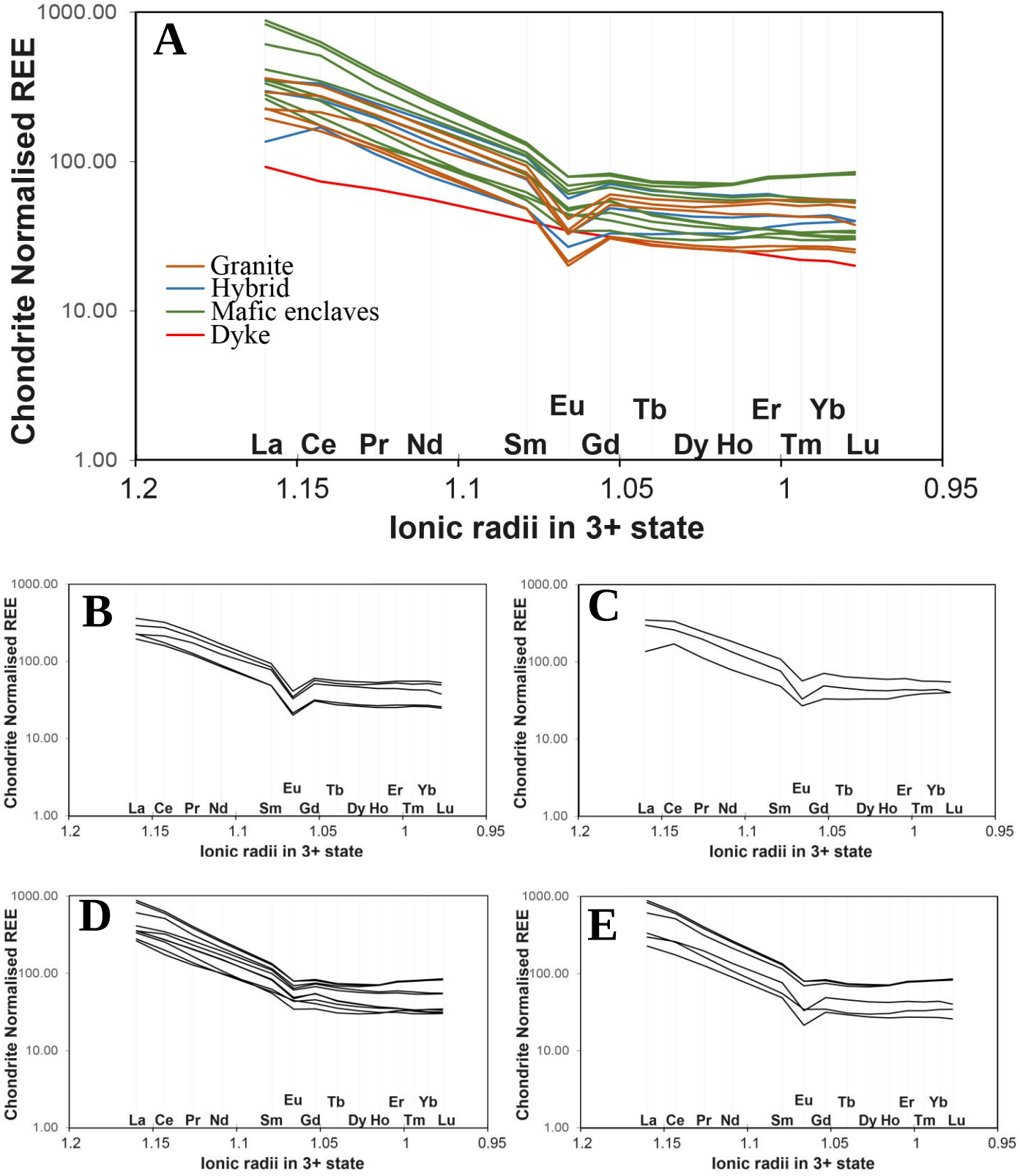

Figure 8: Whole rock rare earth element plots, normalised to CI carbonaceous chondrites. (A) all samples, MG7; the basalt dyke in red, hybrid samples in blue, mafic enclaves in green, granite in orange, (B) granite REE signatures, (C) hybrid REE signatures, (D) mafic enclave REE signatures, (E) sample set 16, ranging from granite, hybridised to mafic enclave REE signatures. Cl Chondrite values from Sun and McDonough (1996).

Individual mineral rare earth analysis

Individual mineral composition trace element analysis was done using LA-ICP-MS in samples: BOUNDARYts002, HYBRIDts006B, ENCLAVEts009 and BOUNDARYts012 for both sulphides and silicates. Titanite (Figure 9) and hornblende (Figure 10) were targeted due to a higher concentration of REEs compared to other silicates and their frequency in the enclaves, hybrid and granite phases (although hornblende is absent in granite). Feldspar and biotite were also targeted. But REE concentration, particularly of HREEs, were below detection limits for accurate analyses.

Titanite REE plots generally present similar trends apart from the Eu anomaly. Samples in mafic enclaves have a small positive or negative Eu anomaly (Figure 9A, B and C), while the titanites in BOUNDARYts016 and BOUNDARYts002 (Figure 9D and E) have a moderate negative Eu anomaly compared to the other REEs, which are all elevated in comparison to the mafic titanites.

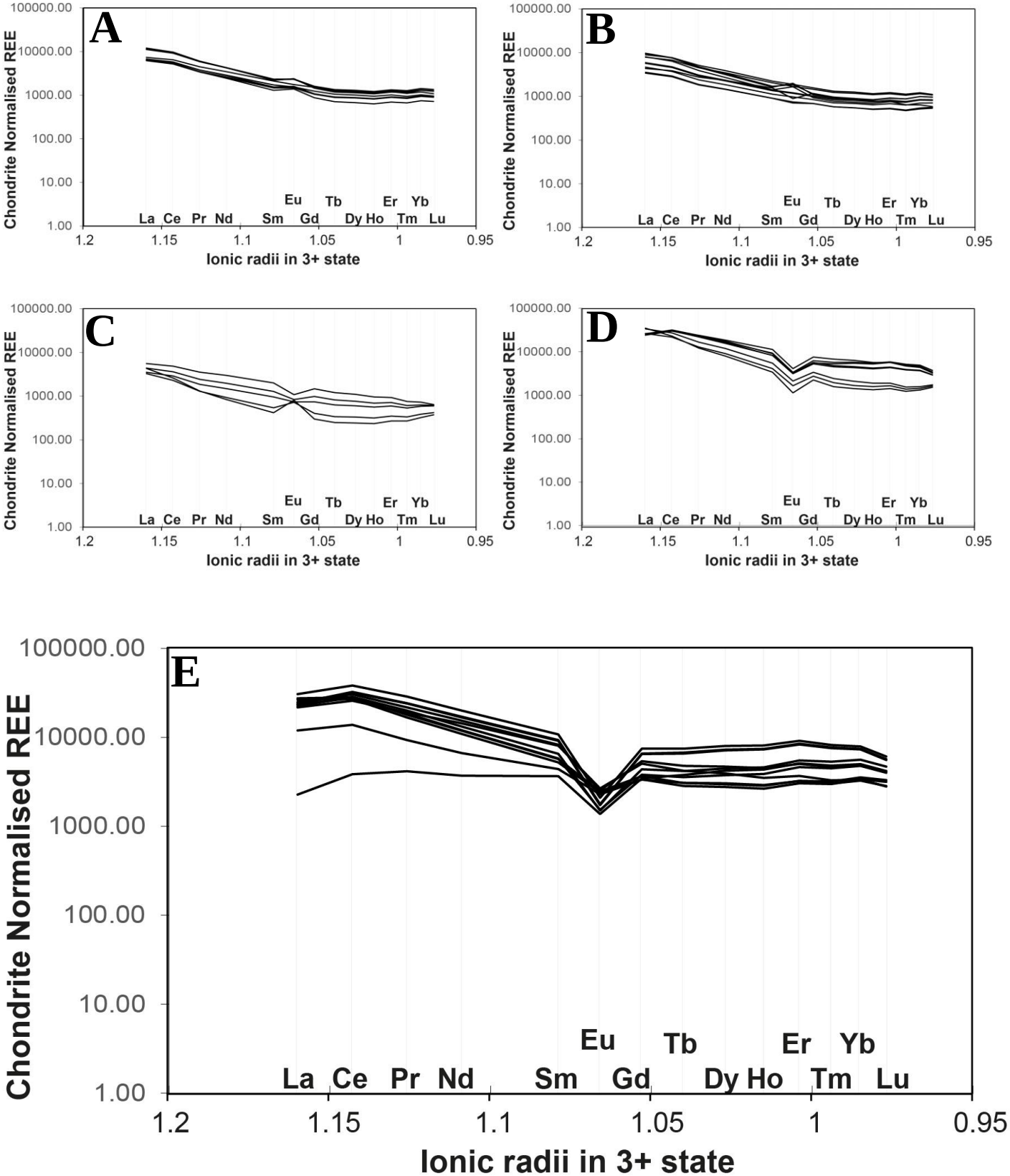

Figure 9: Titanite REE plots: (A) large titanite crystal in mafic enclave associated with a potassium feldspar crystal and a pyrite crystal, (B) large titanite in mafic enclave associated with a potassium feldspar crystal, (C) titanite crystal in mafic enclave associated with a potassium feldspar crystal, (D) subhedral titanite crystals in granite, near boundary with a mafic enclave, (E) euhedral titanite crystal in granite, near boundary with a mafic enclave. Cl Chondrite values from Sun and McDonough (1996).

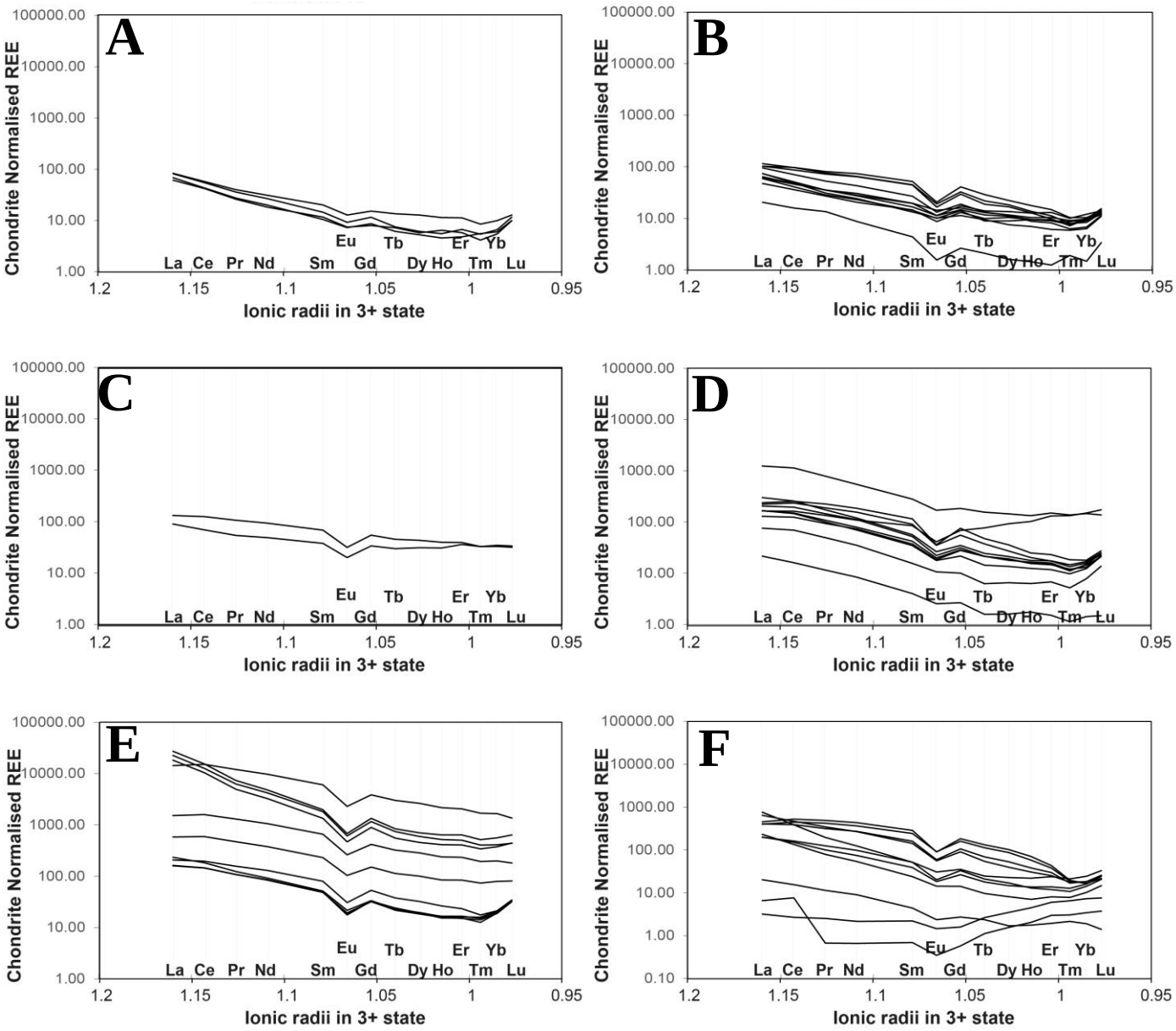

Figure 10: REE plots of hornblende crystals: (A, B, C) hornblende crystals in mafic enclaves, (D) hornblende crystal in mafic enclaves near boundary with granite, (E) hornblende crystals within mafic enclave, associated with a large anhedral mass of hornblende crystals, (F) hornblende crystal within mafic enclave near boundary with granite. Cl Chondrite values from Sun and McDonough (1996).

The REE signatures from hornblende crystals vary, displaying a wide range of REE concentrations with both positive and negative Eu anomalies. Hornblende crystals in ENCLAVEts009 (Figure 10A, B and C) follow a similar trend by having a small negative Eu anomaly. Hornblende crystals in BOUNDARYts002 (Figure 10D) are similar to those in BOUNDARY016 (Figure 10E and F) with hornblendes in BOUNDARYts016 being the most elevated in REEs

Copper concentration

Trace element concentrations of Cu and other transition metals together with sulphur are summarised in Table 9 and show that Cu is in low abundance (<40 ppm) in the Mannum granite samples, the dyke being slightly richer in Cu (50 ppm). Table 8 compares the correlation between transition metals and S or SiO_2.

Table 8: Shows R^2 values for select transition metals and SiO_2 and S, displaying the correlation between them.

	Cu	Co	Ni	Zn
SiO_2	0.647	0.223	0.489	0.387
S	0.818	0.73	0.357	0.433

Cu is most highly correlated with S, and somewhat correlated with SiO_2, while Co, Ni and Zn and are not strongly correlated with either S or SiO_2 (see Table 8). Understanding which minerals the targeted transition metals are concentrated in, enables transport processes to be better understood, and also provides information about possible isotope fractionation. The distribution of Cu appears to be linked with sulphur and this indicates that a volatile phase is transporting Cu, which may cause or drive isotope fractionation. Understanding the behaviour and quantity (Tables 9, 10 and 11) of other transition metals aids in Cu isotope analysis, as Zn and Ni can be used as spikes. However, if Cu purification is unsuccessful and Ni or Zn contaminate the sample, this causes the spike to be imprecise. Plots of Cu, Co, Ni and Zn against S and SiO_2 can be found in Appendix A.

Table 9: Solution ICP-MS analysis of trace elements in the Mannum granite rock suite. Targeted transition metals are shown.

Sample Name	S	Co	Ni	Cu	Zn
MG7	2506	57	85	50	123
HYBRID006B	856	17	5	13	127
HYBRID016B	259	20	2	4	64
HYBRID002A	2016	22	10	21	128
ENCLAVE016D	885	13	5	9	158
ENCLAVE 016E	1743	28	10	20	324
ENCLAVE 016F	1798	26	10	26	309
ENCLAVE 017A	2520	42	35	27	219
ENCLAVE 016C	1524	22	10	20	318
ENCLAVE 002B	2613	25	16	29	206
ENCLAVE 002C	2663	26	16	30	208
ENCLAVE 009B	1257	39	25	15	185
SD001A	867	29	7	14	130
SD001B	871	32	7	11	118
GRANITE012A	49	51	8	7	98
GRANITE 013A	287	17	2	4	60
GRANITE 016A	260	28	2	6	41
GRANITE 006A	322	25	3	4	72
GRANITE 012G	11	18	2	2	37

Measuring the amount of Cu in individual minerals aids in understanding the distribution and behaviour of Cu within the system. Table 10 displays a summary of targeted transition metals in rock forming minerals from LA-ICP-MS analysis and Table 11 summarises the values for pyrite. The data show that Co, Ni and Zn behave differently from Cu in their mineralogical distribution. This shows that Cu isotope analysis cannot necessarily be used to understand the behaviour of other transition metals. Note that Co is at elevated levels in pyrite but was not determined in the rock-forming minerals. EPMA data on sulphides are in Appendix B; the targeted transition metals were mostly below detection limits for EPMA.

Table 10: LA-ICP-MS data of targeted transition metals in rock-forming minerals, showing the average of analysis and the range of values. The number of analyses is displayed next to the mineral name.

Mineral/sample			
BOUNDARY002	**Ni**	**Cu**	**Zn**
Biotite (11)	29	12	930
	(1-66)	(0-56)	(58-1200)
Hornblende (19)	21	20	870
	(0-25)	(0-75)	(2-1300)
Matrix (16)	19	77	23
	(0-26)	(2-210)	(2-850)
HYBRID006B	**Ni**	**Cu**	**Zn**
	24	30	1100
Hornblende (15)	(3-61	(1-300)	(220-1500)
	13	2	450
Biotite (9)	(0-38	(1-6)	(14-1300)
ENCLAVE009	**Ni**	**Cu**	**Zn**
Biotite (25)	92	5	910
	(82-100)	(3-11)	(810-1200)
Hornblende (28)	59	1	680
	(0-120)	(0-6)	(3-820)
Matrix (15)	24	37	160
	(0-120)	(0-170)	(2-870)
BOUNDARY0016	**Ni**	**Cu**	**Zn**
Magnetite (20)	21	9	239
	(2-93)	(0-160)	(56-2000)
Biotite (12)	42	9	1300
	(31-48)	(2-37)	(1200-1600)
Matrix (17)	1	7	61
	(0-8)	(0-30)	(2-520)
Hornblende (43)	20	41	853
	(0-45)	(0-470)	(1-3200)

Table 11: LA-ICP-MS trace element data of transition metal concentrations in pyrite crystals averaged in different samples with minimum and maximum values.

sample	Co	Ni	Cu	Zn
BOUNDARYts002	1500	290	780	660
	(17-12000)	(16-1400)	(0-9700)	(1-27000)
HYBRIDts006C	740	350	5800	76
	(130-2400)	(75-1500)	(2-49000)	(3-370)
ENCLAVEts009	2700	2200	51	350
	(0-13000)	(15-33000)	(0-680)	(0-12000)
BOUNDARYts016	1300	240	260	370
	(9-7500	(17-1000)	(0-6500)	(1-5900)

Copper isotopes

Initial Cu isotope results were inconsistent and standards were approximately -1‰ out (Table 12) from literature values: USGS-BHVO-2 has an accepted value of $\delta^{65}Cu = 0.12$ (Moynier et al., 2017), USGS-GSP-2 has an accepted value of $\delta^{65}Cu = 0.30$ (Liu et al., 2014).

The Mannum granite samples initially showed a wide range of $\delta^{65}Cu$ values from 0.5‰ to -2.9.‰. In an attempt to overcome this problem, further analysis was conducted with samples prepared with hydrofluoric (HF) hotplate digestion. The results showed the standards were far closer to the expected $\delta^{65}Cu$ but still incorrect (Table 12), indicating HF bomb digestion caused fractionation, either through vaporisation and subsequent escape of a high ^{65}Cu vapor out of the bombs or possibly fractionation into fluorides which were undissolved and centrifuged out prior to Cu extraction.

The column ion exchange chromatography procedure was also modified to include two runs, the initial one, with a widened collection window, followed by a second run with the original collection volume; this was done to try and collect all the copper from the sample, then purify it, as impurities, such as Ti and Fe were suspected to alter the $\delta^{65}Cu$ value (Lowczak, 2019). However, this also produced inaccuracies in the standards USGS BHVO-2 and USGS GSP-2

(Table 12). Other metals such as Co, Ni and Zn were also of concern but this proved not to be an issue.

The molarity of HCl which carries samples through columns was investigated and was found to be in the range 5.81 to 5.7 Mol L^{-1}, while the copper column chromatography method calls for 6 Mol L^{-1} HCl. The molarity of the HCl controls the rate at which Cu cuts pass through the column. Maréchal and Albarède (2002) showed with 3 Mol L^{-1} HCl Cu cuts pass through after just 4 ml, while 7 Mol L^{-1} passes through after 20 ml; this drastic change in volume required to separate Cu indicates ^{65}Cu was being lost in the 7.5 ml eluting phase. Maréchal and Albarède (2002) also stated that a 90% collection may result in up to 0.3‰ change in the $\delta^{65}Cu$ value, which can greatly affect results. A Cu extraction was subsequently performed with 6 Mol L^{-1} HCl; only one run through the columns was performed on standard USGS BHVO-2, and a $\delta^{65}Cu$ value of 0.115‰ was achieved compared to the accepted value of 0.12. The other standard, GSP-2, returned a Ga uncorrected analysis of 0.312‰ compared to the accepted value of 0.3 (Moynier et al., 2017 and Liu et al., 2014). As both the BHVO-2 and GSP-2 only returned a single correct value the Cu isotope analysis is considered preliminary. The evolution of the Cu separation method used in this study, with reference to the $\delta^{65}Cu$ values for the standards, is summarised in Table 12.

Table 12: Cu isotope standard experiment results with date and change in method.

Date/change in method	BHVO-2 experimental $\delta^{65}Cu$ ‰	GSP-2 experimental $\delta^{65}Cu$‰
25/08/2021Original	**-0.942959**	**-0.947468**
13/09/2021 No bomb digestion	**-0.0727**	**0.1407**
25/09/2021Wider column collection	**-0.03**	**--**
11/10/2021 and 21/20/2021 Exact molarity of acid	**0.111**	**0.312**

After issues with Cu cuts collection had been solved, nine samples were analysed using MC-ICP-MS (Figure 11). The results for the analysed samples fit within the bounds of Rayleigh fractionation curves, showing that $\delta^{65}Cu$ is related to Cu concentration and becomes more

positive/heavier with decreasing Cu. Unfortunately, the analysis for two of the samples (HYBRID16B and ENCLAVE16D) was unsuccessful and a lack of time prevented repeat runs of these samples.

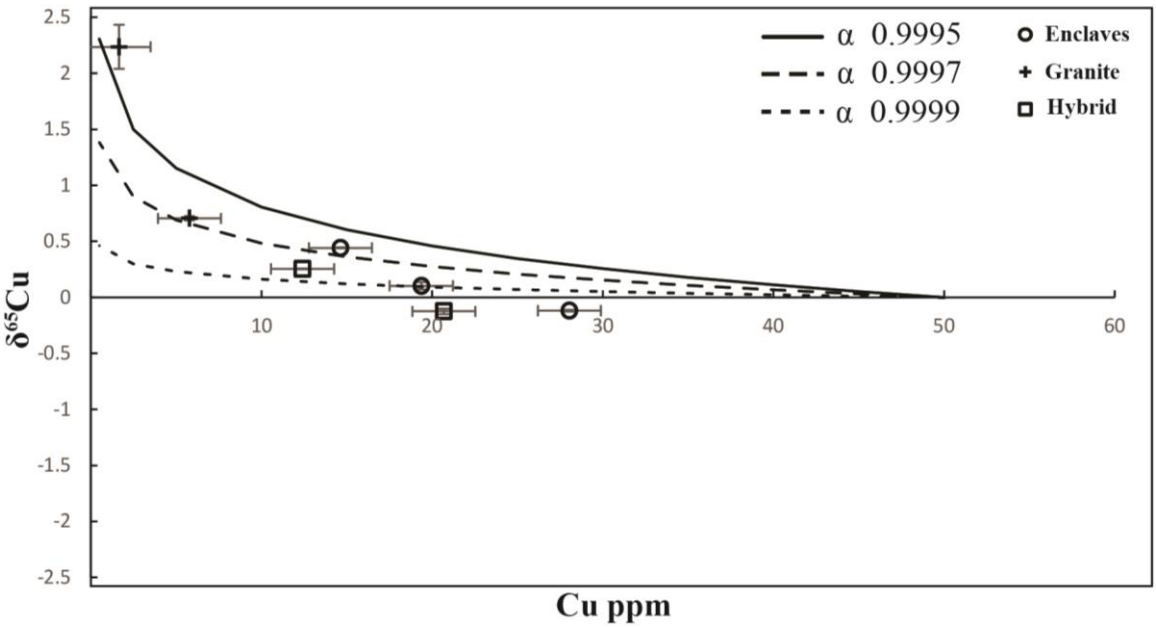

Figure 11: δ^{65}Cu data collected from Mannum granite with enclaves, granite and hybrid phases modelled against Cu concentration, with Rayleigh fractionation curves produced by Rayleigh fractionation factors α.

DISCUSSION

Whole rock textural evolution through mixing/mingling

Varying degrees of mingling and mixing between the mafic enclave and host granite were observed through petrographic analysis. The hybrid zones between the mafic enclaves and host granite vary in size and composition. Sample HYBRIDts006C is interpreted to be a completely mixed hybrid of the enclave and granite, as it possesses rapakivi feldspar, hornblende and plagioclase xenocrysts, and an increased frequency of pyrite and magnetite (Figure 5E). Samples GRANITEts006A and HYBRIDts6B (Figures 5C and 5D respectively) show incomplete mingling, as they lack any mafic minerals with the exception of rapakivi feldspars and minor pyrite. This is interpreted as a Na_2O rich melt/fluid interacting more reactively with the felsic crystal mush (Vernon, 2016). Sample BOUNDARYts001 shows a texturally abrupt granite-enclave boundary, showing no rapakivi texture mantling alkali feldspars (Figure 5A). The variation in the degree of mixing/mingling is possibly attributed to local thermal conditions; pressure is assumed to be constant across the system. Abrupt boundaries form as a result of a large difference in temperature between the granite and enclave, quenching the enclave as it is injected into the granite (Cherry and Trembath, 1978). In contrast the hybrid zones form as a result of the enclave and granite being closer in temperature during injection, preventing quenching. The degree of hybridisation is also associated with the proximity of mafic enclaves to microgranite blocks. Field observations show that the mafic enclaves and microgranite do not interact, with the enclaves deforming around the microgranite blocks. This is most likely due to the microgranite blocks being solid during the injection of the mafic enclaves (Turner and Foden, 1996). Turner and Foden (1996) reported a temperature of $\approx 930\,C^{o}$ after thermal equilibrium was achieved between the granite and the mafic enclaves, with mixing between the two phases likely occurring

before thermal equilibrium was reached. However, mingling may have continued after this point, allowing for more extensive formation of rapakivi feldspars. Several models have been proposed for the formation of rapakivi feldspars. The two main mechanisms proposed are: (1) isothermal decompression, where the feldspar stability field moves from alkali feldspar to plagioclase, and (2) a mechanism of mixing/mingling where mafic magma mingles into a crystal-rich felsic melt (Stewart, 1959; Hibbard, 1981; Calzia and Rämö, 2005). The rapakivi textures in the Mannum granite are strong textural evidence of the mixing/mingling of the magma of the mafic enclaves into the partially crystallized magma of the granite. Pankhurst et al. (2011) suggest multiple mixing events as opposed to mingling may have occurred due to the range in mafic enclave compositions reported by Turner and Foden (1996). Pankhurst et al. (2011) concluded that both the host granite and mafic enclaves had undergone fractional crystallisation and magma mingling/mixing. These two processes provide mechanisms for the transportation of material from a mafic source, such as the mantle, to the crust.

Whole rock geochemical evolution

The degree to which the host granite and mafic enclave phases have interacted, producing a third hybrid phase, was observed through whole rock major element analysis. Figure 12 shows the Harker plots calculated from the data from Figure 6 and Table 6, with added crystallisation vectors showing which minerals exert compositional control (Cortés, 2009). The trends presented in Figure 6 show a continuously evolving system, with two outliers: the mafic dyke, which is interpreted to be a later occurrence and distantly related to the Mannum granite and enclaves, and Sample ENCLAVEts017 which is the most mafic of the enclave samples. The trends visually resemble fractional crystallisation trends in Harker plots; however, they represent mixing/mingling trends in this case.

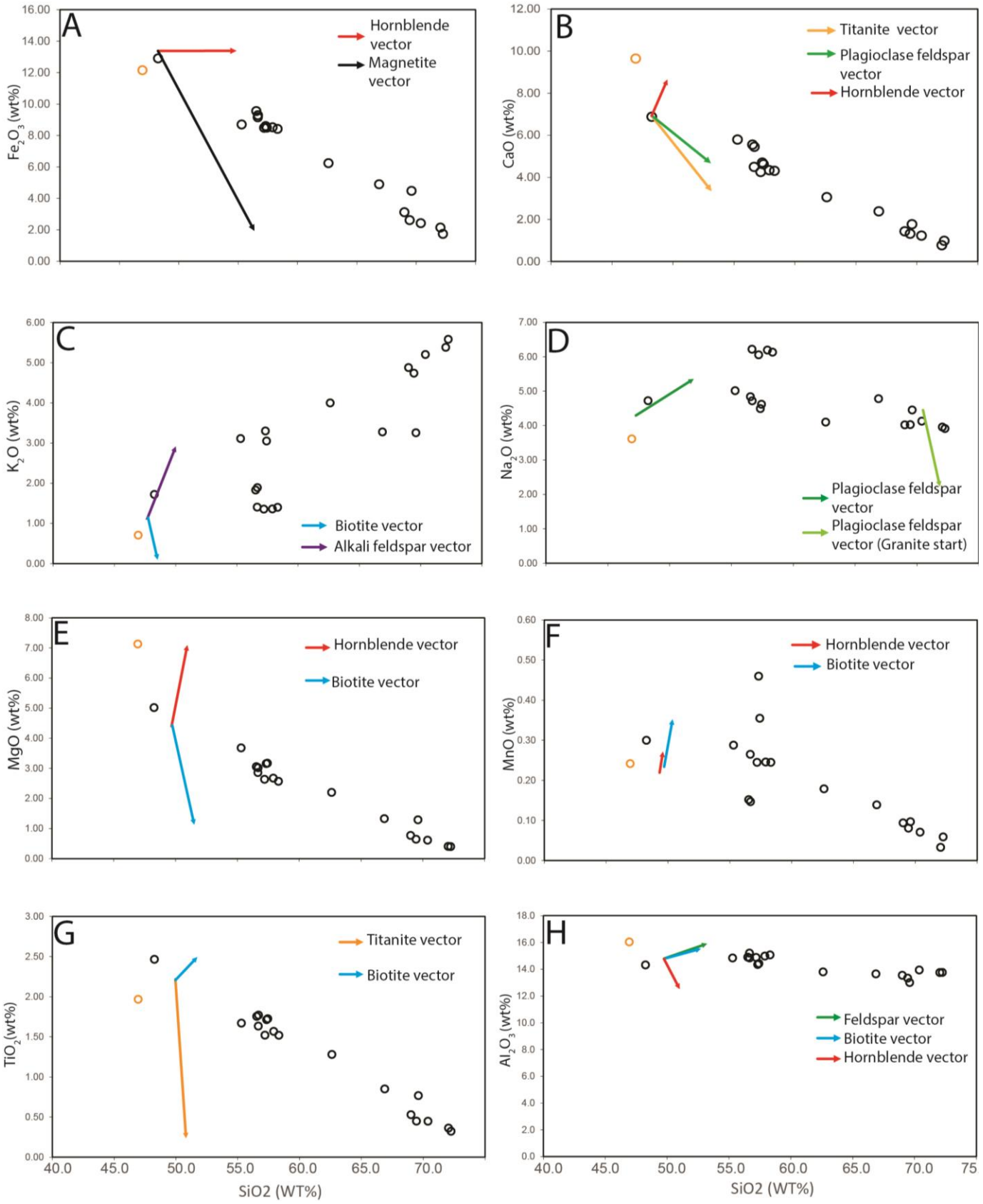

Figure 12: Crystallisation vectors on Harker plots from Figure 6 show the direction composition will take if mineralisation of a specific mineral occurs at 0%, 5%, 10% and 12%. Accessory minerals were modelled at 0% 2%, 4% and 6%, due to the low abundance of them within samples. The length of the vector shows the magnitude of whole rock composition change from the 0% mineralisation of a mineral to 12% mineralisation of a mineral and 6% in the case of accessory minerals.

The crystallisation vectors with Harker plots indicate which minerals control composition (Cortés, 2009; Harker, 1909). Fe_2O_3 is controlled by hornblende and magnetite, with magnetite exerting large control on Fe_2O_3 content; however, magnetite is present only as a trace phase (Figure 12A). Pyrite is also present, but in smaller quantities than magnetite. Fe_2O_3 is likely controlled by hornblende and to a smaller degree magnetite. The CaO content is predominantly controlled by plagioclase feldspar and hornblende. Titanite contains ≈ 28 (wt%) CaO, higher than the 9-12 (wt%) found in high Ca plagioclase feldspar and hornblende (Figure 12B); however, it is an accessory mineral making up at most only 1 -2% of the mineral assemblage in sample ENCLAVEts009. Na_2O is controlled by plagioclase feldspar; crystallisation vectors initially increase towards 57 wt% SiO_2, however Na_2O then decreases beyond this point as samples become more felsic (Figure 12D). K_2O is controlled by alkali feldspar and follows a fractional crystallisation trend (Figure 12C). MgO is controlled by both biotite and hornblende; these two minerals show vectors in opposing directions, however the MgO trend runs between them (Figure 12E). MnO is also controlled by biotite and hornblende and possibly small accessory minerals such as spinels (Figure 12F). TiO_2 is controlled by titanite and biotite, with the TiO_2 content of titanite ≈ 35-36.5 wt%, and is therefore mostly taken up into this mineral (Figure 12G). Al_2O_3 is taken up by biotite, feldspar and hornblende, however the amount of Al_2O_3 changes little in the overall system (Figure 12H). Whole rock chemistry analysis of Turner and Foden (1996) reported similar trends in Fe_2O_3, MnO, CaO and Na_2O vs SiO_2 plots, with the same MnO vertical trend at ≈57 wt% SiO_2; this vertical trend is possibly due to mineralisation of hornblende, and differences in individual enclave chemistries. The crystallisation vectors generally support the Harker plot trends. The Na_2O trend is relatively flat, decreasing only slightly from a central point of 57 wt% SiO_2, thus indicating that Na_2O is more mobile across the system, able to reside in the more felsic samples by forming rapakivi feldspars.

Whole rock rare earth elements

The whole rock REE plots show a negative Eu anomaly (Figure 8), as Eu^{2+} substitutes with Ca^{2+} in Ca-bearing minerals particularly plagioclase feldspar, thus indicating partial crystallisation of the original parental melt before injection of mafic melt into granite (Weill and Drake, 1973; Harrowfield et al., 1999). The low REE concentration of MG7, the Mannum dyke, indicates it originated from a different magma source. The mafic enclaves are slightly more enriched, overall, in REEs compared to the granite and hybrid material, and this may indicate a lack of REE transport or the presence of accessory minerals which can readily take in REEs, such as zircon.

Individual mineral chemical evolution

Hornblende REE patterns show a wide range of values following a general pattern of a small Eu anomaly, due to amphiboles taking up incompatible elements. The wide range of values most likely reflects the changing melt composition; as hornblende crystallises, it takes up incompatible elements. REEs being incorporated into hornblende may explain the higher enrichment of REEs in the mafic enclaves compared to the granite. The large hornblende crystal mass in BOUNDARYts016, shows elevated REEs indicating that it is a possible mafic xenocryst forming in a parental magma before injection.

Initial observations of titanites, in ENCLAVEts009 particularly, indicated that they are xenocrysts due to their association with alkali feldspar. The two minerals possess a euhedral edge with each other while having anhedral edges with the rest of the assemblage; this is interpreted as the titanite and alkali feldspar being xenocrysts from the granite and being assimilated and partially remelted resulting in the external anhedral edge (Figure 5F). Pyrite is also often associated with these titanite-alkali feldspar crystals, indicating a later stage fluid interaction or that these crystals have originated in an immiscible melt. These titanite-alkali

feldspar-pyrite crystals are exclusive to sample ENCLAVEts009 indicating there may have been unique mixing/mingling conditions and behaviours within individual mafic enclaves. REE analysis of the titanites however, reveals that they most likely formed in a mafic environment, as discussed by Pankhurst et al. (2011). REEs are overall depleted in mafic titanites (ENCLAVEts009) compared to felsic titanites (titanites within BOUNDARYts002 and BOUNDARYts016), while mafic titanites display a lesser Eu anomaly (Figure 9A, B and C). REE data indicate that titanites have grown within the mafic enclaves, and are not xenocrysts. However, the euhedral edge association with large alkali feldspars provides evidence towards an assimilation of xenocrysts from the host granite during injection of the mafic enclaves. This possibly indicates that the alkali feldspar xenocrysts are a result of a felsic immiscible melt and that felsic material mingles with the mafic enclaves more readily than the mafic material in the granite, which is restricted to near the enclave-granite boundary or in hybrid zones (Kamenetsky and Kamenetsky, 2010). However, this does not explain the observed relationship with large titanites and pyrite.

LA-ICP-MS analysis also showed the quantity of Cu in individual minerals (see Tables 9, 10 and 11) and that Cu concentration in the individual minerals are generally low, <100 ppm, but there is considerable variation. For example, the pyrite in the ENCLAVEts009 sample carries significantly less Cu than pyrites in other samples; however, the pyrite crystals in this sample may be a late-stage product as these often larger crystals are in association with titanite-alkali feldspar and are anhedral, indicating a product of magmatic fluids (Figure 5F) (Polyakov and Soultanov, 2011). Pyrite in sample HYBRIDts006B has a much higher Cu content (mean of 5800 ppm) compared to other samples (mean of <1000 ppm), indicating that Cu was transported during hybridisation. Cu was shown in Table 8 to correlate with S; the formation of sulphides can lead to a large degree of Cu isotope fractionation (Brzozowski

et al., 2020). Note that Co concentration was determined, as Co is not separated from Cu through column ion exchange chromatography, and may cause interference in MC-ICP-MS at high enough concentrations (>1000 ppb) (Kidder et al., 2020). Ni and Zn were measured as they can be used for internal standard spikes for MC-ICP-MS and will affect the δ^{65}Cu value if not removed through ion exchange chromatography (this was not an issue in this study as Ga was used as an internal standard). In the current study Cu isotope analysis was used to determine if this Cu was fractionated during the formation of pyrites.

Copper isotope behaviour

Preliminary Cu isotope analysis results show that Cu isotope ratios in the Mannum granite-mafic enclave system follow a Rayleigh fractionation distribution (Figure 11). Figure 11 shows that δ^{65}Cu increases with decreasing Cu concentration. As the Mannum granite is a high energy setting, ≈ 930 C^{o}, after thermal equilibrium (Turner and Foden, 1996), very little isotopic fractionation occurred, with the more mafic samples with higher Cu becoming more isotopically lighter (negative δ^{65}Cu). ^{65}Cu has a slight preference for remaining in the melt. Sample ENCLAVE009 shows a slight elevation compared to other enclave samples and even hybrid samples; this may be due to the apparent magmatic fluid movement (Figure 5F). In ENCLAVE009, the ^{65}Cu values still lie within Rayleigh fractionation curves, the higher ^{65}Cu values also showing that the amount of Cu and S measured is accurate. Figure 11 shows that Cu is being transported to some extent from the mafic enclaves to the granite and hybrid phases following the Rayleigh fractionation trend. This indicates that Cu is preferentially remaining in the mafic enclaves, but a small quantity is being transported with the mafic material during mixing/mingling with the granite.

The issues experienced with Cu isotope analysis in this project highlight the importance of the use of high-quality isotopic reference standards. A variety of issues involving sample digestion and separation through ion exchange chromatography were identified through measuring of these isotope standards. The use of bomb digestion was found probably to cause significant Cu fractionation. Bomb digestion was originally used, as certain minerals in the granite such as zircon are very difficult to digest. However, it is not necessary for Cu isotope analysis. The molarity of the HCl proved to be a critical factor in the full separation and collection of Cu. Maréchal and Albarède (2002) stated that 90% collection may result in up to 0.3‰, with a small change in the molarity of HCl leading to incomplete collection. The reason the molarity of HCl is critical is due to the coordination chemistry of copper-aqua-chloro complexes. Brugger et al. (2001) showed at 25°C that the nature of the Cu^{2+} changes considerably with the concentration of the Cl^- ion, at 2 Mol L^{-1} Cl^- $(Cu(H_2O)_6)^{2+}$ is the dominant complex, at 4 Mol L^{-1} Cl^- a mixture of $(Cu(H_2O)_6)^{2+}$, $(Cu^{2+}Cl(H_2O)_5)^+$ and $(Cu^{2+}Cl_2(H_2O)_4)$ occur in roughly equal abundance, and between 6 Mol L^{-1} and 8 Mol L^{-1} the $(Cu^{2+}Cl_2(H_2O)_4)$ complex is most abundant and stable. This complex is a Jahn-Teller distorted octahedral complex with the two Cl ions occupying opposite apical sites (Brugger et al., 2001; Halcrow, 2013). The Cl concentration is critical to the stabilisation of the complex, as at lower concentrations of Cl the complex will move to mixtures of the $(Cu(H_2O)_6)^{2+}$ and $(Cu^{2+}Cl(H_2O)_5$ complexes. This is because H_2O molecules are stronger ligands than Cl ions (Halcrow, 2013). The stability of polar Cu^{2+} complexes enables Cu to be separated out from the other metals in an ion exchange column between the intervals of 7.5 ml to 25.5 ml of 6 Mol L^{-1} HCl (Maréchal and Albarède, 2002). This understanding of Cu complex coordination chemistry can be related to Cl-rich hydrothermal fluids, Cl-rich fluids being able to transport Cu more readily; this may also have an isotopic effect with $^{65}Cu^{2+}Cl_2(H_2O)_4$ being very slightly more stable and less likely to exchange ligands than $^{63}Cu^{2+}Cl_2(H_2O)_4$. In high

temperature and highly saline hydrothermal fluids (greater than 250°C and >10 Mol L^{-1} Cl^-, Cu is transported as a $CuCl_4$ tetrahedral complex (Brugger et al., 2001; Liu et al., 2002). This means ^{65}Cu is preferentially more mobile, leading to the initial few ml of Cu cuts from the ion exchange separation column being enriched in ^{65}Cu. This effect of greater ^{65}Cu mobility is reflected in the measured Cu isotopes results, with ^{65}Cu being slightly more concentrated in the granite, which Cu is transported into. Due to the preliminary nature of the Cu isotope analysis presented in this study, a number scenarios surrounding the Cu isotopic ratios of the Mannum granite have been constructed to show the possible variations in $\delta^{65}Cu$ and the implications these data would have (Figure 13).

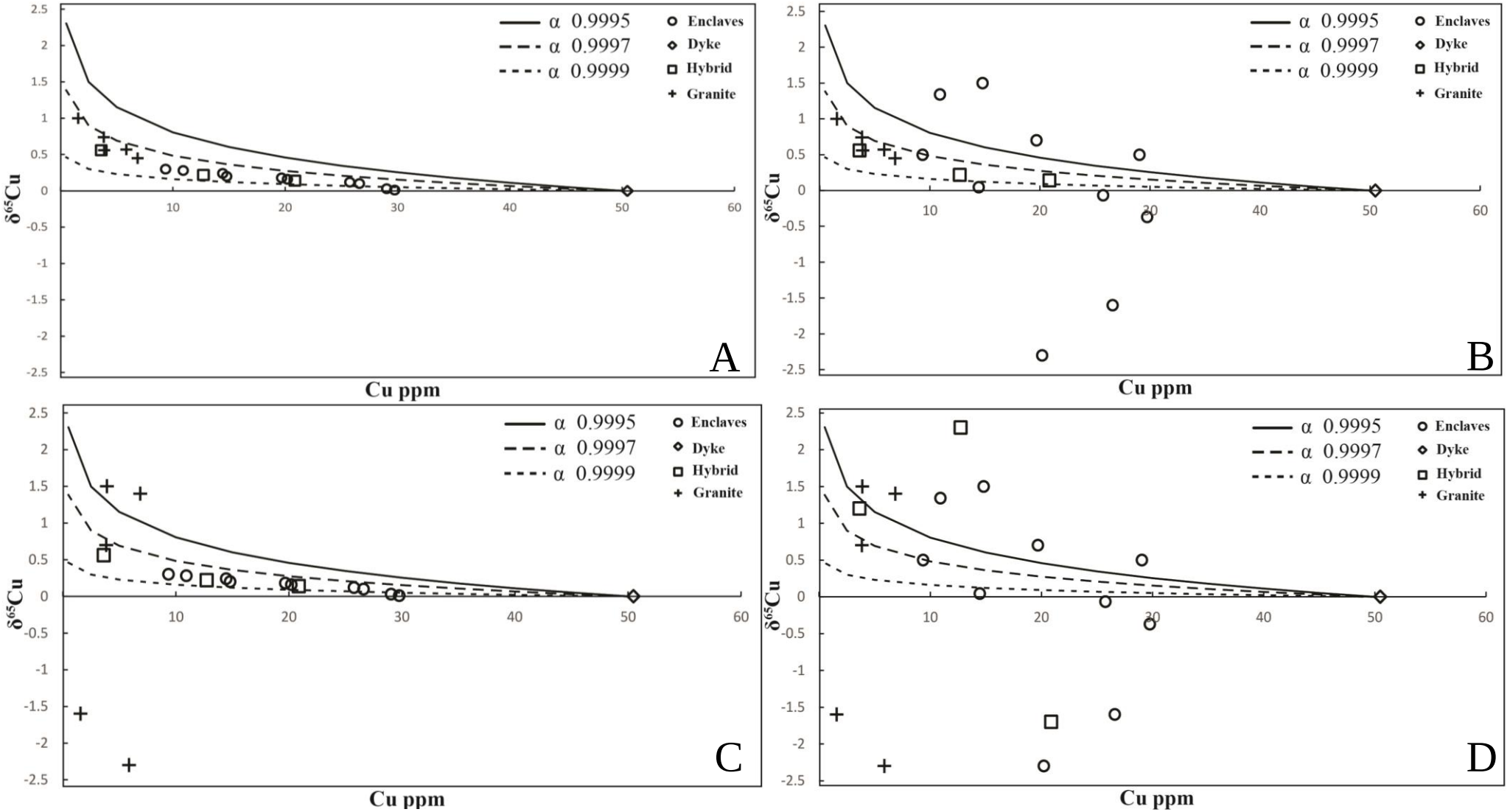

Figure 13: Cu isotope schematics with possible results of Cu isotope analysis modelled with copper concentration in each of the samples. Compositional phases are divided and Rayleigh fractionation curves show the range of isotope fractionations through Rayleigh fractionation factors α. (A) Cu isotope fractionation follows Rayleigh fractionation curve. (B) Mafic enclave samples display a large range of δ^{65}Cu. (C) Granite samples display a large range of δ^{65}Cu. (D) All samples display a large range of δ^{65}Cu.

If Cu isotope data were successfully collected, δ^{65}Cu values may have displayed differences in copper chemistry. Figure 13A shows δ^{65}Cu values controlled by Rayleigh fractionation; very little Cu fractionation has occurred (Mathur et al., 2012), reflecting the preliminary results presented in this study. Figure 13A displays narrow mantle values between -0.15 to 0.18‰ in the enclave samples and up to1‰ in the granite (Liu et al., 2015). The granitic samples, with low Cu content, display a higher δ^{65}Cu due to the relationship between decreasing Cu concentration and increasing δ^{65}Cu (Mathur et al., 2012).

Figure 13B shows a high degree of variation of δ^{65}Cu in mafic enclave samples; this would indicate that the mafic enclaves have undergone a highly fractionating process, such as metasomatism or interaction with magmatic fluids. The granite samples show low variation in δ^{65}Cu, showing that Cu has not been transferred to the granite from the mafic enclaves to any large degree; the hybridised samples show no variation in δ^{65}Cu. In this scenario there has been minimal transfer of Cu between the two phases, or the highly fractionated nature of the Cu in mafic enclaves is a later occurrence. The drastic difference in δ^{65}Cu may also suggest a different origin for the two magmas (Larson et al., 2003).

Figure 13C shows a high degree of variation of δ^{65}Cu in granite samples, showing the copper within the host granite to be highly fractionated, possibly from metasomatism, assimilation of country rock, or interaction with magmatic fluids. The mafic enclaves, however, originate from a less fractionated source, with respect to Cu, or have not been exposed to any processes which would lead to a large degree of Cu isotope fractionation (Larson et al., 2003).

In Figure 13D both the granite and mafic enclaves are highly fractionated. This indicates that the parental magma of both enclaves and granite is a highly fractionated source, or that a process or multiple processes have caused a large variation in δ^{65}Cu, such as metasomatism, assimilation of a highly fractionated Cu source, or interaction with magmatic fluids. Alternatively, either the granite or enclaves may possess the large variation of δ^{65}Cu, such as

in Figures 13B and 13C, and the Cu has been transferred between the two phases, resulting in overall change of δ^{65}Cu (Liu et al., 2014).

Clearly, due to the preliminary nature of the δ^{65}Cu fractionation results, a number of replicate analyses need to be undertaken before more definite conclusions can be reached on the mechanism of Cu fractionation in this system.

CONCLUSIONS

The Mannum granite provides insight into the transfer of material between two magmatic phases of different composition and gives insight into the behaviour of Cu isotopes in an evolving magmatic system. Whole rock and mineral major and trace element analysis and Cu isotope analysis support the following conclusions:

1. Magma mingling and to a smaller extent mixing show the transfer of plagioclase feldspar into the granite phase leading to the formation of rapakivi feldspars. They also show the transfer of xenocrysts of minerals such as hornblende, alkali feldspar, pyrite and plagioclase, between the two phases, concentrating in a third hybrid phase.
2. The origins of the titanite-alkali feldspar-pyrite associations are unresolved. The euhedral relationship between the titanite and alkali feldspar indicates that they grew together, while titanite REE signatures, small Eu anomaly and lower overall REEs compared to titanites in the granite, indicate that titanites have grown in the mafic enclaves. Both titanite and alkali feldspar display anhedral edges with the surrounding mafic enclave, possibly from reabsorption into the mafic melt. Alternatively, titanite and alkali feldspar resulted from immiscible melt inclusions, hence the euhedral internal and anhedral external edges. The association with pyrite may indicate fluid mobility or a high Fe and S content of the immiscible fluid.

3. Preliminary Cu isotope analysis showed that $\delta^{65}Cu$ positive increase is correlated to decreasing Cu concentration. $\delta^{65}Cu$ values follow a Rayleigh fractionation curve as the heavier isotope remains in the magma slightly more readily than the light isotope. The small range of ^{65}Cu values in the enclaves and hybrid samples measured shows an apparent lack of fluid mobility.

FUTURE WORK

Drill core samples or fresh samples from within the Mannum granite, in contrast with the exposed outcrop sequences used in this study, would likely provide more certainty to whole rock chemistry and possibly allow for the full extent of the mafic enclaves within the granite to be explored. Cu, Fe and Zn isotopes could be used to compare the role of hydrothermal fluids and magmatism in metal transport, as Redox sensitivity and petrogenesis can be better constrained (Fernandez and Borrok, 2009; Foden et al., 2015). Thermometry and more extensive REE analysis may show the origin of the alkali feldspar-titanite-pyrite associations. Though the alkali feldspar is clearly a xenocryst either from an immiscible melt or from the granite phase, the titanites, as evidenced by REE signatures, are native to the mafic enclaves. Thermometry will show the temperature at which large titanites formed relative to the surrounding mafic enclaves. Extensive analysis of titanites within all phases may well aid in discriminating titanite growth generations. REE analysis of titanites within the mafic enclaves which are not associated with alkali feldspar or pyrite may indicate if there are multiple generations of titanite growth and may provide information on the origin of titanites in the mafic enclaves. SEM imaging of titanites may show zoning; McLeod et al. (2010) showed that zoning in titanite is related to mixing/mingling. Further investigation into the formation

of Cu complexes, and how Cu isotopes fractionate in response, in magmatic rocks would aid in the understanding of the role of mafic magmas in Cu transport.

ACKNOWLEDGMENTS

I would like to thank my supervisors Lucy McGee and Justin Payne for their continuous support, guidance and patience throughout the year, particularly during the Cu isotope period of this project. I am grateful to MinEx CRC for the financial support and to John Foden for his knowledge on the Mannum granite and transition metal isotopes, and for his support during the year. The staff at Adelaide Microscopy, Sarah Gilbert, Aoife McFadden and Benjamin Wade, have been a huge source of assistance. Big thanks to Robert Klaebe for continuous help and inductions, along with Bradly Cave and Zara Woolston for their help in the clean laboratory. Thanks to Claire Wright at the CSIRO Waite campus for help with Cu isotope analysis. Derrick Hasterok and Katie Howard are acknowledged for all the effort and time that they have put into coordinating Honours this year. Thanks to all the other Honours students for mutual support. Thank you to my parents for help with proofreading.

REFERENCES (LEVEL 1 HEADING)

BARNES, C. G., WERTS, K., MEMETI, V., PATERSON, S. R., BREMER, R., (2021), A tale of five enclaves: Mineral perspectives on origins of mafic enclaves in the Tuolumne Intrusive Complex, *Geosphere*, 17, 352–374.

BEA, F., PEREIRA, M. D., STROH, A. S., (1994), Mineral/leucosome trace-element partitioning in a peraluminous migmatite (a laser ablation-ICP-MS study), *Chemical Geology*, 117, 291-312.

BIGELEISEN, J., MAYER, M. G., (1947), Calculation of Equilibrium Constants for Isotopic Exchange Reactions, *Journal of Chemical Physics*, 15, 261-267.

BRUGGER, J., MCPHAIL, D. C., BLACK, J., SPICCIA, L., (2001), Complexation of metal ions in brines: application of electronic spectroscopy in the study of the Cu(II)-LiCl-H2O system between 25 and 90°C, *Geochemica et Cosmochimica Acta*, 65, 2691-2708.

BRZOZOWSKI, M. J., GOOD, D. J., WU, C., LI, W., (2020), Cu isotope systematics of conduit-type Cu–PGE mineralization in the Eastern Gabbro, Coldwell Complex, Canada, *Mineralium Deposita*, 56, 707–724.

CALZIA, J. P., RÄMÖ, O. T., (2005), Miocene rapakivi granites in the southern Death Valley region, California, USA. *Earth Science Reviews*, 73, 221–243.

CHERRY, M. E., TREMBATH, L. T., (1978), The pressure quench formation of rapakivi texture, *Contributions to Mineralogy and Petrology*, 68, 1–6.

CORTÉS, A. J., (2009), On the Harker Variation; A Comment on "The Statistical Analysis of Compositional Data. Where Are We and Where Should We Be Heading?" by Aitchison and Egozcue (2005), *Mathematical Geosciences*, 41, 817-828.

COX, D., WATT, S. F. L., JENNER, F. E., HASTIE, A. R., HAMMOND, S. J., KUNZ, B., (2020), Elevated magma fluxes deliver high-Cu magmas to the upper crust, Geology, 48, 957-960.

DEPAOLO, D. J., (1981), Trace element and isotopic effects of combined wallrock assimilation and fractional crystallization, *Earth and Planetary Science Letters*, 53, 189-202.

FROST, B. R., BARNES, C. G., COLLINS, W. J., ARCULUS, R. J., ELLIES, D. J., FROST, C. D., (2001), A Geochemical Classification for Granitic Rocks, *Journal of Petrology*, 42, 2033-2048.

FERNANDEZ, A., BORROK, D. M., (2009), Fractionation of Cu, Fe, and Zn isotopes during the oxidative weathering of sulfide-rich rocks, *Chemical Geology*, 264, 1-12.

FODEN, J., ELBURG, M. A., DOUGHERTY-PAGE, J., BURTT, A., (2006), The timing and duration of the Delamerian Orogeny: Correlation with the Ross Orogen and implications for Gondwana Assembly, *The Journal of Geology*, 114, 189-210.

FODEN, J., ELBURG, M., TURNER, S., CLARK, C., BLADES, M. L., COX, G., COLLINS, A. S., WOLFF, K., GEORGE, C., (2020), Cambro-Ordovician magmatism in the Delamerian orogeny: Implications for tectonic development of the southern Gondwanan margin, *Gondwana Research*, 81, 490-521.

FODEN, J. D., ELBURG, M. A., TURNER, S. P., SANDIFORD, M., O'CALLAGHAN, J., MITCHELL, S., (2002), Granite production in the Delamerian Orogen, South Australia, *Journal of the Geological Society*, 159, 557-575.

FODEN, J., SOSSI, P. A., WAWRYK, C. M., (2015), Fe isotopes and the contrasting petrogenesis of A-, I- and S-type granite, *Lithos*, 212, 32-44.

FODEN, J., SONG, S. H., TURNER, S., ELBURG, M., SMITH, P. B., DER STELDT, B. V., PENGLIS, D. V., (2002), Geochemical evolution of lithospheric mantle beneath S.E. South Australia, *Chemical Geology*, 182, 663-695.

GIBSON, G. M., CHAMPION, D. C., IRELAND, T. R., (2015), Preservation of a fragmented late Neoproterozoic–earliest Cambrian hyper-extended continental-margin sequence in the Australian Delamerian Orogen, *Geological Society, London, Special Publications*, 413, 269-299.

HALCROW, M. A., (2013), Jahn–Teller distortions in transition metal compounds, and their importance in functional molecular and inorganic materials, *Royal Society of Chemistry*, 42, 1784-1795.

HARKER, A., (1909), *The Natural History of Igneous Rocks*, Cambridge University Press.

HARROWFIELD. J. M, OGDEN, M. I., RICHMOND, W. R., WHITE, A. H., (1999), Lanthanide ions as calcium substitutes: a structural comparison of europium and calcium complexes of a ditopic calixarene, *J. Chem. Soc., Dalton Trans*., 1991, 2153-2160.

HIBBARD, M. J., (1981), The magma mixing origin of mantled feldspars. *Contributions to Mineralogy and Petrology* 76, 158–170.

HOGAN, J. P., GILBERT, M. C., PRICE, J. D., (2000), Crystallisation of fine- and coarse-grained A-type granite sheets of the Southern Oklahoma Aulacogen, U.S.A. *Transactions of the Royal Society of Edinburgh Earth Sciences*, 91, 139–150.

HUANG, J., LIU, S., GAO, Y., XIAO, Y., CHEN, SHA., (2016), Copper and zinc isotope systematics of altered oceanic crust at IODP Site 1256 in the eastern equatorial Pacific, *Journal of Geophysical Research: Solid Earth*, 121, 7086-7100.

KAMENETSKY. V. S., KAMENETSKY. M. B., (2010), Magmatic fluids immiscible with silicate melts: example from inclusions in phenocrysts and glasses, and implications for magma evolution and melt transport, *Geofluids*, 10, 293-311.

KENDALL, C,, CALDWELL, E. A,, (1998), Fundamentals of Isotope Geochemistry, In KENDALL, C, and MCDONNELL J. J. (eds), *Isotope Tracers in Catchment Hydrology*, Elsevier Science.

KIDDER, J. A., VOINOT, A., SULIVAN, K. V., CHIPLEY, D., VALENTINO, M., LAYTON-MATTHEWS, D, L. EYBOURNE, M., (2020), Improved ion-exchange column chromatography for Cu purification from high-Na matrices and isotopic analysis by MC-ICPMS, *Journal of Analytical Atomic Spectrometry*, 35, 776-783.

LARSON, P. B., MAHER, K., RAMOS, F. C., CHANG, Z., GASPAR, M., MEINERT, L. D., (2003), Copper isotope ratios in magmatic and hydrothermal ore-forming environments, *Chemical Geology*, 201, 337-350.

LIU, W., BRUGGER, J., MCPHAIL, D. C., SPICCIA, L., (2002), A spectrophotometric study of aqueous copper(I)–chloride complexes in LiCl solutions between 100 °C and 250 °C, *Geochimica et Cosmochimica Acta*, 66, 3615-2633.

LIU, S., HUANG, J., LIU, J., WÖRNER, G., YANG, W., TANG, Y., CHEN, Y., TANG, L., ZHENG, J., LI, S., (2015), Copper isotopic composition of the silicate Earth, *Earth and Planetary Science Letters*, 427, 95-103.

LIU, S., LI, D., LI, S., TENG, F., KE, S., HE, Y., LU, Y., (2014), High-precision copper and iron isotope analysis of igneous rock standards by MC-ICP-MS, *Journal of Analytical Atomic Spectrometry*, 29, 122-133.

LIU, S., LI, Y., LIU, J., YANG, Z., LIU, J., SHI, Y., (2021), Equilibrium Cu isotope fractionation in copper minerals: a first-principles study, *Chemical Geology*, 564, 120060.

LOWCZAK, C. R., (2019), *Copper isotope method development for determining the source of mineralised provinces*, Honours thesis, The University of Adelaide.

LV, N., BAO, Z., CHEN, L., CHEN, K., ZHANG, Y., YUAN, H., (2020), Accurate determination of Cu isotope compositions in Cu-bearing minerals using microdrilling and MC-ICP-MS, *International Journal of Mass Spectrometry*, 457, 116414.

MARÉCHAL, C., ALBARÈDE, F., (2002), Ion-exchange fractionation of copper and zinc isotopes, *Geochimica et Cosmochimica Acta*, 66, 1499-1509.
MARÉCHAL, C. N., TÉLOUK, P., ALBARÈDE, F., (1999), Precise analysis of copper and zinc isotopic compositions by plasma-source mass spectrometry, *chemical geology*, 156, 251-273.
MATHUR, R., JIN, L., PRUSH, V., PAUL, J., EBERSOLE, C., FORNADEL, A., WILLIAMS, J. Z., BRANTLEY, S., (2012), Cu isotopes and concentrations during weathering of black shale of the Marcellus Formation, Huntingdon County, Pennsylvania (USA), *Chemical Geology*, 305, 175-184.
MCDONOUGH, W. F., SUN, S., (1995), The composition of the Earth, *Chemical Geology*, 120, 223-253.
MILLER, J. MCL., PHILLIPS, D., WILSON, C. J. L., DUGDALE, L. J. (2005), Evolution of a reworked orogenic zone: The boundary between the delamerian and lachlan fold belts, southeastern Australia, *Australian Journal of Earth Sciences*, 52, 6, 921-940.
MOYNIER, F, VANCE, D, FUJI, T, Savage, P., (2017), The Isotope Geochemistry of Zinc and Copper, *Reviews in mineralogy and Geochemistry*, 82, 543-600.
NEKVASIL, H., (1991), Ascent of felsic magmas and formation of rapakivi. *American Mineralogist* 76, 1279–1290.
PANKHURST, M. J., VERNON, R. H., TURNER, S. P., SCHAEFER, B. F., FODEN, J. D., (2011), Contrasting Sr and Nd isotopic behaviour during magma mingling; new insights from the Mannum A-type granite, *Lithos*, 126, 135-146.
PLAIL, M., BARCLAY, J., HUMPHREYS, M. C. S., EDMONDS, M., HERD, R. A., CHRISTOPHER, T. E., (2014), Chapter 18 Characterization of mafic enclaves in the erupted products of Soufrière Hills Volcano, Montserrat, 2009 to 2010, *Geological Society, London, Memoirs*, 39, 343-360.
POLYAKOV, V. B., SOULTANOV, D. M,, (2011) New data on equilibrium iron isotope fractionation among sulfides: Constraints on mechanisms of sulfide formation in hydrothermal and igneous systems, *Geochimica et Cosmochimica Acta*, 75, 1957-1974
RAYMOND, L. A., (1943), Petrology: the study of igneous, sedimentary, metamorphic rocks. Dubuque, Iowa : Wm. C. Brown
SHIELDS, W. R., MURPHY, T. J., GARNER, E. L., (1964), Absolute isotopic abundance ratio and the atomic weight of a reference sample of copper, *Journal of Research of the National Bureau of Standards Section A: Physics and Chemistry*, 68A, 6, 589.
STEWART, D.B., 1959. Rapakivi granite from eastern Penobscot Bay, Maine. *20th International Geological Congress, Mexico*, pp. 293–320.
SUN, W, WANG, J, ZHANG, L, ZANG, C, LI H, LING, M, DING, X, LI, C, LIANG, H, (2017), The formation of porphyry copper deposits, *Acta Geochim*, 36, , 9-15.
TURNER, S. P., (1996), Petrogenesis of the late-Delamerian gabbroic complex at Black Hill, South Australia: implications for convective thinning of the lithospheric mantle. *Mineralogy and Petrology* , 56, 51-98.
TURNER, S. P., and FODEN, J., (1996), Magma mingling in late-Delamerian A-type granites at Mannum, South Australia, *Mineralogy and Petrology*, 56, 147-169.
TURNER, S. P., FODEN, J. D., MORRISON, R. S., (1992), Derivation of some A-type magmas by fractionation of basaltic magma: An example from the Padthaway Ridge, South Australia, *Lithos*, 28, 151-179.
UREY, H. C., (1947), The thermodynamic properties of isotopic substances, *Journal of the Chemical Society*, 562.
VERNON, R. H. (2016), Rapakivi granite problems: plagioclase mantles and ovoid megacrysts, *Australian Journal of Earth Sciences*, 63, 675-700.
WARK, D.A., STIMAC, J.A., (1991). Origin of mantled (rapakivi) feldspars; experimental evidence of control by a dissolution- and diffusion-controlled mechanism. Eos, Transactions, American Geophysical Union 72, 304.
WEILL, D.F, DRAKE, M. J, (1973), Europium Anomaly in Plagioclase Feldspar: Experimental results and Semiquantitative model, *Science*, 180, 4090, 1059-1060.
WU, F., LIU, X., JI, W., WANG, J., YANG, L. (2017), Highly fractionated granites: Recognition and research, *Science China Earth Sciences*, 60, 7, 1201-1219.
YAXLEY, G. M. (2000), Experimental study of the phase and melting relations of homogeneous basalt mathplus peridotite mixtures and implications for the petrogenesis of flood basalts, *Contributions to Mineralogy and Petrology*, 139, 3, 326-338.
ZHENG, Y., LIU, S., WU, C., GRIFFIN, W, L., LI, Z., XU, B., YANG, Z., HOU, Z., O'REILLY, S, Y., (2018),Cu isotopes reveal initial Cu enrichment in sources of giant porphyry deposits in a collisional setting, geology, 47, 135-138

APPENDIX A

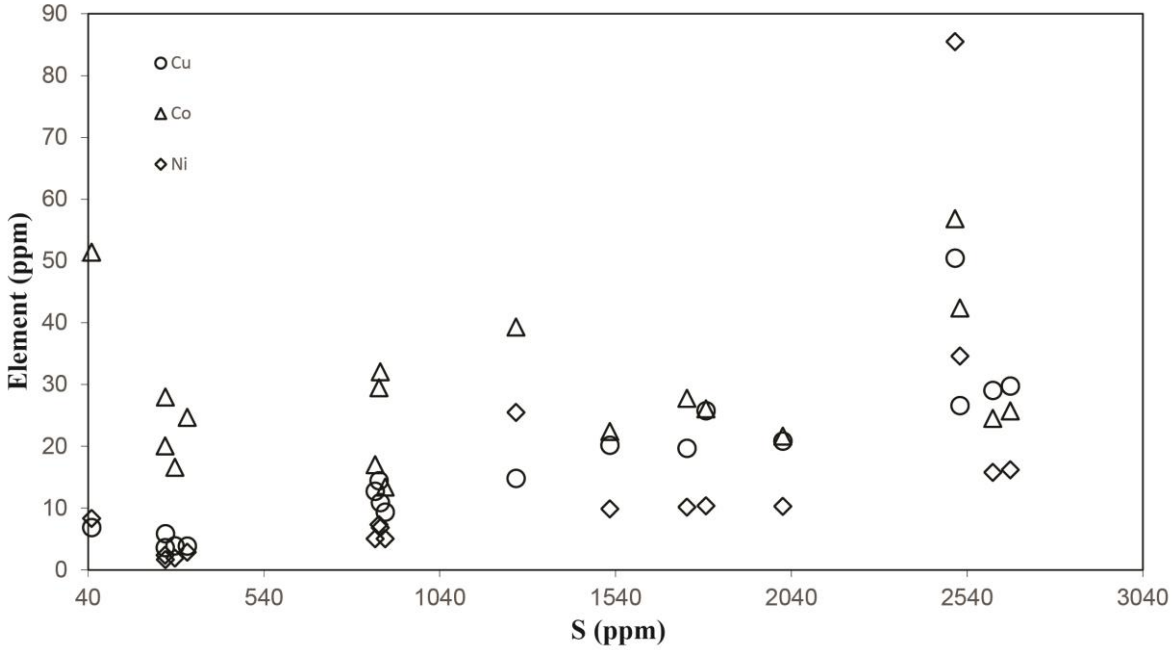

Figure a. Plot of trace transition metal concentrations vs the concentration of S. Note that in general Cu and Co correlation with sulphur value while the correlation is poorer for Ni. Co (triangles), Ni (diamonds), and Cu (curricles).

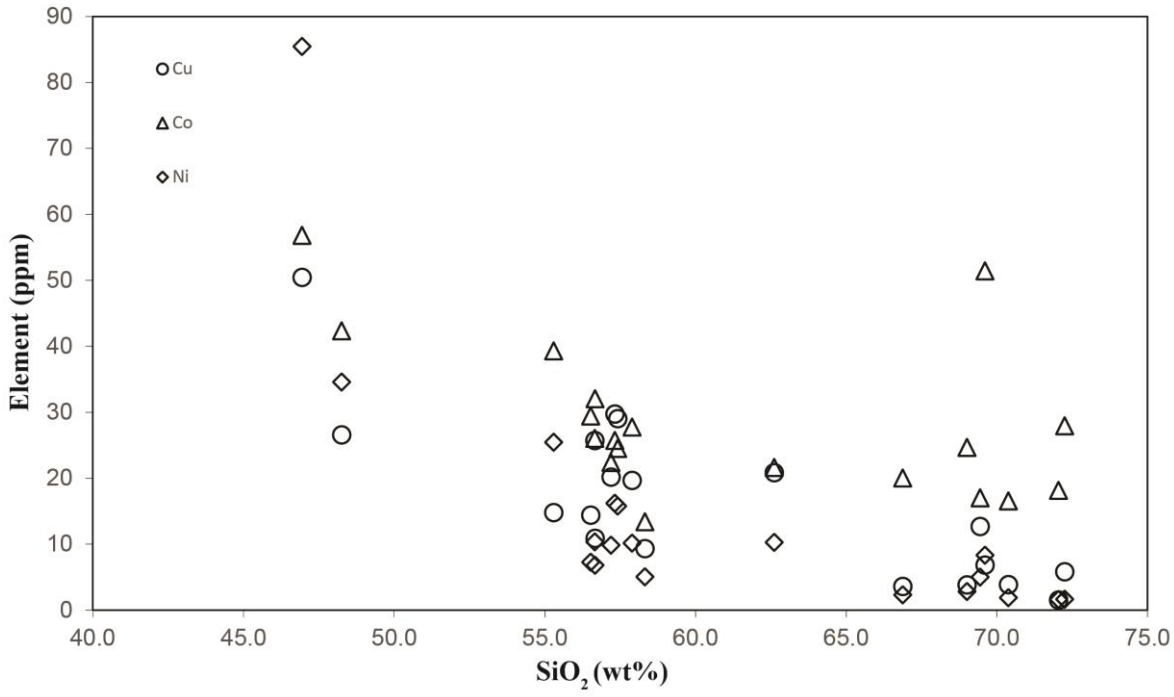

Figure b Plot of trace transition metal concentrations vs the concentration of SiO_2. Note that there is a general inverse correlation for Co (triangles), Ni (diamonds), and Cu (curricles).

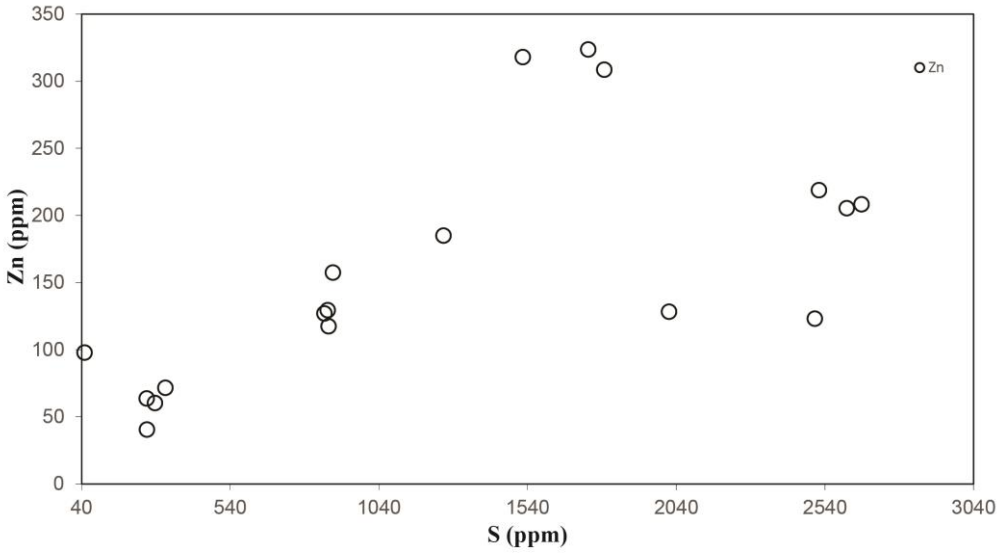

Figure c whole rock Zn concentrations modelled against whole rock S concentration

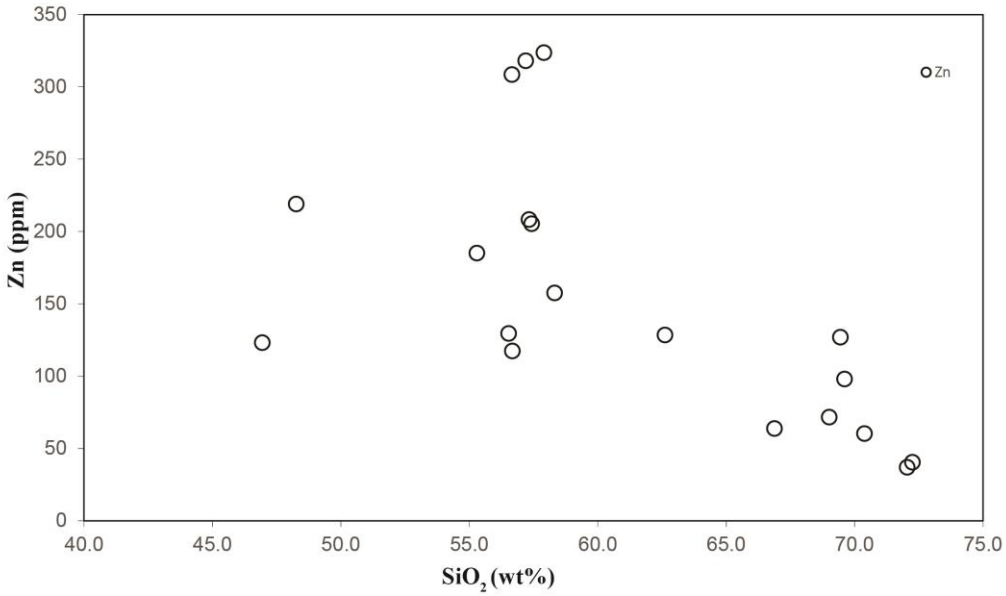

Figure d whole rock Zn concentrations modelled against whole rock SiO_2 concentration.

APPENDIX B

Whole rock chemistry

Sample Name	32 -> 64 S	34 -> 66 S	45 -> 61 Sc	47 -> 79 Ti	49 -> 81 Ti	51 -> 67 V
22:USG-BHVO-2*	150	149	9	14827	14798	304
21:USGS-GSR2	498	515	5	4654	4659	52
MG7 32	2506	2593	10	7797	7951	259
OPMG_006B 24	856	879	3	5641	5778	70
OPMG_016B 104*	259	264	5	3316	3281	32
OPMG_002A 33*	2016	2011	9	6343	6345	81
OPMG_016D 38	885	878	3	5245	5192	80
OPMG_016E 34	1743	1795	16	11912	11658	153
OPMG_016F 13*	1798	1831	15	11798	11797	158
OPMG_017A 26	2520	2565	12	13007	12516	305
OPMG_016C 20	1524	1548	11	10652	10428	146
OPMG_002B 31	2613	2609	12	12142	12066	160
OPMG_002C 45	2663	2700	17	8422	8219	130
OPMG_009B 40	1257	1278	14	10105	10029	189
OPMGB_001A 37	867	882	16	11878	11601	185
OPMGB_001B 35	871	868	11	11245	11155	177
OPMG_012A 36	49	48	6	5808	5728	79
OPMG_013A 7	287	302	4	3441	3402	28
OPMG_016A 27	260	250	3	2186	2179	16
OPMG_006A39	322	310	6	3988	3864	39
OPMG_012G 30	11	<18.7383780234833	3	2732	2694	23

Sample Name	52 -> 52 Cr	53 -> 69 Cr	55 -> 71 Mn	59 -> 59 Co	59 -> 75 Co	60 -> 60 Ni
22:USG-BHVO-2*	284	293	1281	48	44	114
21:USGS-GSR2	24	23	333	8	8	17
MG7 32	137	131	1977	61	57	83
OPMG_006B 24	8	7	1037	18	17	5
OPMG_016B 104*	2	2	710	22	20	2
OPMG_002A 33*	11	11	1537	23	22	10
OPMG_016D 38	9	8	980	15	13	5
OPMG_016E 34	20	18	2095	30	28	10
OPMG_016F 13*	21	19	2127	29	26	10
OPMG_017A 26	31	28	2462	47	42	34
OPMG_016C 20	20	17	1981	25	22	10
OPMG_002B 31	16	15	2906	27	25	16
OPMG_002C 45	17	15	3734	29	26	16
OPMG_009B 40	16	16	2277	43	39	25
OPMGB_001A 37	19	18	1260	32	29	7
OPMGB_001B 35	18	16	1170	35	32	7
OPMG_012A 36	5	5	852	56	51	8
OPMG_013A 7	2	2	640	18	17	2
OPMG_016A 27	1		511	30	28	2
OPMG_006A39	3	3	812	27	25	3
OPMG_012G 30	1	1	293	19	18	1

Sample Name	60 -> 76 Ni	63 -> 63 Cu	65 -> 65 Cu	66 -> 66 Zn	66 -> 82 Zn	69 -> 69 Ga
22:USG-BHVO-2*	117	123	120	97	153	34
21:USGS-GSR2	17	47	46	117	133	195
MG7 32	85	50	50	123	157	36
OPMG_006B 24	5	13	12	127	151	51
OPMG_016B 104*	2	4	4	64	80	94
OPMG_002A 33*	10	21	21	128	165	78
OPMG_016D 38	5	9	9	158	185	17
OPMG_016E 34	10	20	19	324	382	41
OPMG_016F 13*	10	26	25	309	354	40
OPMG_017A 26	35	27	27	219	282	41
OPMG_016C 20	10	20	20	318	363	36
OPMG_002B 31	16	29	28	206	256	58
OPMG_002C 45	16	30	29	208	250	72
OPMG_009B 40	25	15	15	185	232	61
OPMGB_001A 37	7	14	14	130	174	111
OPMGB_001B 35	7	11	11	118	162	102
OPMG_012A 36	8	7	7	98	121	74
OPMG_013A 7	2	4	4	60	73	115
OPMG_016A 27	2	6	6	41	49	102
OPMG_006A39	3	4	4	72	90	89
OPMG_012G 30	2	2	2	37	48	101

Sample Name	71 -> 71 Ga	85 -> 85 Rb	88 -> 104 Sr	89 -> 105 Y	90 -> 122 Zr	93 -> 125 Nb
22:USG-BHVO-2*	22	8	396	20	163	10
21:USGS-GSR2	34	195	223	24	442	26
MG7 32	22	21	432	30	176	4
OPMG_006B 24	24	25	63	39	307	70
OPMG_016B 104*	25	197	157	61	178	56
OPMG_002A 33*	28	87	152	82	340	30
OPMG_016D 38	15	23	67	44	221	34
OPMG_016E 34	34	118	159	107	447	85
OPMG_016F 13*	35	96	157	109	447	90
OPMG_017A 26	26	117	294	46	264	15
OPMG_016C 20	34	54	125	102	413	79
OPMG_002B 31	31	79	141	77	285	48
OPMG_002C 45	32	134	174	83	283	25
OPMG_009B 40	25	64	221	44	278	24
OPMGB_001A 37	28	64	556	51	369	41
OPMGB_001B 35	26	49	520	52	350	36
OPMG_012A 36	28	138	169	76	334	77
OPMG_013A 7	27	154	186	58	235	54
OPMG_016A 27	24	192	150	37	200	42
OPMG_006A39	27	147	149	70	259	70
OPMG_012G 30	25	133	161	29	230	51

Sample Name	118 -> 118 [In]	118 -> 118 [In]	133 -> 133 Cs	137 -> 153 Ba	139 -> 155 La	140 -> 156 Ce
22:USG-BHVO-2*	2	2	0	132	13	32
21:USGS-GSR2	7	7	1	1405	158	386
MG7 32	1	1	1	146	22	45
OPMG_006B 24	6	6	1	265	32	104
OPMG_016B 104*	4	4	3	625	70	159
OPMG_002A 33*	5	5	2	524	82	204
OPMG_016D 38	4	4	0	55	79	156
OPMG_016E 34	10	9	2	141	197	365
OPMG_016F 13*	5	5	2	126	208	387
OPMG_017A 26	4	4	3	172	62	107
OPMG_016C 20	9	9	1	96	144	314
OPMG_002B 31	7	7	2	274	84	198
OPMG_002C 45	6	6	2	385	98	211
OPMG_009B 40	5	5	1	346	66	122
OPMGB_001A 37	3	3	2	717	84	167
OPMGB_001B 35	3	3	1	680	85	166
OPMG_012A 36	6	6	4	438	85	197
OPMG_013A 7	4	4	3	748	53	131
OPMG_016A 27	3	3	3	673	54	107
OPMG_006A39	5	5	3	565	69	168
OPMG_012G 30	4	4	2	660	46	98

Sample Name	141 -> 157 Pr	146 -> 162 Nd]	147 -> 163 Sm [	153 -> 169 Eu	157 -> 173 Gd	159 -> 175 Tb
22:USG-BHVO-2*	5	22	6	2	6	1
21:USGS-GSR2	50	186	25	2	12	1
MG7 32	6	26	6	2	6	1
OPMG_006B 24	10	36	7	2	7	1
OPMG_016B 104*	18	62	11	2	10	2
OPMG_002A 33*	23	85	16	3	14	2
OPMG_016D 38	15	49	8	2	7	1
OPMG_016E 34	35	116	19	4	16	3
OPMG_016F 13*	37	121	20	4	17	3
OPMG_017A 26	12	46	9	2	9	1
OPMG_016C 20	29	97	17	4	15	2
OPMG_002B 31	22	78	15	3	13	2
OPMG_002C 45	24	89	16	4	14	2
OPMG_009B 40	13	45	9	2	8	1
OPMGB_001A 37	19	69	12	3	11	2
OPMGB_001B 35	19	69	12	3	11	2
OPMG_012A 36	22	76	14	2	12	2
OPMG_013A 7	16	57	12	2	10	2
OPMG_016A 27	12	41	7	1	6	1
OPMG_006A39	19	68	12	2	11	2
OPMG_012G 30	11	39	7	1	6	1

Sample Name	163 -> 179 Dy	165 -> 181 Ho	166 -> 182 Er	169 -> 185 Tm	172 -> 188 Yb]	175 -> 191 Lu
22:USG-BHVO-2*	5	1	2	0	2	0
21:USGS-GSR2	6	1	2	0	2	0
MG7 32	6	1	4	1	3	0
OPMG_006B 24	8	2	6	1	6	1
OPMG_016B 104*	11	2	7	1	7	1
OPMG_002A 33*	15	3	10	1	9	1
OPMG_016D 38	7	2	5	1	6	1
OPMG_016E 34	17	4	12	2	13	2
OPMG_016F 13*	18	4	13	2	13	2
OPMG_017A 26	9	2	6	1	5	1
OPMG_016C 20	17	4	12	2	13	2
OPMG_002B 31	14	3	9	1	9	1
OPMG_002C 45	15	3	9	1	9	1
OPMG_009B 40	8	2	5	1	5	1
OPMGB_001A 37	10	2	6	1	5	1
OPMGB_001B 35	10	2	6	1	5	1
OPMG_012A 36	13	3	9	1	9	1
OPMG_013A 7	11	2	7	1	7	1
OPMG_016A 27	7	1	4	1	4	1
OPMG_006A39	12	3	8	1	8	1
OPMG_012G 30	6	1	4	1	4	1

Sample Name	178 -> 178 Hf	178 -> 194 Hf	181 -> 181 Ta	181 -> 197 Ta	206 -> 206 [Pb]	207 -> 207 [Pb]
22:USG-BHVO-2*	4	4	1	1	2	2
21:USGS-GSR2	12	12	1	1	34	34
MG7 32	4	4	0	0	3	3
OPMG_006B 24	8	8	3	3	28	25
OPMG_016B 104*	5	5	3	4	12	10
OPMG_002A 33*	8	8	2	2	20	18
OPMG_016D 38	5	5	1	1	50	44
OPMG_016E 34	10	11	3	3	101	92
OPMG_016F 13*	11	10	3	3	109	98
OPMG_017A 26	6	7	1	1	81	74
OPMG_016C 20	10	10	3	3	107	95
OPMG_002B 31	7	7	3	3	42	39
OPMG_002C 45	7	7	1	1	36	33
OPMG_009B 40	7	7	1	1	41	37
OPMGB_001A 37	8	9	2	2	8	7
OPMGB_001B 35	8	8	2	2	8	7
OPMG_012A 36	9	9	5	5	15	13
OPMG_013A 7	6	6	4	4	14	12
OPMG_016A 27	5	6	3	3	12	11
OPMG_006A39	7	7	5	5	11	10
OPMG_012G 30	7	7	3	3	10	9

Sample Name	208 -> 208 Pb	232 -> 232 Th	238 -> 238 U
22:USG-BHVO-2*	2	1	0
21:USGS-GSR2	41	98	2
MG7 32	3	1	2
OPMG_006B 24	27	8	32
OPMG_016B 104*	11	13	8
OPMG_002A 33*	19	14	16
OPMG_016D 38	47	9	73
OPMG_016E 34	94	22	161
OPMG_016F 13*	101	22	156
OPMG_017A 26	78	5	21
OPMG_016C 20	98	18	161
OPMG_002B 31	41	13	7
OPMG_002C 45	35	15	6
OPMG_009B 40	40	16	10
OPMGB_001A 37	8	8	3
OPMGB_001B 35	8	9	3
OPMG_012A 36	14	17	10
OPMG_013A 7	13	22	4
OPMG_016A 27	12	25	5
OPMG_006A39	11	14	9
OPMG_012G 30	9	21	2

Appendix D EMPA data
EMPA data from sample BOUNDARYts002

SAMPLE	CaO	K2O	BaO	F	TiO2	P2O5	Na2O	SiO2	MgO	Al2O3	FeO	MnO	Cr2O3	NiO	ZnO	SO3	O	TOTAL
OPMG_002_Bio	0	10	0	3	1	0	0	40	18	12	13	1	0	0	0	0	0	98
OPMG_002_Bio	0	10	0	3	1	0	0	41	18	12	14	1	0	0	0	0	0	99
OPMG_002_Bio	0	10	0	3	1	0	0	40	18	12	14	1	0	0	0	0	0	98
OPMG_002_Bio	0	10	0	3	1	0	0	40	18	12	14	1	0	0	0	0	0	98
OPMG_002_Bio	0	10	0	3	1	0	0	41	18	12	14	1	0	0	0	0	0	99
OPMG_002_Bio	0	10	0	3	1	0	0	40	17	12	14	1	0	0	0	0	0	99
OPMG_002_Bio	0	10	0	3	1	0	0	41	18	12	13	1	0	0	0	0	0	98
OPMG_002_Bio	0	10	0	3	1	0	0	41	18	12	13	1	0	0	0	0	0	99
OPMG_002_Bio	0	10	0	3	1	0	0	40	18	12	13	1	0	0	0	0	0	98
OPMG_002_Bio	0	10	0	3	1	0	0	41	18	12	13	1	0	0	0	0	0	98
OPMG_002_Bio	0	10	0	4	1	0	0	41	18	12	13	1	0	0	0	0	0	99
OPMG_002_Bio	0	10	0	4	1	0	0	42	18	12	13	1	0	0	0	0	0	99
OPMG_002_Bio	0	10	0	3	1	0	0	41	18	12	14	1	0	0	0	0	0	99
OPMG_002_Bio	0	10	0	3	1	0	0	41	18	12	14	1	0	0	0	0	0	99
OPMG_002_Bio	0	10	0	3	1	0	0	40	17	13	14	1	0	0	0	0	0	99
OPMG_002_Bio	0	10	0	3	1	0	0	41	18	12	13	1	0	0	0	0	0	99
OPMG_002_Bio	0	10	0	3	1	0	0	40	18	13	13	1	0	0	0	0	0	98
OPMG_002_Bio	0	6	0	2	0	0	0	25	11	7	7	0	0	0	0	0	0	60
OPMG_002_Bio	0	10	0	4	1	0	0	41	19	11	13	1	0	0	0	0	0	100
OPMG_002_Bio	0	10	0	3	1	0	0	40	18	12	13	1	0	0	0	0	0	99
SAMPLE	CaO	K2O	BaO	F	TiO2	P2O5	Na2O	SiO2	MgO	Al2O3	FeO	MnO	Cr2O3	NiO	ZnO	SO3	O	TOTAL
OPMG_002_Titanite	26	0	1	1	34	0	0	29	0	1	3	0	0	0	0	0	0	95

OPMG_002_Titanite	28	0	0	2	32	0	0	31	0	4	2	0	0	0	0	0	0	99
OPMG_002_Titanite	25	0	1	1	35	0	0	28	0	2	3	0	0	0	0	0	0	95
OPMG_002_Titanite	20	0	1	1	43	0	0	24	0	1	3	0	0	0	0	0	0	94
SAMPLE	CaO	K2O	BaO	F	TiO2	P2O5	Na2O	SiO2	MgO	Al2O3	FeO	MnO	Cr2O3	NiO	ZnO	SO3	O	TOTAL
OPMG_002_KSP	0	15	0	0	0	0	1	65	0	18	0	0	0	0	0	0	0	100
OPMG_002_KSP	1	8	0	0	0	0	5	68	0	18	0	0	0	0	0	0	0	101
OPMG_002_KSP	0	11	0	0	0	0	4	66	0	19	0	0	0	0	0	0	0	101
OPMG_002_KSP	0	14	0	0	0	0	2	65	0	19	0	0	0	0	0	0	0	101
OPMG_002_KSP	2	0	0	0	0	0	10	64	0	21	0	0	0	0	0	0	0	98
OPMG_002_KSP	0	15	0	0	0	0	1	65	0	18	0	0	0	0	0	0	0	100
OPMG_002_KSP	0	12	0	0	0	0	3	66	0	19	0	0	0	0	0	0	0	100
OPMG_002_KSP	0	16	0	0	0	0	0	65	0	19	0	0	0	0	0	0	0	101
OPMG_002_KSP	0	16	0	0	0	0	1	64	0	19	0	0	0	0	0	0	0	100
OPMG_002_KSP	0	16	0	0	0	0	1	65	0	19	0	0	0	0	0	0	0	100
OPMG_002_KSP	0	15	0	0	0	0	1	65	0	19	0	0	0	0	0	0	0	100
OPMG_002_KSP	0	16	0	0	0	0	1	65	0	18	0	0	0	0	0	0	0	101
OPMG_002_KSP	0	14	0	0	0	0	2	65	0	19	0	0	0	0	0	0	0	100
OPMG_002_KSP	0	15	0	0	0	0	1	65	0	19	0	0	0	0	0	0	0	100
OPMG_002_KSP	0	15	0	0	0	0	1	65	0	19	0	0	0	0	0	0	0	101
OPMG_002_KSP	0	16	0	0	0	0	1	65	0	19	0	0	0	0	0	0	0	101
OPMG_002_KSP	0	12	0	0	0	0	3	65	0	19	0	0	0	0	0	0	0	100
OPMG_002_KSP	0	15	0	0	0	0	1	65	0	19	0	0	0	0	0	0	0	100
OPMG_002_KSP	0	15	0	0	0	0	1	65	0	19	0	0	0	0	0	0	0	101
OPMG_002_KSP	0	16	0	0	0	0	1	65	0	19	0	0	0	0	0	0	0	101
OPMG_002_KSP	0	15	0	0	0	0	1	65	0	19	0	0	0	0	0	0	0	100
OPMG_002_KSP	0	16	0	0	0	0	0	65	0	19	0	0	0	0	0	0	0	101
OPMG_002_KSP	0	15	0	0	0	0	1	65	0	19	0	0	0	0	0	0	0	100
OPMG_002_KSP	0	15	0	0	0	0	1	65	0	19	0	0	0	0	0	0	0	100
SAMPLE	CaO	K2O	BaO	F	TiO2	P2O5	Na2O	SiO2	MgO	Al2O3	FeO	MnO	Cr2O3	NiO	ZnO	SO3	O	TOTAL

OPMG_002_KSP	0	16	0	0	0	0	0	64	0	19	0	0	0	0	0	0	0	100
OPMG_002_KSP	0	16	0	0	0	0	1	65	0	19	0	0	0	0	0	0	0	100
OPMG_002_KSP	0	16	0	0	0	0	1	65	0	19	0	0	0	0	0	0	0	100
OPMG_002_KSP	0	16	0	0	0	0	0	65	0	19	0	0	0	0	0	0	0	100
OPMG_002_KSP	1	5	0	0	0	0	8	66	0	20	0	0	0	0	0	0	0	100
OPMG_002_KSP	0	14	0	0	0	0	2	65	0	19	0	0	0	0	0	0	0	100
OPMG_002_KSP	0	15	0	0	0	0	1	65	0	19	0	0	0	0	0	0	0	100
OPMG_002_KSP	1	1	0	0	0	0	10	65	0	22	1	0	0	0	0	0	0	100
OPMG_002_KSP	2	0	0	0	0	0	11	67	0	21	0	0	0	0	0	0	0	101
OPMG_002_KSP	1	0	0	0	0	0	11	66	0	21	0	0	0	0	0	0	0	100
OPMG_002_KSP	0	16	0	0	0	0	0	65	0	19	0	0	0	0	0	0	0	100
OPMG_002_KSP	2	4	0	0	0	0	8	66	0	21	0	0	0	0	0	0	0	101
OPMG_002_KSP	0	16	0	0	0	0	1	65	0	19	0	0	0	0	0	0	0	100
OPMG_002_KSP	0	16	0	0	0	0	0	65	0	19	0	0	0	0	0	0	0	101
SAMPLE	CaO	K2O	BaO	F	TiO2	P2O5	Na2O	SiO2	MgO	Al2O3	FeO	MnO	Cr2O3	NiO	ZnO	SO3	O	TOTAL
OPMG_002_HORN?	6	0	0	0	0	0	7	58	0	25	1	0	0	0	0	0	0	98
OPMG_002_HORN?	7	0	0	0	0	0	8	59	0	26	0	0	0	0	0	0	0	101
OPMG_002_HORN?	7	0	0	0	0	0	7	58	0	26	1	0	0	0	0	0	0	99
OPMG_002_HORN?	8	0	0	0	0	0	7	59	0	26	0	0	0	0	0	0	0	101
OPMG_002_HORN?	1	0	0	0	0	0	2	54	1	24	4	0	0	0	0	0	0	87
OPMG_002_HORN?	8	0	0	0	0	0	7	59	0	27	0	0	0	0	0	0	0	101
OPMG_002_HORN?	1	0	0	0	0	0	2	50	2	14	14	0	0	0	0	0	0	83
OPMG_002_HORN?	3	0	0	0	0	0	10	65	0	22	0	0	0	0	0	0	0	101
OPMG_002_HORN?	3	0	0	0	0	0	9	62	0	22	2	0	0	0	0	0	0	98
OPMG_002_HORN?	5	0	0	0	0	0	9	63	0	24	0	0	0	0	0	0	0	101
SAMPLE	CaO	K2O	BaO	F	TiO2	P2O5	Na2O	SiO2	MgO	Al2O3	FeO	MnO	Cr2O3	NiO	ZnO	SO3	O	TOTAL
OPMG_002_Bio	0	10	0	3	1	0	0	39	17	13	15	1	0	0	0	0	0	98
OPMG_002_Bio	0	10	0	3	1	0	0	39	17	12	15	1	0	0	0	0	0	98
OPMG_002_Bio	0	10	0	3	1	0	0	38	16	12	15	1	0	0	0	0	0	96

SAMPLE	CaO	K2O	BaO	F	TiO2	P2O5	Na2O	SiO2	MgO	Al2O3	FeO	MnO	Cr2O3	NiO	ZnO	SO3	O	TOTAL
OPMG_002_Titanite	11	1	0	2	0	0	2	46	13	6	16	1	0	0	0	0	0	99
OPMG_002_Titanite	12	1	0	2	0	0	2	47	13	6	16	1	0	0	0	0	0	100
OPMG_002_Titanite	11	1	0	2	1	0	2	46	12	7	16	1	0	0	0	0	0	97
OPMG_002_Titanite	18	0	0	1	17	0	1	39	6	5	8	1	0	0	0	0	0	96
OPMG_002_Titanite	12	1	0	1	2	0	1	45	11	7	15	1	0	0	0	0	0	96
OPMG_002_Titanite	28	0	1	1	35	0	0	31	0	2	3	0	0	0	0	0	0	99
OPMG_002_Titanite	27	0	1	1	34	0	0	30	0	2	2	0	0	0	0	0	0	98
OPMG_002_Titanite	28	0	1	1	35	0	0	31	0	2	3	0	0	0	0	0	0	100
OPMG_002_Titanite	28	0	1	1	36	0	0	31	0	1	2	0	0	0	0	0	0	100
OPMG_002_Titanite	28	0	1	1	36	0	0	31	0	1	2	0	0	0	0	0	0	100
SAMPLE	CaO	K2O	BaO	F	TiO2	P2O5	Na2O	SiO2	MgO	Al2O3	FeO	MnO	Cr2O3	NiO	ZnO	SO3	O	TOTAL
OPMG_002_Feld	3	0	0	0	0	0	10	65	0	22	0	0	0	0	0	0	0	100
OPMG_002_Feld	5	0	0	0	0	0	9	62	0	24	0	0	0	0	0	0	0	101
OPMG_002_Feld	2	0	0	0	0	0	10	65	0	22	1	0	0	0	0	0	0	101
OPMG_002_Feld	3	0	0	0	0	0	10	64	0	23	0	0	0	0	0	0	0	100
OPMG_002_Feld	3	0	0	0	0	0	10	65	0	22	0	0	0	0	0	0	0	101
OPMG_002_Feld	3	0	0	0	0	0	10	65	0	22	0	0	0	0	0	0	0	100
OPMG_002_Feld	3	0	0	0	0	0	10	64	0	22	0	0	0	0	0	0	0	100
OPMG_002_Feld	3	0	0	0	0	0	10	65	0	22	0	0	0	0	0	0	0	101
SAMPLE	CaO	K2O	BaO	F	TiO2	P2O5	Na2O	SiO2	MgO	Al2O3	FeO	MnO	Cr2O3	NiO	ZnO	SO3	O	TOTAL
OPMG_002_Bio	0	10	0	3	1	0	0	40	17	12	14	1	0	0	0	0	0	98
OPMG_002_Bio	0	10	0	3	1	0	0	39	16	13	15	1	0	0	0	0	0	98
OPMG_002_Bio	0	10	0	3	1	0	0	39	17	12	15	1	0	0	0	0	0	98
OPMG_002_Bio	0	9	0	3	2	0	0	39	17	12	14	1	0	0	0	0	0	97
OPMG_002_Bio	0	10	0	4	1	0	0	40	18	12	14	1	0	0	0	0	0	99
OPMG_002_Bio	0	10	0	3	1	0	0	39	16	12	16	1	0	0	0	0	0	98
OPMG_002_Bio	1	10	0	3	1	0	0	39	16	12	15	1	0	0	0	0	0	98
OPMG_002_Bio	56	0	0	4	0	42	0	1	0	0	0	0	0	0	0	1	0	104

OPMG_002_Bio	0	10	0	3	1	0	0	39	16	12	15	1	0	0	0	0	0	99
OPMG_002_Bio	0	10	0	3	1	0	0	39	16	12	15	1	0	0	0	0	0	98
OPMG_002_Bio	0	10	0	3	1	0	0	39	16	12	15	1	0	0	0	0	0	98
OPMG_002_Bio	0	10	0	3	1	0	0	39	16	12	16	1	0	0	0	0	0	98
OPMG_002_Bio	0	10	0	3	1	0	0	39	16	12	15	1	0	0	0	0	0	98
OPMG_002_Bio	0	10	0	3	1	0	0	40	17	12	14	1	0	0	0	0	0	98
SAMPLE	CaO	K2O	BaO	F	TiO2	P2O5	Na2O	SiO2	MgO	Al2O3	FeO	MnO	Cr2O3	NiO	ZnO	SO3	O	TOTAL
OPMG_002_Horn	11	1	0	2	0	0	2	46	12	7	17	1	0	0	0	0	0	98
OPMG_002_Horn	11	1	0	1	1	0	2	46	11	7	16	1	0	0	0	0	0	98
OPMG_002_Horn	11	1	0	1	1	0	2	47	12	6	16	1	0	0	0	0	0	99
OPMG_002_Horn	11	1	0	1	1	0	2	47	12	6	16	1	0	0	0	0	0	99
OPMG_002_Horn	11	1	0	1	1	0	2	46	12	7	16	1	0	0	0	0	0	97
OPMG_002_Horn	11	1	0	2	1	0	2	47	12	6	16	1	0	0	0	0	0	99
OPMG_002_Horn	0	10	0	3	1	0	0	41	19	12	12	1	0	0	0	0	0	99
OPMG_002_Horn	0	10	0	3	1	0	0	41	19	12	12	1	0	0	0	0	0	97
OPMG_002_Horn	11	1	0	1	0	0	2	47	12	6	17	1	0	0	0	0	0	99
OPMG_002_Horn	8	1	0	1	0	0	1	41	8	9	13	1	0	0	0	0	0	83
OPMG_002_Horn	9	1	0	1	0	0	1	45	10	8	14	1	0	0	0	0	0	91
OPMG_002_Horn	11	1	0	1	1	0	2	46	12	6	17	1	0	0	0	0	0	99
OPMG_002_Horn	11	1	0	1	0	0	2	47	11	8	15	1	0	0	0	0	0	97
SAMPLE	CaO	K2O	BaO	F	TiO2	P2O5	Na2O	SiO2	MgO	Al2O3	FeO	MnO	Cr2O3	NiO	ZnO	SO3	O	TOTAL
OPMG_002_plag	3	0	0	0	0	0	10	65	0	22	0	0	0	0	0	0	0	100
OPMG_002_plag	3	0	0	0	0	0	9	62	0	21	0	0	0	0	0	0	0	96
OPMG_002_plag	3	0	0	0	0	0	10	65	0	22	0	0	0	0	0	0	0	100
OPMG_002_plag	3	0	0	0	0	0	10	65	0	22	0	0	0	0	0	0	0	101
OPMG_002_plag	3	0	0	0	0	0	10	66	0	22	0	0	0	0	0	0	0	101
OPMG_002_plag	2	0	0	0	0	0	10	65	0	21	0	0	0	0	0	0	0	99
OPMG_002_plag	3	0	0	0	0	0	10	65	0	22	0	0	0	0	0	0	0	101
OPMG_002_plag	3	0	0	0	0	0	11	65	0	22	0	0	0	0	0	0	0	101

OPMG_002_plag	2	0	0	0	0	0	10	65	1	21	1	0	0	0	0	0	0	101
OPMG_002_plag	2	0	0	0	0	0	10	66	0	22	0	0	0	0	0	0	0	101
OPMG_002_plag	3	0	0	0	0	0	11	66	0	22	0	0	0	0	0	0	0	102
OPMG_002_plag	3	0	0	0	0	0	10	64	1	21	1	0	0	0	0	0	0	100
OPMG_002_plag	3	0	0	0	0	0	11	66	0	22	0	0	0	0	0	0	0	101
OPMG_002_plag	3	0	0	0	0	0	10	63	0	22	0	0	0	0	0	0	0	99
OPMG_002_plag	5	0	0	0	0	0	8	60	3	18	4	0	0	0	0	0	0	100

EMPA data from sample HYBRIDts006B

SAMPLE	K2O	BaO	F	TiO2	P2O5	Na2O	SiO2	MgO	Al2O3	FeO	MnO	Cr2O3	NiO	ZnO	SO3	O	TOTAL
OPMG_006B_Titanite	0	1	1	33	0	0	29	0	2	3	0	0	0	0	0	0	95
OPMG_006B_Titanite	0	1	1	34	0	0	29	0	1	3	0	0	0	0	0	0	95
OPMG_006B_Titanite	0	0	1	31	0	0	30	0	4	2	0	0	0	0	0	0	92
OPMG_006B_Titanite	0	1	1	34	0	0	29	0	2	3	0	0	0	0	0	0	95
OPMG_006B_Titanite	0	1	1	33	0	0	30	0	2	3	0	0	0	0	0	0	96
OPMG_006B_Titanite	0	0	1	22	0	0	21	0	2	2	0	0	0	0	0	0	68
OPMG_006B_Titanite	0	1	1	34	0	0	29	0	1	3	0	0	0	0	0	0	95
OPMG_006B_Titanite	0	0	1	26	0	0	25	0	3	3	0	0	0	0	0	0	82
OPMG_006B_Titanite	0	0	4	0	40	0	1	0	0	0	0	0	0	0	0	0	99
OPMG_006B_Titanite	0	1	1	34	0	0	29	0	1	2	0	0	0	0	0	0	94
OPMG_006B_Titanite	0	1	1	32	0	0	29	0	2	3	0	0	0	0	0	0	95
OPMG_006B_Titanite	0	1	1	32	0	0	29	0	2	3	0	0	0	0	0	0	95
SAMPLE	K2O	BaO	F	TiO2	P2O5	Na2O	SiO2	MgO	Al2O3	FeO	MnO	Cr2O3	NiO	ZnO	SO3	O	TOTAL
OPMG_006B_KSP_27	0	0	0	0	0	11	67	0	21	0	0	0	0	0	0	0	101
OPMG_006B_KSP_27	0	0	0	0	0	11	66	0	21	0	0	0	0	0	0	0	101
OPMG_006B_KSP_27	0	0	0	0	0	11	66	0	22	0	0	0	0	0	0	0	101

OPMG_006B_KSP_27	0	0	0	0	0	10	65	0	21	0	0	0	0	0	0	0	99
OPMG_006B_KSP_27	7	0	0	0	0	6	64	0	19	0	0	0	0	0	0	0	97
OPMG_006B_KSP_27	16	0	0	0	0	0	65	0	19	0	0	0	0	0	0	0	100
OPMG_006B_KSP_27	15	0	0	0	0	1	65	0	19	0	0	0	0	0	0	0	100
OPMG_006B_KSP_27	15	0	0	0	0	2	65	0	19	0	0	0	0	0	0	0	100
OPMG_006B_KSP_27	16	0	0	0	0	0	65	0	19	0	0	0	0	0	0	0	100
OPMG_006B_KSP_27	16	0	0	0	0	1	65	0	18	0	0	0	0	0	0	0	100
OPMG_006B_KSP_27	16	0	0	0	0	0	65	0	19	0	0	0	0	0	0	0	100
OPMG_006B_KSP_27	0	0	0	0	0	11	67	0	21	0	0	0	0	0	0	0	100
OPMG_006B_KSP_27	15	0	0	0	0	1	65	0	19	0	0	0	0	0	0	0	100
OPMG_006B_KSP_27	16	0	0	0	0	0	64	0	19	0	0	0	0	0	0	0	99
OPMG_006B_KSP_27	16	0	0	0	0	0	64	0	18	0	0	0	0	0	0	0	100
OPMG_006B_KSP_27	15	0	0	0	0	1	65	0	19	0	0	0	0	0	0	0	100
OPMG_006B_KSP_27	0	0	0	0	0	11	66	0	21	0	0	0	0	0	0	0	101
OPMG_006B_KSP_27	0	0	0	0	0	11	66	0	21	0	0	0	0	0	0	0	100
OPMG_006B_KSP_27	0	0	0	0	0	11	66	0	21	1	0	0	0	0	0	0	100
OPMG_006B_KSP_27	0	0	0	0	0	11	66	0	21	0	0	0	0	0	0	0	100
SAMPLE	K2O	BaO	F	TiO2	P2O5	Na2O	SiO2	MgO	Al2O3	FeO	MnO	Cr2O3	NiO	ZnO	SO3	O	TOTAL
OPMG_006B_KSP_28rim	0	0	0	0	0	10	65	0	21	1	0	0	0	0	0	0	99
OPMG_006B_KSP_28rim	0	0	0	0	0	10	65	0	22	0	0	0	0	0	0	0	100
OPMG_006B_KSP_28rim	0	0	0	0	0	10	65	0	22	0	0	0	0	0	0	0	100
OPMG_006B_KSP_28rim	0	0	0	0	0	0	101	0	0	0	0	0	0	0	0	0	101
OPMG_006B_KSP_28rim	0	0	0	0	0	11	66	0	22	0	0	0	0	0	0	0	101
OPMG_006B_KSP_28rim	0	0	0	0	0	10	64	0	21	1	0	0	0	0	0	0	98
OPMG_006B_KSP_28rim	0	0	0	0	0	11	66	0	22	0	0	0	0	0	0	0	100
OPMG_006B_KSP_28rim	0	0	0	0	0	11	66	0	21	0	0	0	0	0	0	0	100
OPMG_006B_KSP_28rim	0	0	0	0	0	11	66	0	21	0	0	0	0	0	0	0	101
OPMG_006B_KSP_28rim	0	0	0	0	0	11	66	0	21	0	0	0	0	0	0	0	100
OPMG_006B_KSP_28rim	13	0	0	0	0	2	65	0	19	0	0	0	0	0	0	0	100

OPMG_006B_KSP_28rim	16	0	0	0	0	0	64	0	19	0	0	0	0	0	0	0	100
OPMG_006B_KSP_28rim	0	0	0	0	0	10	64	0	21	1	0	0	0	0	0	0	99
OPMG_006B_KSP_28rim	0	0	0	0	0	10	62	0	21	0	0	0	0	0	0	0	97
OPMG_006B_KSP_28rim	0	0	0	0	0	10	65	0	22	0	0	0	0	0	0	0	101
OPMG_006B_KSP_28rim	0	0	0	0	0	11	66	0	22	0	0	0	0	0	0	0	101
OPMG_006B_KSP_28rim	0	0	0	0	0	10	65	0	22	0	0	0	0	0	0	0	100
OPMG_006B_KSP_28rim	0	0	0	1	0	11	64	0	19	4	0	0	0	0	0	0	100
OPMG_006B_KSP_28rim	0	0	0	0	0	10	63	0	20	0	0	0	0	0	0	0	96
OPMG_006B_KSP_28rim	0	0	0	0	0	10	62	0	20	0	0	0	0	0	0	0	95
OPMG_006B_KSP_28rim	0	0	0	0	0	11	65	0	22	0	0	0	0	0	0	0	100
OPMG_006B_KSP_28rim	1	0	0	0	0	10	64	0	23	0	0	0	0	0	0	0	100
SAMPLE	K2O	BaO	F	TiO2	P2O5	Na2O	SiO2	MgO	Al2O3	FeO	MnO	Cr2O3	NiO	ZnO	SO3	O	TOTAL
OPMG_006B_Titanite_29	0	1	1	34	0	0	29	0	2	3	0	0	0	0	0	0	94
OPMG_006B_Titanite_29	0	1	1	33	0	0	29	0	2	3	0	0	0	0	0	0	93
OPMG_006B_Titanite_29	0	1	1	32	0	0	29	0	2	3	0	0	0	0	0	0	95
OPMG_006B_Titanite_29	0	1	1	32	0	0	28	0	2	3	0	0	0	0	0	0	93
OPMG_006B_Titanite_29	0	1	1	34	0	0	29	0	1	3	0	0	0	0	0	0	95
OPMG_006B_Titanite_29	0	1	1	32	0	0	30	0	2	3	0	0	0	0	0	0	96
OPMG_006B_Titanite_29	0	1	1	34	0	0	29	0	1	3	0	0	0	0	0	0	95
OPMG_006B_Titanite_29	0	1	1	34	0	0	29	0	2	3	0	0	0	0	0	0	96
OPMG_006B_Titanite_29	0	1	1	32	0	0	30	0	2	3	0	0	0	0	0	0	97
SAMPLE	K2O	BaO	F	TiO2	P2O5	Na2O	SiO2	MgO	Al2O3	FeO	MnO	Cr2O3	NiO	ZnO	SO3	O	TOTAL
OPMG_006B_BIO_30	10	0	3	1	0	0	39	16	12	15	1	0	0	0	0	0	98
OPMG_006B_BIO_30	10	0	3	1	0	0	39	16	12	16	1	0	0	0	0	0	98
OPMG_006B_BIO_30	10	0	3	1	0	0	40	16	12	16	1	0	0	0	0	0	99
OPMG_006B_BIO_30	9	0	3	4	0	0	39	15	12	16	1	0	0	0	0	0	99
OPMG_006B_BIO_30	10	0	3	1	0	0	40	16	12	16	1	0	0	0	0	0	99
OPMG_006B_BIO_30	10	0	3	1	0	0	39	16	12	16	1	0	0	0	0	0	99
OPMG_006B_BIO_30	10	0	3	1	0	0	39	16	12	16	1	0	0	0	0	0	98

OPMG_006B_BIO_30	10	0	3	1	0	0	39	16	12	16	1	0	0	0	0	0	98
OPMG_006B_BIO_30	10	0	3	1	0	0	39	16	12	16	1	0	0	0	0	0	98
OPMG_006B_BIO_30	0	1	1	33	0	0	30	0	2	3	0	0	0	0	0	0	97
OPMG_006B_BIO_30	10	0	3	1	0	0	39	16	12	16	1	0	0	0	0	0	98
OPMG_006B_BIO_30	10	0	3	1	0	0	39	16	12	16	1	0	0	0	0	0	98
OPMG_006B_BIO_30	10	0	3	1	0	0	40	17	12	14	1	0	0	0	0	0	98
SAMPLE	K2O	BaO	F	TiO2	P2O5	Na2O	SiO2	MgO	Al2O3	FeO	MnO	Cr2O3	NiO	ZnO	SO3	O	TOTAL
OPMG_006B_Titanite_31	0	1	1	33	0	0	29	0	2	3	0	0	0	0	0	0	95
OPMG_006B_Titanite_31	0	1	1	33	0	0	30	0	2	3	0	0	0	0	0	0	96
OPMG_006B_Titanite_31	0	1	1	33	0	0	29	0	2	3	0	0	0	0	0	0	96
OPMG_006B_Titanite_31	0	1	1	33	0	0	29	0	2	3	0	0	0	0	0	0	95
OPMG_006B_Titanite_31	0	1	1	34	0	0	29	0	2	3	0	0	0	0	0	0	95
OPMG_006B_Titanite_31	0	1	2	31	0	0	30	0	2	3	0	0	0	0	0	0	97
OPMG_006B_Titanite_31	0	1	1	34	0	0	29	0	2	3	0	0	0	0	0	0	95
OPMG_006B_Titanite_31	0	1	1	34	0	0	30	0	2	3	0	0	0	0	0	0	96
OPMG_006B_Titanite_31	0	1	1	34	0	0	29	0	1	3	0	0	0	0	0	0	95
OPMG_006B_Titanite_31	0	1	1	34	0	0	29	0	1	3	0	0	0	0	0	0	95
OPMG_006B_Titanite_31	0	1	1	33	0	0	29	0	2	3	0	0	0	0	0	0	94
SAMPLE	K2O	BaO	F	TiO2	P2O5	Na2O	SiO2	MgO	Al2O3	FeO	MnO	Cr2O3	NiO	ZnO	SO3	O	TOTAL
OPMG_006B_HORN_32	1	0	2	1	0	2	47	12	5	16	1	0	0	0	0	0	98
OPMG_006B_HORN_32	1	0	2	1	0	2	47	12	5	16	1	0	0	0	0	0	99
OPMG_006B_HORN_32	1	0	2	1	0	2	46	12	5	16	2	0	0	0	0	0	96
OPMG_006B_HORN_32	1	0	1	0	0	2	47	12	6	16	2	0	0	0	0	0	98
OPMG_006B_HORN_32	1	0	1	0	0	2	47	12	6	17	2	0	0	0	0	0	100
OPMG_006B_HORN_32	0	0	0	0	0	0	15	10	9	11	3	0	0	0	0	0	71
OPMG_006B_HORN_32	1	0	1	0	0	2	46	11	6	17	2	0	0	0	0	0	98
OPMG_006B_HORN_32	10	0	3	0	0	0	39	16	13	13	1	0	0	0	0	0	97
OPMG_006B_HORN_32	10	0	3	2	0	0	39	16	12	14	1	0	0	0	0	0	97
OPMG_006B_HORN_32	1	0	1	1	0	2	46	11	6	17	1	0	0	0	0	0	98

OPMG_006B_HORN_32	1	0	1	0	0	2	47	12	6	17	2	0	0	0	0	0	98
OPMG_006B_HORN_32	1	0	2	1	0	2	46	12	6	17	2	0	0	0	0	0	99
OPMG_006B_HORN_32	1	0	1	0	0	2	46	11	6	18	2	0	0	0	0	0	99
OPMG_006B_HORN_32	1	0	1	0	0	1	45	11	7	17	2	0	0	0	0	0	96
OPMG_006B_HORN_32	1	0	1	0	0	2	46	11	6	17	2	0	0	0	0	0	98
OPMG_006B_HORN_32	2	0	2	0	0	2	45	11	7	17	1	0	0	0	0	0	97
OPMG_006B_HORN_32	1	0	1	0	0	2	46	11	6	17	2	0	0	0	0	0	99
OPMG_006B_HORN_32	1	0	1	0	0	2	46	11	6	17	2	0	0	0	0	0	99
OPMG_006B_HORN_32	1	0	2	0	0	2	46	11	6	17	2	0	0	0	0	0	97
OPMG_006B_HORN_32	10	0	3	1	0	0	41	18	12	12	1	0	0	0	0	0	98
OPMG_006B_HORN_32	9	0	3	0	0	0	41	19	12	11	1	0	0	0	0	0	97
OPMG_006B_HORN_32	1	0	1	1	0	2	46	11	6	17	2	0	0	0	0	0	98
OPMG_006B_HORN_32	1	0	1	1	0	2	46	11	6	17	2	0	0	0	0	0	99
OPMG_006B_HORN_32	1	0	1	1	0	2	47	12	6	17	2	0	0	0	0	0	99
OPMG_006B_HORN_32	1	0	1	1	0	2	46	12	6	17	2	0	0	0	0	0	98

EMPA data from sample ENCLAVEts009

SAMPLE	K2O	BaO	F	TiO2	P2O5	Na2O	SiO2	MgO	Al2O3	FeO	MnO	Cr2O3	NiO	ZnO	SO3	O	TOTAL
OPMG_009 _001 ALK-feld	15	0	0	0	0	1	64	0	20	0	0	0	0	0	0	0	101
OPMG_009 _001 ALK-feld	16	0	0	0	0	1	65	0	19	0	0	0	0	0	0	0	101
OPMG_009 _001 ALK-feld	16	0	0	0	0	1	65	0	19	0	0	0	0	0	0	0	101
OPMG_009 _001 ALK-feld	13	0	0	0	0	1	60	1	18	3	0	0	0	0	0	0	96
OPMG_009 _001 ALK-feld	16	0	0	0	0	0	63	0	19	0	0	0	0	0	0	0	99
OPMG_009 _001 ALK-feld	8	0	0	0	0	6	65	0	19	1	0	0	0	0	0	0	100
OPMG_009 _001 ALK-feld	15	0	0	0	0	1	65	0	19	0	0	0	0	0	0	0	100
OPMG_009 _001 ALK-feld	15	0	0	0	0	1	65	0	19	0	0	0	0	0	0	0	100
OPMG_009 _001 ALK-feld	15	0	0	0	0	1	65	0	19	0	0	0	0	0	0	0	100
OPMG_009 _001 ALK-feld	15	0	0	0	0	1	65	0	19	0	0	0	0	0	0	0	100
OPMG_009 _001 ALK-feld	15	0	0	0	0	1	65	0	19	0	0	0	0	0	0	0	100
OPMG_009 _001 ALK-feld	15	0	0	0	0	1	65	0	19	0	0	0	0	0	0	0	100

OPMG_009 _001 ALK-feld	15	0	0	0	0	1	64	0	19	0	0	0	0	0	0	0	100
OPMG_009 _001 ALK-feld	15	0	0	0	0	1	65	0	19	0	0	0	0	0	0	0	100
OPMG_009 _001 ALK-feld	15	0	0	0	0	1	64	0	19	0	0	0	0	0	0	0	100
OPMG_009 _001 ALK-feld	15	0	0	0	0	1	65	0	19	0	0	0	0	0	0	0	100
OPMG_009 _001 ALK-feld	14	0	0	0	0	2	64	0	19	0	0	0	0	0	0	0	99
OPMG_009 _001 ALK-feld	16	0	0	0	0	1	64	0	19	0	0	0	0	0	0	0	100
OPMG_009 _001 ALK-feld	15	0	0	0	0	1	65	0	19	0	0	0	0	0	0	0	100
OPMG_009 _001 ALK-feld	15	0	0	0	0	2	65	0	19	0	0	0	0	0	0	0	100
OPMG_009 _001 ALK-feld	15	0	0	0	0	1	64	0	19	0	0	0	0	0	0	0	100
OPMG_009 _001 ALK-feld	16	0	0	0	0	0	63	0	19	1	0	0	0	0	0	0	99
SAMPLE	K2O	BaO	F	TiO2	P2O5	Na2O	SiO2	MgO	Al2O3	FeO	MnO	Cr2O3	NiO	ZnO	SO3	O	TOTAL
OPMG_009 _002 Amphibol	1	0	1	0	0	2	46	12	7	17	1	0	0	0	0	0	99
OPMG_009 _002 Amphibol	1	0	2	0	0	2	48	13	6	16	1	0	0	0	0	0	99
OPMG_009 _002 Amphibol	1	0	2	0	3	1	44	11	6	15	1	0	0	0	0	0	97
OPMG_009 _002 Amphibol	1	0	1	11	0	2	38	11	5	21	2	0	0	0	0	0	101
OPMG_009 _002 Amphibol	1	0	2	0	15	1	31	8	4	11	1	0	0	0	0	0	99
OPMG_009 _002 Amphibol	1	0	2	1	4	1	41	11	7	14	1	0	0	0	0	0	96
OPMG_009 _002 Amphibol	1	0	1	1	0	1	44	11	7	14	1	0	0	0	0	0	90
OPMG_009 _002 Amphibol	1	0	2	1	0	2	47	13	6	16	1	0	0	0	0	0	100
OPMG_009 _002 Amphibol	1	0	2	1	0	2	47	13	6	16	1	0	0	0	0	0	100
OPMG_009 _002 Amphibol	1	0	2	0	0	2	47	12	6	17	1	0	0	0	0	0	99
OPMG_009 _002 Amphibol	1	0	2	0	0	2	46	13	6	16	1	0	0	0	0	0	99
SAMPLE	K2O	BaO	F	TiO2	P2O5	Na2O	SiO2	MgO	Al2O3	FeO	MnO	Cr2O3	NiO	ZnO	SO3	O	TOTAL
OPMG_009 _003 Plag	0	0	0	0	0	7	57	0	28	0	0	0	0	0	0	0	101
OPMG_009 _003 Plag	0	0	0	0	0	5	54	0	29	0	0	0	0	0	0	0	100
OPMG_009 _003 Plag	0	0	0	0	0	6	54	0	29	0	0	0	0	0	0	0	100
OPMG_009 _003 Plag	0	0	0	0	0	6	54	0	29	0	0	0	0	0	0	0	100
OPMG_009 _003 Plag	0	0	0	0	0	5	53	0	30	1	0	0	0	0	0	0	100
OPMG_009 _003 Plag	0	0	0	0	0	5	53	0	30	0	0	0	0	0	0	0	100

OPMG_009 _003 Plag	0	0	0	0	0	5	53	0	30	0	0	0	0	0	0	0	100
OPMG_009 _003 Plag	0	0	0	0	0	5	53	0	30	0	0	0	0	0	0	0	100
OPMG_009 _003 Plag	0	0	0	0	0	5	53	0	30	0	0	0	0	0	0	0	99
OPMG_009 _003 Plag	0	0	0	0	0	5	52	0	30	0	0	0	0	0	0	0	99
OPMG_009 _003 Plag	0	0	0	0	0	5	35	0	22	1	0	0	0	0	0	0	74
OPMG_009 _003 Plag	0	0	0	0	0	4	34	0	21	1	0	0	0	0	0	0	72
OPMG_009 _003 Plag	0	0	0	0	0	5	34	0	21	0	0	0	0	0	0	0	71
OPMG_009 _003 Plag	0	0	0	0	0	5	53	0	30	0	0	0	0	0	0	0	100
OPMG_009 _003 Plag	0	0	0	0	0	5	52	0	30	0	0	0	0	0	0	0	99
OPMG_009 _003 Plag	0	0	0	0	0	5	52	0	29	1	0	0	0	0	0	0	100
OPMG_009 _003 Plag	0	0	0	0	0	5	53	0	30	0	0	0	0	0	0	0	101
OPMG_009 _003 Plag	0	0	0	0	0	5	53	0	30	0	0	0	0	0	0	0	101
OPMG_009 _003 Plag	0	0	0	0	0	5	53	0	30	0	0	0	0	0	0	0	101
OPMG_009 _003 Plag	0	0	0	0	0	4	33	0	20	0	0	0	0	0	0	0	68
OPMG_009 _003 Plag	0	0	0	0	0	5	53	0	30	0	0	0	0	0	0	0	100
OPMG_009 _003 Plag	0	0	0	0	0	5	53	0	30	0	0	0	0	0	0	0	101
OPMG_009 _003 Plag	0	0	0	0	0	5	53	0	30	0	0	0	0	0	0	0	100
OPMG_009 _003 Plag	0	0	0	0	0	5	53	0	30	1	0	0	0	0	0	0	100
OPMG_009 _003 Plag	0	0	0	0	0	5	53	0	30	0	0	0	0	0	0	0	100
OPMG_009 _003 Plag	0	0	0	0	0	5	53	0	30	0	0	0	0	0	0	0	100
OPMG_009 _003 Plag	0	0	0	0	0	5	53	0	30	0	0	0	0	0	0	0	100
OPMG_009 _003 Plag	0	0	0	0	0	5	53	0	30	0	0	0	0	0	0	0	100
OPMG_009 _003 Plag	0	0	0	0	0	5	52	0	29	1	0	0	0	0	0	0	100
OPMG_009 _003 Plag	0	0	0	0	0	5	53	0	30	0	0	0	0	0	0	0	100
OPMG_009 _003 Plag	0	0	0	0	0	5	53	0	30	1	0	0	0	0	0	0	101
OPMG_009 _003 Plag	0	0	0	0	0	5	52	0	30	0	0	0	0	0	0	0	99
OPMG_009 _003 Plag	0	0	0	0	0	5	52	0	29	1	0	0	0	0	0	0	100
OPMG_009 _003 Plag	0	0	0	0	0	5	53	0	30	0	0	0	0	0	0	0	101
OPMG_009 _003 Plag	0	0	0	0	0	5	53	0	30	0	0	0	0	0	0	0	100

OPMG_009 _003 Plag	0	0	0	0	0	5	52	0	30	1	0	0	0	0	0	0	100
OPMG_009 _003 Plag	0	0	0	0	0	5	52	0	30	1	0	0	0	0	0	0	100
OPMG_009 _003 Plag	0	0	0	0	0	5	52	0	30	0	0	0	0	0	0	0	100
OPMG_009 _003 Plag	0	0	0	0	0	5	52	0	30	0	0	0	0	0	0	0	100
OPMG_009 _003 Plag	0	0	0	0	0	5	53	0	30	0	0	0	0	0	0	0	100
OPMG_009 _003 Plag	0	0	0	0	0	5	53	0	30	0	0	0	0	0	0	0	100
OPMG_009 _003 Plag	0	0	0	0	0	5	53	0	30	0	0	0	0	0	0	0	100
OPMG_009 _003 Plag	0	0	0	0	0	5	52	0	30	0	0	0	0	0	0	0	99
OPMG_009 _003 Plag	0	0	0	0	0	5	52	0	30	0	0	0	0	0	0	0	100
OPMG_009 _003 Plag	0	0	0	0	0	5	53	0	30	0	0	0	0	0	0	0	101
OPMG_009 _003 Plag	0	0	0	0	0	5	52	0	30	0	0	0	0	0	0	0	100
OPMG_009 _003 Plag	0	0	0	0	0	5	52	0	30	0	0	0	0	0	0	0	99
OPMG_009 _003 Plag	0	0	0	0	0	5	53	0	30	0	0	0	0	0	0	0	100
OPMG_009 _003 Plag	0	0	0	0	0	5	53	0	30	1	0	0	0	0	0	0	100
OPMG_009 _003 Plag	0	0	0	0	0	6	55	0	29	0	0	0	0	0	0	0	100
SAMPLE	K2O	BaO	F	TiO2	P2O5	Na2O	SiO2	MgO	Al2O3	FeO	MnO	Cr2O3	NiO	ZnO	SO3	O	TOTAL
OPMG_009 _004 amphibol	1	0	2	0	0	2	45	12	6	16	1	0	0	0	0	0	96
OPMG_009 _004 amphibol	1	0	2	0	0	2	47	13	6	16	1	0	0	0	0	0	99
OPMG_009 _004 amphibol	1	0	2	0	0	2	47	13	6	16	1	0	0	0	0	0	99
OPMG_009 _004 amphibol	1	0	1	0	0	2	47	13	6	16	1	0	0	0	0	0	99
OPMG_009 _004 amphibol	1	0	2	0	0	1	47	13	6	16	1	0	0	0	0	0	99
OPMG_009 _004 amphibol	1	0	2	0	0	1	47	13	6	16	1	0	0	0	0	0	99
OPMG_009 _004 amphibol	1	0	1	0	0	2	47	13	6	16	1	0	0	0	0	0	99
OPMG_009 _004 amphibol	1	0	2	0	0	2	47	13	6	16	1	0	0	0	0	0	100
SAMPLE	K2O	BaO	F	TiO2	P2O5	Na2O	SiO2	MgO	Al2O3	FeO	MnO	Cr2O3	NiO	ZnO	SO3	O	TOTAL
OPMG_009 _005 amphibol rim	1	0	2	0	0	2	46	12	6	17	1	0	0	0	0	0	99
OPMG_009 _005 amphibol rim	1	0	2	0	0	2	45	12	7	16	1	0	0	0	0	0	96

OPMG_009 _005 amphibol rim	1	0	1	0	0	2	46	12	7	17	1	0	0	0	0	0	99
OPMG_009 _005 amphibol rim	1	0	2	0	0	2	46	12	6	17	1	0	0	0	0	0	99
OPMG_009 _005 amphibol rim	1	0	2	0	0	2	45	12	7	17	1	0	0	0	0	0	98
OPMG_009 _005 amphibol rim	1	0	2	1	0	2	46	12	6	16	1	0	0	0	0	0	98
OPMG_009 _005 amphibol rim	1	0	2	1	0	2	47	13	6	17	1	0	0	0	0	0	100
OPMG_009 _005 amphibol rim	1	0	2	0	0	2	45	12	6	16	1	0	0	0	0	0	97
OPMG_009 _005 amphibol rim	1	0	2	0	0	2	46	12	6	16	1	0	0	0	0	0	98
OPMG_009 _005 amphibol rim	1	0	2	1	0	2	46	12	6	17	1	0	0	0	0	0	98
OPMG_009 _005 amphibol rim	1	0	2	1	0	2	45	12	6	17	1	0	0	0	0	0	98
OPMG_009 _005 amphibol rim	1	0	2	1	0	2	47	13	5	15	1	0	0	0	0	0	97
OPMG_009 _005 amphibol rim	1	0	2	1	0	2	48	13	5	15	1	0	0	0	0	0	98
OPMG_009 _005 amphibol rim	1	0	2	1	0	2	48	13	5	16	1	0	0	0	0	0	99
OPMG_009 _005 amphibol rim	1	0	2	1	0	2	46	12	6	17	1	0	0	0	0	0	99
OPMG_009 _005 amphibol rim	1	0	2	1	0	2	46	12	6	17	1	0	0	0	0	0	99
OPMG_009 _005 amphibol rim	1	0	1	0	0	4	48	8	9	13	1	0	0	0	0	0	93
OPMG_009 _005 amphibol rim	1	0	1	0	0	2	46	12	7	16	1	0	0	0	0	0	97
OPMG_009 _005 amphibol rim	1	0	1	0	0	4	49	9	10	12	1	0	0	0	0	0	95

OPMG_009 _005 amphibol rim	1	0	1	0	0	3	49	11	8	14	1	0	0	0	0	0	98
OPMG_009 _005 amphibol rim	1	0	1	0	0	5	52	8	11	11	1	0	0	0	0	0	100
OPMG_009 _005 amphibol rim	1	0	1	0	0	3	48	11	8	15	1	0	0	0	0	0	98
OPMG_009 _005 amphibol rim	1	0	2	0	0	2	46	12	6	17	1	0	0	0	0	0	99
OPMG_009 _005 amphibol rim	1	0	2	0	0	2	47	13	6	16	1	0	0	0	0	0	99
OPMG_009 _005 amphibol rim	1	0	2	1	0	2	46	12	6	16	1	0	0	0	0	0	99
SAMPLE	K2O	BaO	F	TiO2	P2O5	Na2O	SiO2	MgO	Al2O3	FeO	MnO	Cr2O3	NiO	ZnO	SO3	O	TOTAL
OPMG_009 _006 amphibol transsect	1	0	2	1	0	2	47	13	6	16	1	0	0	0	0	0	100
OPMG_009 _006 amphibol transsect	1	0	2	1	0	2	48	13	5	16	1	0	0	0	0	0	99
OPMG_009 _006 amphibol transsect	1	0	2	1	0	2	48	13	5	16	1	0	0	0	0	0	100
OPMG_009 _006 amphibol transsect	1	0	2	1	0	2	48	13	5	16	1	0	0	0	0	0	99
OPMG_009 _006 amphibol transsect	1	0	2	1	0	2	48	13	5	16	1	0	0	0	0	0	100
OPMG_009 _006 amphibol transsect	1	0	2	1	0	2	48	13	5	16	1	0	0	0	0	0	99
OPMG_009 _006 amphibol transsect	1	0	2	1	0	2	48	13	5	16	1	0	0	0	0	0	99
OPMG_009 _006 amphibol transsect	1	0	2	1	0	2	48	13	5	16	1	0	0	0	0	0	99
OPMG_009 _006 amphibol transsect	1	0	2	1	0	2	48	13	5	16	1	0	0	0	0	0	100
OPMG_009 _006 amphibol transsect	1	0	2	1	0	2	48	13	5	16	1	0	0	0	0	0	99

OPMG_009 _006 amphibol transsect	1	0	2	1	0	2	48	13	5	16	1	0	0	0	0	100
OPMG_009 _006 amphibol transsect	1	0	2	1	0	2	48	13	5	16	1	0	0	0	0	99
OPMG_009 _006 amphibol transsect	1	0	2	1	0	2	48	13	5	15	1	0	0	0	0	98
OPMG_009 _006 amphibol transsect	1	0	2	1	0	2	48	13	5	15	1	0	0	0	0	99
OPMG_009 _006 amphibol transsect	1	0	2	1	0	2	48	13	5	16	1	0	0	0	0	98
OPMG_009 _006 amphibol transsect	1	0	2	1	0	2	47	12	6	16	1	0	0	0	0	97
SAMPLE	K2O	BaO	F	TiO2	P2O5	Na2O	SiO2	MgO	Al2O3	FeO	MnO	Cr2O3	NiO	ZnO	SO3	O	TOTAL
OPMG_009 _007 Titanite	0	1	1	36	0	0	31	0	1	2	0	0	0	0	0	0	101
OPMG_009 _007 Titanite	0	1	1	36	0	0	30	0	1	2	0	0	0	0	0	0	100
OPMG_009 _007 Titanite	0	1	1	37	0	0	30	0	1	2	0	0	0	0	0	0	100
OPMG_009 _007 Titanite	0	1	1	36	0	0	30	0	1	2	0	0	0	0	0	0	99
OPMG_009 _007 Titanite	0	1	1	37	0	0	30	0	1	2	0	0	0	0	0	0	100
OPMG_009 _007 Titanite	0	1	1	37	0	0	30	0	1	2	0	0	0	0	0	0	99
OPMG_009 _007 Titanite	0	1	1	37	0	0	30	0	1	2	0	0	0	0	0	0	99
OPMG_009 _007 Titanite	0	1	1	37	0	0	30	0	1	2	0	0	0	0	0	0	99
OPMG_009 _007 Titanite	0	1	1	37	0	0	31	0	1	2	0	0	0	0	0	0	100
OPMG_009 _007 Titanite	0	1	1	36	0	0	30	0	1	2	0	0	0	0	0	0	99
OPMG_009 _007 Titanite	0	1	1	36	0	0	30	0	1	2	0	0	0	0	0	0	99
OPMG_009 _007 Titanite	0	1	1	37	0	0	30	0	1	2	0	0	0	0	0	0	99
OPMG_009 _007 Titanite	0	1	1	38	0	0	30	0	1	1	0	0	0	0	0	0	99
OPMG_009 _007 Titanite	0	1	1	37	0	0	30	0	1	2	0	0	0	0	0	0	99
OPMG_009 _007 Titanite	0	1	1	37	0	0	30	0	1	2	0	0	0	0	0	0	99
OPMG_009 _007 Titanite	0	1	1	37	0	0	30	0	1	2	0	0	0	0	0	0	99
SAMPLE	K2O	BaO	F	TiO2	P2O5	Na2O	SiO2	MgO	Al2O3	FeO	MnO	Cr2O3	NiO	ZnO	SO3	O	TOTAL
OPMG_009 _008 Titanite rim	0	1	1	36	0	0	30	0	2	2	0	0	0	0	0	0	100

OPMG_009 _008 Titanite rim	0	1	1	36	0	0	30	0	2	2	0	0	0	0	0	0	100
OPMG_009 _008 Titanite rim	0	1	1	36	0	0	30	0	2	2	0	0	0	0	0	0	100
OPMG_009 _008 Titanite rim	0	1	1	36	0	0	30	0	2	2	0	0	0	0	0	0	100
OPMG_009 _008 Titanite rim	0	1	1	35	0	0	30	0	2	2	0	0	0	0	0	0	99
OPMG_009 _008 Titanite rim	0	1	1	32	0	0	21	0	1	2	0	0	0	0	0	0	85
OPMG_009 _008 Titanite rim	0	1	1	34	0	0	31	0	2	2	0	0	0	0	0	0	99
OPMG_009 _008 Titanite rim	0	1	1	32	0	0	31	0	3	3	0	0	0	0	0	0	97
OPMG_009 _008 Titanite rim	0	1	1	34	0	0	30	0	2	3	0	0	0	0	0	0	99
OPMG_009 _008 Titanite rim	0	1	1	36	0	0	30	0	2	2	0	0	0	0	0	0	99
OPMG_009 _008 Titanite rim	0	1	1	36	0	0	31	0	1	2	0	0	0	0	0	0	100
OPMG_009 _008 Titanite rim	0	1	1	36	0	0	30	0	1	2	0	0	0	0	0	0	99
OPMG_009 _008 Titanite rim	0	1	1	36	0	0	30	0	1	2	0	0	0	0	0	0	99
OPMG_009 _008 Titanite rim	0	1	1	36	0	0	30	0	2	2	0	0	0	0	0	0	99
OPMG_009 _008 Titanite rim	0	1	1	36	0	0	30	0	2	2	0	0	0	0	0	0	100
OPMG_009 _008 Titanite rim	0	1	1	36	0	0	30	0	2	2	0	0	0	0	0	0	100
OPMG_009 _008 Titanite rim	0	1	1	37	0	0	30	0	1	2	0	0	0	0	0	0	100
OPMG_009 _008 Titanite rim	0	1	1	37	0	0	29	0	1	2	0	0	0	0	0	0	99
OPMG_009 _008 Titanite rim	0	1	1	37	0	0	30	0	1	2	0	0	0	0	0	0	99
OPMG_009 _008 Titanite rim	0	1	1	37	0	0	30	0	1	2	0	0	0	0	0	0	100
OPMG_009 _008 Titanite rim	0	1	1	36	0	0	30	0	1	2	0	0	0	0	0	0	100
OPMG_009 _008 Titanite rim	0	1	1	37	0	0	30	0	1	2	0	0	0	0	0	0	100
OPMG_009 _008 Titanite rim	0	1	1	37	0	0	31	0	1	2	0	0	0	0	0	0	100
OPMG_009 _008 Titanite rim	0	1	1	36	0	0	30	0	1	2	0	0	0	0	0	0	100
OPMG_009 _008 Titanite rim	0	1	1	35	0	0	30	0	2	2	0	0	0	0	0	0	100
OPMG_009 _008 Titanite rim	0	1	1	36	0	0	30	0	2	2	0	0	0	0	0	0	99
OPMG_009 _008 Titanite rim	0	1	1	36	0	0	30	0	2	2	0	0	0	0	0	0	100
OPMG_009 _008 Titanite rim	0	1	1	35	0	0	30	0	2	2	0	0	0	0	0	0	99
OPMG_009 _008 Titanite rim	0	1	1	36	0	0	30	0	2	2	0	0	0	0	0	0	99
OPMG_009 _008 Titanite rim	0	1	1	36	0	0	30	0	2	2	0	0	0	0	0	0	99

OPMG_009 _008 Titanite rim	0	1	1	37	0	0	30	0	1	2	0	0	0	0	0	0	99
OPMG_009 _008 Titanite rim	0	1	1	35	0	0	30	0	2	3	0	0	0	0	0	0	97
OPMG_009 _008 Titanite rim	0	1	1	37	0	0	30	0	1	2	0	0	0	0	0	0	98
OPMG_009 _008 Titanite rim	6	0	0	20	0	0	44	0	9	1	0	0	0	0	0	0	99
OPMG_009 _008 Titanite rim	0	1	1	37	0	0	30	0	1	2	0	0	0	0	0	0	99
SAMPLE	K2O	BaO	F	TiO2	P2O5	Na2O	SiO2	MgO	Al2O3	FeO	MnO	Cr2O3	NiO	ZnO	SO3	O	TOTAL
OPMG_009 _009 Titanite transcet	0	1	1	36	0	0	30	0	2	2	0	0	0	0	0	0	99
OPMG_009 _009 Titanite transcet	0	1	1	36	0	0	30	0	2	2	0	0	0	0	0	0	99
OPMG_009 _009 Titanite transcet	0	1	1	36	0	0	30	0	2	2	0	0	0	0	0	0	100
OPMG_009 _009 Titanite transcet	0	1	1	36	0	0	30	0	2	2	0	0	0	0	0	0	100
OPMG_009 _009 Titanite transcet	0	1	1	36	0	0	30	0	2	2	0	0	0	0	0	0	100
OPMG_009 _009 Titanite transcet	0	1	1	36	0	0	30	0	2	2	0	0	0	0	0	0	100
OPMG_009 _009 Titanite transcet	0	1	1	36	0	0	30	0	2	2	0	0	0	0	0	0	99
OPMG_009 _009 Titanite transcet	0	1	1	36	0	0	30	0	2	2	0	0	0	0	0	0	100
OPMG_009 _009 Titanite transcet	0	1	1	36	0	0	30	0	2	2	0	0	0	0	0	0	100
OPMG_009 _009 Titanite transcet	0	1	1	35	0	0	30	0	2	2	0	0	0	0	0	0	99
OPMG_009 _009 Titanite transcet	0	1	1	35	0	0	30	0	2	2	0	0	0	0	0	0	99
OPMG_009 _009 Titanite transcet	0	1	1	35	0	0	30	0	2	2	0	0	0	0	0	0	99
OPMG_009 _009 Titanite transcet	0	1	1	36	0	0	30	0	2	2	0	0	0	0	0	0	99

OPMG_009 _009 Titanite transcet	0	1	1	36	0	0	30	0	2	2	0	0	0	0	0	0	99
OPMG_009 _009 Titanite transcet	0	1	1	36	0	0	30	0	2	2	0	0	0	0	0	0	99
OPMG_009 _009 Titanite transcet	0	1	1	35	0	0	30	0	2	2	0	0	0	0	0	0	99
OPMG_009 _009 Titanite transcet	0	1	1	36	0	0	30	0	2	2	0	0	0	0	0	0	99
OPMG_009 _009 Titanite transcet	0	1	1	37	0	0	30	0	1	2	0	0	0	0	0	0	99
OPMG_009 _009 Titanite transcet	0	1	1	37	0	0	30	0	1	2	0	0	0	0	0	0	99
OPMG_009 _009 Titanite transcet	0	1	1	37	0	0	30	0	1	2	0	0	0	0	0	0	99
OPMG_009 _009 Titanite transcet	0	1	1	37	0	0	30	0	1	2	0	0	0	0	0	0	99
OPMG_009 _009 Titanite transcet	0	1	1	37	0	0	30	0	1	2	0	0	0	0	0	0	99
OPMG_009 _009 Titanite transcet	1	1	1	33	0	0	32	0	3	2	0	0	0	0	0	0	98
SAMPLE	K2O	BaO	F	TiO2	P2O5	Na2O	SiO2	MgO	Al2O3	FeO	MnO	Cr2O3	NiO	ZnO	SO3	O	TOTAL
OPMG_009 _010 amphibol	1	0	2	1	0	2	46	13	6	16	1	0	0	0	0	0	99
OPMG_009 _010 amphibol	1	0	2	1	0	2	48	14	5	15	1	0	0	0	0	0	99
OPMG_009 _010 amphibol	1	0	2	1	0	2	47	13	5	15	1	0	0	0	0	0	98
OPMG_009 _010 amphibol	1	0	2	1	0	2	47	13	6	15	1	0	0	0	0	0	100
OPMG_009 _010 amphibol	0	0	4	0	42	0	0	0	0	0	0	0	0	0	0	0	102
OPMG_009 _010 amphibol	0	0	4	0	41	0	0	0	0	0	0	0	0	0	0	0	101
SAMPLE	K2O	BaO	F	TiO2	P2O5	Na2O	SiO2	MgO	Al2O3	FeO	MnO	Cr2O3	NiO	ZnO	SO3	O	TOTAL
OPMG_009 _011 AlK fled	16	0	0	0	0	1	64	0	19	0	0	0	0	0	0	0	100
OPMG_009 _011 AlK fled	16	0	0	0	0	1	64	0	19	0	0	0	0	0	0	0	100
OPMG_009 _011 AlK fled	16	0	0	0	0	0	64	0	19	0	0	0	0	0	0	0	100
OPMG_009 _011 AlK fled	11	0	0	0	0	4	65	0	19	0	0	0	0	0	0	0	100

OPMG_009 _011 AlK fled	0	0	0	0	0	12	66	0	20	0	0	0	0	0	0	0	99
OPMG_009 _011 AlK fled	16	0	0	0	0	1	65	0	19	0	0	0	0	0	0	0	100
OPMG_009 _011 AlK fled	16	0	0	0	0	0	64	0	19	0	0	0	0	0	0	0	100
OPMG_009 _011 AlK fled	16	0	0	0	0	1	64	0	19	0	0	0	0	0	0	0	100
OPMG_009 _011 AlK fled	14	0	0	0	0	2	65	0	19	0	0	0	0	0	0	0	100
OPMG_009 _011 AlK fled	16	0	0	0	0	1	64	0	19	0	0	0	0	0	0	0	100
OPMG_009 _011 AlK fled	15	0	0	0	0	1	65	0	19	0	0	0	0	0	0	0	100
OPMG_009 _011 AlK fled	15	0	0	0	0	1	63	0	19	0	0	0	0	0	0	0	99
OPMG_009 _011 AlK fled	14	0	0	0	0	1	64	0	19	0	0	0	0	0	0	0	99
OPMG_009 _011 AlK fled	16	0	0	0	0	1	64	0	19	0	0	0	0	0	0	0	99
OPMG_009 _011 AlK fled	8	0	0	0	0	0	32	0	10	0	1	0	0	0	0	0	78
OPMG_009 _011 AlK fled	0	0	0	0	0	11	65	0	22	0	0	0	0	0	0	0	101
OPMG_009 _011 AlK fled	16	0	0	0	0	0	63	0	19	0	0	0	0	0	0	0	99
OPMG_009 _011 AlK fled	0	0	0	0	0	11	65	0	22	0	0	0	0	0	0	0	100
OPMG_009 _011 AlK fled	0	0	0	0	0	10	64	0	22	0	0	0	0	0	0	0	99
OPMG_009 _011 AlK fled	16	0	0	0	0	0	64	0	19	0	0	0	0	0	0	0	100
OPMG_009 _011 AlK fled	0	0	0	0	0	11	65	0	22	0	0	0	0	0	0	0	101
OPMG_009 _011 AlK fled	0	0	0	0	0	10	65	0	22	0	0	0	0	0	0	0	101
OPMG_009 _011 AlK fled	0	0	0	0	0	10	64	0	22	0	0	0	0	0	0	0	100
SAMPLE	K2O	BaO	F	TiO2	P2O5	Na2O	SiO2	MgO	Al2O3	FeO	MnO	Cr2O3	NiO	ZnO	SO3	O	TOTAL
OPMG_009 _012 AlK rim	16	0	0	0	0	0	64	0	19	0	0	0	0	0	0	0	99
OPMG_009 _012 AlK rim	16	0	0	0	0	1	65	0	19	0	0	0	0	0	0	0	100
OPMG_009 _012 AlK rim	15	0	0	0	0	1	64	0	19	0	0	0	0	0	0	0	99
OPMG_009 _012 AlK rim	15	0	0	0	0	2	65	0	19	0	0	0	0	0	0	0	100
OPMG_009 _012 AlK rim	15	0	0	0	0	1	64	0	19	0	0	0	0	0	0	0	100
OPMG_009 _012 AlK rim	15	0	0	0	0	1	64	0	19	0	0	0	0	0	0	0	100
OPMG_009 _012 AlK rim	15	0	0	0	0	1	64	0	19	0	0	0	0	0	0	0	99
OPMG_009 _012 AlK rim	0	0	0	0	0	11	66	0	22	0	0	0	0	0	0	0	101
OPMG_009 _012 AlK rim	0	0	0	0	0	11	65	0	22	0	0	0	0	0	0	0	101

OPMG_009 _012 AlK rim	14	0	0	0	0	2	65	0	19	0	0	0	0	0	0	0	101
OPMG_009 _012 AlK rim	16	0	0	0	0	1	64	0	19	0	0	0	0	0	0	0	100
OPMG_009 _012 AlK rim	0	0	0	0	0	10	63	0	22	1	0	0	0	0	0	0	99
OPMG_009 _012 AlK rim	0	0	0	0	0	10	64	0	23	0	0	0	0	0	0	0	100
OPMG_009 _012 AlK rim	0	0	0	0	0	10	63	0	23	0	0	0	0	0	0	0	100
OPMG_009 _012 AlK rim	0	0	0	0	0	11	62	0	21	0	0	0	0	0	0	0	97

EMPA data from sample BOUNDARYts016

SAMPLE	K2O	BaO	F	TiO2	P2O5	Na2O	SiO2	MgO	Al2O3	FeO	MnO	Cr2O3	NiO	ZnO	SO3	O	TOTAL
OPMG_016_Titanite	0	1	1	33	0	0	30	0	2	3	0	0	0	0	0	0	97
OPMG_016_Titanite	0	0	2	32	0	0	31	0	3	3	0	0	0	0	0	0	98
OPMG_016_Titanite	0	1	1	32	0	0	30	0	3	3	0	0	0	0	0	0	98
OPMG_016_Titanite	0	0	1	32	0	0	29	0	2	3	0	0	0	0	0	0	96
OPMG_016_Titanite	0	1	2	32	0	0	30	0	3	3	0	0	0	0	0	0	97
OPMG_016_Titanite	0	1	0	79	0	0	2	0	0	5	0	0	0	0	0	0	90
OPMG_016_Titanite	0	1	1	34	0	0	29	0	2	3	0	0	0	0	0	0	95
OPMG_016_Titanite	0	0	2	31	0	0	30	0	3	3	0	0	0	0	0	0	96
OPMG_016_Titanite	0	1	1	34	0	0	29	0	2	2	0	0	0	0	0	0	96
OPMG_016_Titanite	0	1	1	34	0	0	29	0	2	3	0	0	0	0	0	0	94
OPMG_016_Titanite	0	1	1	31	0	0	29	0	3	3	0	0	0	0	0	0	94
OPMG_016_Titanite	0	1	2	31	0	0	30	0	3	3	0	0	0	0	0	0	97
SAMPLE	K2O	BaO	F	TiO2	P2O5	Na2O	SiO2	MgO	Al2O3	FeO	MnO	Cr2O3	NiO	ZnO	SO3	O	TOTAL
OPMG_016_spinel	0	1	0	61	0	0	0	0	0	22	2	0	0	0	0	0	87
OPMG_016_spinel	0	1	0	58	0	0	0	0	0	27	9	0	0	0	0	0	96
OPMG_016_spinel	0	0	0	0	0	0	0	0	0	92	0	0	0	0	0	0	92
OPMG_016_spinel	0	0	0	0	0	0	0	0	0	92	0	0	0	0	0	0	93
SAMPLE	K2O	BaO	F	TiO2	P2O5	Na2O	SiO2	MgO	Al2O3	FeO	MnO	Cr2O3	NiO	ZnO	SO3	O	TOTAL
OPMG_016_KSP	16	0	0	0	0	0	65	0	19	0	0	0	0	0	0	0	100
OPMG_016_KSP	16	0	0	0	0	0	65	0	19	0	0	0	0	0	0	0	100

OPMG_016_KSP	16	0	0	0	0	1	65	0	19	0	0	0	0	0	0	0	100
OPMG_016_KSP	16	0	0	0	0	0	65	0	19	0	0	0	0	0	0	0	101
OPMG_016_KSP	14	0	0	0	0	2	65	0	19	0	0	0	0	0	0	0	100
OPMG_016_KSP	0	0	0	0	0	1	42	0	0	0	0	0	0	0	0	0	45
SAMPLE	K2O	BaO	F	TiO2	P2O5	Na2O	SiO2	MgO	Al2O3	FeO	MnO	Cr2O3	NiO	ZnO	SO3	O	TOTAL
OPMG_016_KSP	16	0	0	0	0	1	65	0	19	0	0	0	0	0	0	0	100
OPMG_016_KSP	16	0	0	0	0	0	65	0	19	0	0	0	0	0	0	0	100
OPMG_016_KSP	16	0	0	0	0	1	65	0	19	0	0	0	0	0	0	0	101
OPMG_016_KSP	16	0	0	0	0	0	65	0	19	0	0	0	0	0	0	0	100
OPMG_016_KSP	16	0	0	0	0	0	64	0	19	0	0	0	0	0	0	0	100
OPMG_016_KSP	16	0	0	0	0	1	65	0	19	0	0	0	0	0	0	0	101
OPMG_016_KSP	16	0	0	0	0	0	64	0	19	0	0	0	0	0	0	0	99
OPMG_016_KSP	16	0	0	0	0	1	65	0	19	0	0	0	0	0	0	0	100
OPMG_016_KSP	16	0	0	0	0	0	64	0	19	0	0	0	0	0	0	0	100
OPMG_016_KSP	16	0	0	0	0	0	64	0	18	0	0	0	0	0	0	0	99
OPMG_016_KSP	0	0	0	0	0	11	66	0	20	0	0	0	0	0	0	0	99
SAMPLE	K2O	BaO	F	TiO2	P2O5	Na2O	SiO2	MgO	Al2O3	FeO	MnO	Cr2O3	NiO	ZnO	SO3	O	TOTAL
OPMG_016_Titanite	0	1	1	34	0	0	30	0	2	3	0	0	0	0	0	0	96
OPMG_016_Titanite	0	1	1	34	0	0	29	0	2	3	0	0	0	0	0	0	95
OPMG_016_Titanite	0	1	2	32	0	0	22	0	1	3	0	0	0	0	0	0	82
OPMG_016_Titanite	0	1	1	35	0	0	27	0	2	3	0	0	0	0	0	0	92
OPMG_016_Titanite	0	1	1	33	0	0	29	0	2	3	0	0	0	0	0	0	95
OPMG_016_Titanite	0	1	1	34	0	0	30	0	2	3	0	0	0	0	0	0	96
OPMG_016_Titanite	0	1	1	33	0	0	29	0	2	3	0	0	0	0	0	0	96
SAMPLE	K2O	BaO	F	TiO2	P2O5	Na2O	SiO2	MgO	Al2O3	FeO	MnO	Cr2O3	NiO	ZnO	SO3	O	TOTAL
OPMG_016_Titanite	0	1	1	34	0	0	30	0	2	3	0	0	0	0	0	0	96
OPMG_016_Titanite	0	1	1	33	0	0	28	0	2	3	0	0	0	0	0	0	93
OPMG_016_Titanite	0	1	1	32	0	0	29	0	2	3	0	0	0	0	0	0	94
OPMG_016_Titanite	0	1	1	38	0	0	26	0	1	4	0	0	0	0	0	0	94

OPMG_016_Titanite	0	1	1	36	0	0	29	0	2	2	0	0	0	0	0	0	97
OPMG_016_Titanite	0	1	1	35	0	0	27	0	2	2	0	0	0	0	0	0	92
OPMG_016_Titanite	0	1	1	35	0	0	30	0	2	2	0	0	0	0	0	0	99
OPMG_016_Titanite	0	1	1	31	0	0	29	0	2	4	0	0	0	0	0	0	94
OPMG_016_Titanite	0	1	1	32	0	0	30	0	2	3	0	0	0	0	0	0	97
OPMG_016_Titanite	0	1	2	30	0	0	30	0	4	3	0	0	0	0	0	0	95
OPMG_016_Titanite	0	0	4	0	41	0	1	0	0	0	0	0	0	0	1	0	102
OPMG_016_Titanite	0	1	1	33	0	0	30	0	3	2	0	0	0	0	0	0	98
OPMG_016_Titanite	0	1	1	30	0	0	30	0	2	3	0	0	0	0	0	0	90
OPMG_016_Titanite	0	0	0	0	0	0	100	0	0	0	0	0	0	0	0	0	100
OPMG_016_Titanite	0	0	0	1	0	0	100	0	0	0	0	0	0	0	0	0	102
OPMG_016_Titanite	0	0	0	0	0	0	101	0	0	0	0	0	0	0	0	0	101
SAMPLE	K2O	BaO	F	TiO2	P2O5	Na2O	SiO2	MgO	Al2O3	FeO	MnO	Cr2O3	NiO	ZnO	SO3	O	TOTAL
OPMG_016_Titanite	0	1	1	34	0	0	29	0	2	3	0	0	0	0	0	0	96
OPMG_016_Titanite	0	1	1	34	0	0	29	0	2	3	0	0	0	0	0	0	96
OPMG_016_Titanite	0	1	1	35	0	0	29	0	2	2	0	0	0	0	0	0	95
OPMG_016_Titanite	0	0	1	29	0	0	27	0	2	3	0	0	0	0	0	0	86
OPMG_016_Titanite	0	1	1	41	0	0	20	0	2	3	0	0	0	0	0	0	86
OPMG_016_Titanite	0	1	1	34	0	0	29	0	2	3	0	0	0	0	0	0	96
OPMG_016_Titanite	0	1	1	34	0	0	29	0	2	3	0	0	0	0	0	0	96
OPMG_016_Titanite	0	1	1	34	0	0	29	0	2	3	0	0	0	0	0	0	96
SAMPLE	K2O	BaO	F	TiO2	P2O5	Na2O	SiO2	MgO	Al2O3	FeO	MnO	Cr2O3	NiO	ZnO	SO3	O	TOTAL
OPMG_016_KSP	15	0	0	0	0	0	61	0	18	1	2	0	0	0	0	0	98
OPMG_016_KSP	16	0	0	0	0	1	65	0	18	0	0	0	0	0	0	0	100
OPMG_016_KSP	16	0	0	0	0	1	65	0	19	0	0	0	0	0	0	0	100
OPMG_016_KSP	16	0	0	0	0	1	65	0	18	0	0	0	0	0	0	0	100
OPMG_016_KSP	16	0	0	0	0	0	65	0	19	0	0	0	0	0	0	0	101
OPMG_016_KSP	15	0	0	0	0	1	65	0	19	0	0	0	0	0	0	0	100
OPMG_016_KSP	8	0	0	0	0	6	66	0	19	0	0	0	0	0	0	0	99

OPMG_016_KSP	15	0	0	0	0	1	65	0	19	0	0	0	0	0	0	0	100
OPMG_016_KSP	15	0	0	0	0	1	65	0	19	0	0	0	0	0	0	0	100
OPMG_016_KSP	16	0	0	0	0	0	65	0	19	0	0	0	0	0	0	0	100
OPMG_016_KSP	16	0	0	0	0	1	65	0	19	0	0	0	0	0	0	0	100
OPMG_016_KSP	16	0	0	0	0	1	65	0	18	0	0	0	0	0	0	0	100
OPMG_016_KSP	15	0	0	0	0	1	65	0	18	0	0	0	0	0	0	0	100
OPMG_016_KSP	16	0	0	0	0	0	65	0	18	0	0	0	0	0	0	0	100
OPMG_016_KSP	16	0	0	0	0	1	66	0	18	0	0	0	0	0	0	0	100
OPMG_016_KSP	16	0	0	0	0	1	65	0	18	0	0	0	0	0	0	0	100
OPMG_016_KSP	16	0	0	0	0	1	65	0	18	0	0	0	0	0	0	0	100
OPMG_016_KSP	15	0	0	0	0	1	65	0	18	0	0	0	0	0	0	0	100
OPMG_016_KSP	15	0	0	0	0	1	65	0	18	0	0	0	0	0	0	0	100
OPMG_016_KSP	15	0	0	0	0	1	65	0	18	0	0	0	0	0	0	0	100
OPMG_016_KSP	15	0	0	0	0	1	65	0	19	0	0	0	0	0	0	0	100
OPMG_016_KSP	16	0	0	0	0	0	65	0	18	0	0	0	0	0	0	0	100
OPMG_016_KSP	16	0	0	0	0	1	65	0	19	0	0	0	0	0	0	0	100
OPMG_016_KSP	16	0	0	0	0	1	65	0	18	0	0	0	0	0	0	0	100

SAMPLE	K2O	BaO	F	TiO2	P2O5	Na2O	SiO2	MgO	Al2O3	FeO	MnO	Cr2O3	NiO	ZnO	SO3	O	TOTAL
OPMG_016_HORN	1	0	2	1	0	2	45	11	6	17	1	0	0	0	0	0	97
OPMG_016_HORN	1	0	2	0	0	2	46	12	7	17	1	0	0	0	0	0	99
OPMG_016_HORN	1	0	2	0	0	2	46	12	6	17	1	0	0	0	0	0	99
OPMG_016_HORN	1	0	1	0	0	1	36	9	5	14	1	0	0	0	0	0	78
OPMG_016_HORN	1	0	2	0	0	2	46	12	6	17	1	0	0	0	0	0	98
OPMG_016_HORN	1	0	2	0	0	2	45	11	7	17	1	0	0	0	0	0	98
OPMG_016_HORN	1	0	2	0	0	2	46	12	7	17	1	0	0	0	0	0	99
OPMG_016_HORN	1	0	2	0	0	2	47	12	6	17	1	0	0	0	0	0	99
OPMG_016_HORN	1	0	2	0	0	2	46	12	6	17	1	0	0	0	0	0	99
OPMG_016_HORN	1	0	2	0	0	2	46	12	6	17	1	0	0	0	0	0	99
OPMG_016_HORN	1	0	2	0	0	2	46	12	6	17	1	0	0	0	0	0	99

OPMG_016_HORN	1	0	1	0	0	2	41	10	6	15	1	0	0	0	0	0	88
OPMG_016_HORN	1	0	2	0	0	2	45	11	7	17	1	0	0	0	0	0	97
OPMG_016_HORN	1	0	2	0	0	2	46	12	7	17	1	0	0	0	0	0	99
OPMG_016_HORN	1	0	2	0	0	2	45	11	7	17	1	0	0	0	0	0	98
OPMG_016_HORN	1	0	2	0	0	2	46	12	6	17	1	0	0	0	0	0	98
OPMG_016_HORN	1	0	2	0	0	2	46	12	6	17	1	0	0	0	0	0	99
SAMPLE	K2O	BaO	F	TiO2	P2O5	Na2O	SiO2	MgO	Al2O3	FeO	MnO	Cr2O3	NiO	ZnO	SO3	O	TOTAL
OPMG_016_Plag	0	0	0	0	0	0	0	0	0	0	0	0	0	0	0	0	1
OPMG_016_Plag	0	0	0	0	0	0	0	0	0	0	0	0	0	0	0	0	1
OPMG_016_Plag	0	0	0	0	0	0	0	0	0	0	0	0	0	0	0	0	1
SAMPLE	K2O	BaO	F	TiO2	P2O5	Na2O	SiO2	MgO	Al2O3	FeO	MnO	Cr2O3	NiO	ZnO	SO3	O	TOTAL
OPMG_016_HORN	1	0	2	0	0	2	47	12	6	17	1	0	0	0	0	0	99
OPMG_016_HORN	1	0	1	0	0	1	44	6	12	12	1	0	0	0	0	0	83
OPMG_016_HORN	1	0	2	0	0	2	47	12	6	17	1	0	0	0	0	0	99
OPMG_016_HORN	1	0	1	0	0	2	47	12	6	17	1	0	0	0	0	0	99
OPMG_016_HORN	1	0	2	1	0	2	44	10	6	15	1	0	0	0	0	0	90
OPMG_016_HORN	1	0	2	0	0	2	46	12	6	17	1	0	0	0	0	0	98
OPMG_016_HORN	1	0	1	0	0	1	47	12	6	17	1	0	0	0	0	0	99
OPMG_016_HORN	1	0	2	0	0	2	47	12	6	17	1	0	0	0	0	0	99
OPMG_016_HORN	0	0	4	0	41	0	1	0	0	0	0	0	0	0	0	0	102
SAMPLE	K2O	BaO	F	TiO2	P2O5	Na2O	SiO2	MgO	Al2O3	FeO	MnO	Cr2O3	NiO	ZnO	SO3	O	TOTAL
OPMG_016_HORN	0	0	0	0	0	0	0	0	0	0	2	0	0	0	0	0	57
OPMG_016_HORN	0	0	0	0	0	0	0	0	0	0	2	0	0	0	0	0	56
OPMG_016_HORN	0	0	0	0	0	0	0	0	0	0	2	0	0	0	0	0	58
OPMG_016_HORN	0	0	0	0	0	0	0	0	0	0	2	0	0	0	0	0	57
SAMPLE	K2O	BaO	F	TiO2	P2O5	Na2O	SiO2	MgO	Al2O3	FeO	MnO	Cr2O3	NiO	ZnO	SO3	O	TOTAL
OPMG_016_Plag	0	0	0	0	0	10	62	0	19	0	0	0	0	0	0	0	95
OPMG_016_Plag	0	0	0	0	0	10	65	0	22	0	0	0	0	0	0	0	99
OPMG_016_Plag	0	0	0	0	0	10	65	0	22	0	0	0	0	0	0	0	100

OPMG_016_Plag	0	0	0	0	0	11	66	0	20	0	0	0	0	0	0	0	100
SAMPLE	K2O	BaO	F	TiO2	P2O5	Na2O	SiO2	MgO	Al2O3	FeO	MnO	Cr2O3	NiO	ZnO	SO3	O	TOTAL
OPMG_016_BIO	10	0	3	1	0	0	40	17	12	15	1	0	0	0	0	0	99
OPMG_016_BIO	10	0	3	1	0	0	39	16	12	15	1	0	0	0	0	0	99
OPMG_016_BIO	10	0	3	1	0	0	39	16	12	15	1	0	0	0	0	0	98
OPMG_016_BIO	10	0	4	1	0	0	39	16	12	15	1	0	0	0	0	0	99
OPMG_016_BIO	10	0	3	1	0	0	39	16	12	15	1	0	0	0	0	0	99
OPMG_016_BIO	10	0	3	1	0	0	39	16	12	16	1	0	0	0	0	0	99
OPMG_016_BIO	10	0	3	1	0	0	39	16	12	15	1	0	0	0	0	0	99
OPMG_016_BIO	10	0	4	1	0	0	39	16	12	15	1	0	0	0	0	0	99
OPMG_016_BIO	10	0	4	1	0	0	40	17	12	14	1	0	0	0	0	0	99
SAMPLE	K2O	BaO	F	TiO2	P2O5	Na2O	SiO2	MgO	Al2O3	FeO	MnO	Cr2O3	NiO	ZnO	SO3	O	TOTAL
OPMG_016_HORN	10	0	4	1	0	0	41	18	11	13	1	0	0	0	0	0	99
OPMG_016_HORN	10	0	3	0	0	0	40	18	12	14	1	0	0	0	0	0	98
OPMG_016_HORN	1	0	1	0	0	1	53	10	5	16	1	0	0	0	0	0	99
OPMG_016_HORN	1	0	1	0	0	1	47	11	6	17	1	0	0	0	0	0	97
OPMG_016_HORN	1	0	1	0	0	1	47	12	6	17	1	0	0	0	0	0	99
OPMG_016_HORN	1	0	1	0	0	1	44	10	7	16	1	0	0	0	0	0	92
OPMG_016_HORN	1	0	1	1	0	2	46	12	6	17	1	0	0	0	0	0	98
OPMG_016_HORN	1	0	1	0	0	2	46	12	6	17	1	0	0	0	0	0	99
OPMG_016_HORN	1	0	2	0	0	2	46	11	6	17	1	0	0	0	0	0	98
OPMG_016_HORN	1	0	1	0	0	2	47	12	6	17	1	0	0	0	0	0	99
OPMG_016_HORN	1	0	1	0	0	2	46	11	6	17	1	0	0	0	0	0	98
OPMG_016_HORN	1	0	2	0	0	2	46	12	6	17	1	0	0	0	0	0	99

EMPA data of pyrite in samples ENCLAVE009 and HYBRID006A

SAMPLE	Fe WT%	Ni WT%	Zn WT%	S WT%	Cu WT%	As WT%	O WT%	TOTAL
009_001 - Pyrite	46.66	0	0	54.15	0.04	0.01	0	100.86
009_001 - Pyrite	46.73	0.17	0	54.10	0	0.06	0	101.06
009_001 - Pyrite	46.63	0	0	54.03	0	0.01	0	100.68
009_001 - Pyrite	45.03	1.47	0	53.92	0.01	0.03	0	100.46
006A_016 - pyrite	44.69	0.03	0	53.88	0	0.03	0	98.62
006A_016 - pyrite	46.15	0	0	53.56	0	0	0	99.71
006A_016 - pyrite	46.32	0	03	53.21	0.02	0.03	0	99.58
006A_016 - pyrite	46.45	0.01	0.02	53.64	0	0	0	100.12
009_012 - Pyrite	45.36	0	0	53.53	0	0.04	0	98.93
009_012 - Pyrite	45.44	0	0	53.08	0	0	0	98.51
009_012 - Pyrite	45.74	0	0.01	53.41	0.03	0.07	0	99.26
009_012 - Pyrite	46.17	0.19	0	53.01	0	0.03	0	99.39

APPENDIX C

LA-ICP-MS REE element data

Analysis	139La	140Ce	141Pr	146Nd	147Sm	153Eu	157Gd	159Tb	163Dy	165Ho	166Er	169Tm	172Yb	175Lu
OPMG_009_Anorthite - 1	3.4	5.1	0.4	1.5	0.2	0.6	0.2	0.0	0.1	0.0	0.0	0.0	0.0	0.0
OPMG_009_Anorthite - 2	2.2	3.8	0.4	1.5	0.2	0.6	0.1	0.0	0.0	0.0	0.0	0.0	0.0	0.0
OPMG_009_Anorthite - 3	2.9	4.1	0.4	1.4	0.2	0.5	0.2	0.0	0.1	0.0	0.1	0.0	0.1	0.0
OPMG_009_Anorthite - 4	2.1	3.0	0.3	1.2	0.1	0.5	0.2	0.0	0.2	0.0	0.2	0.0	0.1	0.0
OPMG_009_Anorthite - 5	1.8	3.2	0.3	1.2	0.2	0.6	0.2	0.0	0.1	0.0	0.0	0.0	0.0	0.0
OPMG_009_Anorthite - 6	1.7	3.2	0.3	1.3	0.1	0.5	0.2	0.0	0.1	0.0	0.0	0.0	0.0	0.0
OPMG_009_Anorthite - 7	2.3	4.0	0.4	1.7	0.2	0.6	0.2	0.0	0.1	0.0	0.1	0.0	0.0	0.0
OPMG_009_Anorthite - 8	2.5	3.7	0.4	1.4	0.2	0.5	0.2	0.0	0.2	0.0	0.1	0.0	0.1	0.0
OPMG_009_Anorthite - 9	1.5	2.8	0.3	1.2	0.2	0.5	0.1	0.0	0.1	0.0	0.0	0.0	0.0	0.0
OPMG_009_Anorthite - 10	1.7	2.9	0.3	1.3	0.2	0.6	0.2	0.0	0.1	0.0	0.0	0.0	0.0	0.0
OPMG_009_Anorthite - 11	3.2	5.1	0.5	2.1	0.2	0.6	0.2	0.0	0.1	0.0	0.1	0.0	0.0	0.0
OPMG_009_Anorthite_rim - 1	8.0	10.6	0.9	3.0	0.4	1.0	0.2	0.0	0.2	0.0	0.1	0.0	0.1	0.0
OPMG_009_Anorthite_rim - 2	4.8	6.8	0.6	1.8	0.3	1.0	0.1	0.0	0.1	0.0	0.0	0.0	0.0	0.0
OPMG_009_Anorthite_rim - 3	1.9	1.7	0.1	0.3	0.1	0.2	0.1	0.0	0.0	0.0	0.0	0.0	0.0	0.0
OPMG_009_Anorthite_rim - 4	2.3	4.0	0.4	1.4	0.2	0.6	0.3	0.0	0.1	0.0	0.0	0.0	0.1	0.0
OPMG_009_Anorthite_rim - 5	2.0	3.5	0.4	1.5	0.3	0.7	0.2	0.0	0.1	0.0	0.0	0.0	0.0	0.0
OPMG_009_Anorthite_rim - 6	2.8	4.6	0.5	1.7	0.3	0.6	0.2	0.0	0.0	0.0	0.0	0.0	0.0	0.0
OPMG_009_Anorthite_rim - 7	7.1	7.0	0.5	1.5	0.2	0.5	0.2	0.0	0.1	0.0	0.1	0.0	0.1	0.0
OPMG_009_Anorthite_rim - 8	1.9	3.3	0.3	1.4	0.1	0.6	0.3	0.0	0.1	0.0	0.0	0.0	0.0	0.0
OPMG_009_Anorthite_rim - 9	9.9	11.2	0.8	2.5	0.3	1.0	0.1	0.0	0.1	0.0	0.0	0.0	0.1	0.0
OPMG_009_Titan - 1	1490.5	3275.4	321.7	1182.3	222.2	84.3	211.6	32.8	215.9	45.3	145.5	21.5	155.2	22.5
OPMG_009_Titan - 2	1593.7	3524.9	350.1	1276.8	229.2	89.8	214.3	32.3	213.2	44.7	142.5	21.2	155.3	22.7
OPMG_009_Titan - 3	2842.9	5930.8	559.6	1950.9	324.5	134.3	288.6	42.5	278.6	58.2	187.9	28.2	208.4	30.9
OPMG_009_Titan - 4	2720.5	5754.2	551.6	1935.5	328.0	132.1	294.2	43.5	283.4	59.4	190.4	28.2	207.6	30.2

OPMG_009_Titan - 5	2634.5	5609.3	540.8	1930.1	338.1	129.9	308.4	46.1	300.5	62.9	200.7	29.5	213.3	31.1
OPMG_009_Titan - 6	2667.4	5638.7	545.4	1955.9	345.1	132.1	319.7	48.5	317.6	66.5	212.6	31.4	228.4	33.3
OPMG_009_Titan - 7	1731.5	3968.5	414.7	1575.9	311.8	98.7	302.0	46.4	302.0	61.9	191.3	27.1	190.2	26.6
OPMG_009_Titan - 8	1539.3	3436.4	349.4	1312.5	254.7	87.0	245.7	37.8	247.6	51.3	161.5	23.1	163.8	23.5
OPMG_009_Titan - 9	1475.2	3211.6	317.8	1170.0	220.6	83.4	211.4	32.5	214.2	45.1	143.9	21.2	152.9	22.4
OPMG_009_Titan - 10	1462.0	3172.4	314.7	1153.3	216.8	82.6	208.8	31.9	212.8	44.4	142.1	20.8	150.7	22.0
OPMG_009_Titan - 11	1531.7	3293.2	317.0	1115.6	191.2	77.9	173.4	25.6	165.2	34.6	111.1	16.5	120.4	17.7
OPMG_009_Titan - 12	1413.4	3158.5	316.4	1156.7	214.8	78.7	201.7	30.7	202.1	41.6	131.5	19.2	136.7	19.2
OPMG_009_Titan - 13	3059.5	6631.2	646.7	2311.4	410.8	150.6	380.8	57.4	376.5	78.8	251.0	37.0	268.1	38.5
OPMG_009_Titan - 14	2620.8	5331.5	502.7	1748.4	299.7	113.4	270.9	40.3	259.8	53.7	167.9	24.2	171.6	24.5
OPMG_009_KSP - 1	1.5	0.6	0.0	0.1	0.0	0.2	0.0	0.0	0.0	0.0	0.0	0.0	0.0	0.0
OPMG_009_KSP - 2	1.4	0.5	0.0	0.0	0.0	0.2	0.0	0.0	0.0	0.0	0.0	0.0	0.0	0.0
OPMG_009_KSP - 3	1.6	0.7	0.0	0.1	0.0	0.3	0.0	0.0	0.0	0.0	0.0	0.0	0.0	0.0
OPMG_009_KSP - 4	1.4	0.9	0.0	0.1	0.0	0.3	0.0	0.0	0.0	0.0	0.0	0.0	0.0	0.0
OPMG_009_KSP - 5	1.8	1.1	0.0	0.1	0.0	0.3	0.0	0.0	0.0	0.0	0.0	0.0	0.0	0.0
OPMG_009_KSP - 6	1.3	0.6	0.0	0.0	0.0	0.2	0.0	0.0	0.0	0.0	0.0	0.0	0.0	0.0
OPMG_009_KSPrim - 1	1.2	0.4	0.0	0.0	0.0	0.3	0.0	0.0	0.0	0.0	0.0	0.0	0.0	0.0
OPMG_009_KSPrim - 2	2.6	1.2	0.1	0.1	0.0	0.2	0.0	0.0	0.0	0.0	0.0	0.0	0.0	0.0
OPMG_009_KSPrim - 3	1.1	0.3	0.0	0.0	0.0	0.1	0.0	0.0	0.0	0.0	0.0	0.0	0.0	0.0
OPMG_009_KSPrim - 4	2.6	1.5	0.1	0.2	0.0	0.2	0.0	0.0	0.0	0.0	0.0	0.0	0.1	0.0
OPMG_009_KSPrim - 5	2.6	1.5	0.1	0.1	0.0	0.2	0.0	0.0	0.0	0.0	0.0	0.0	0.0	0.0
OPMG_009_KSPrim - 6	3.1	1.4	0.0	0.1	0.0	0.2	0.0	0.0	0.0	0.0	0.0	0.0	0.0	0.0
OPMG_009_KSPrim - 7	2.9	1.2	0.0	0.1	0.0	0.2	0.0	0.0	0.0	0.0	0.0	0.0	0.0	0.0
OPMG_009_BIO - 1	4.9	9.6	1.1	3.7	0.6	0.1	0.5	0.1	0.5	0.1	0.3	0.0	0.3	0.0
OPMG_009_BIO - 2	4.9	9.5	1.1	4.1	0.6	0.1	0.5	0.1	0.5	0.1	0.3	0.0	0.4	0.0
OPMG_009_BIO - 3	4.9	9.6	1.1	3.8	0.7	0.1	0.4	0.1	0.5	0.1	0.3	0.0	0.3	0.0
OPMG_009_BIO - 4	4.8	9.6	1.1	3.7	0.6	0.1	0.6	0.1	0.4	0.1	0.2	0.0	0.3	0.0
OPMG_009_BIO - 5	4.9	9.6	1.1	3.7	0.7	0.1	0.5	0.1	0.5	0.1	0.3	0.0	0.3	0.0
OPMG_009_matrix - 1	620.5	698.7	52.6	169.6	24.6	4.9	23.7	2.8	16.7	3.4	10.1	1.2	7.9	1.3

OPMG_009_matrix - 2	28.0	45.6	3.7	10.0	0.8	0.3	0.5	0.0	0.2	0.0	0.1	0.0	0.1	0.0
OPMG_009_matrix - 3	20.1	39.8	4.5	17.6	3.4	0.7	3.5	0.5	2.7	0.5	1.2	0.2	1.3	0.3
OPMG_009_matrix - 4	58.9	78.5	7.1	25.3	4.5	1.0	4.2	0.5	2.6	0.5	1.3	0.2	1.4	0.3
OPMG_009_matrix - 5	5.2	6.0	0.3	0.8	0.1	0.1	0.1	0.0	0.1	0.0	0.1	0.0	0.1	0.0
OPMG_009_matrix - 6	12.4	20.7	2.1	8.1	1.5	0.4	1.5	0.2	1.1	0.2	0.6	0.1	0.6	0.1
OPMG_009_matrix - 7	2.8	1.2	0.1	0.2	0.0	0.1	0.0	0.0	0.0	0.0	0.0	0.0	0.0	0.0
OPMG_009_matrix - 8	4.4	1.8	0.1	0.1	0.0	0.1	0.0	0.0	0.0	0.0	0.0	0.0	0.0	0.0
OPMG_009_horn - 1	16.2	26.4	2.5	9.1	1.5	0.4	1.7	0.2	1.3	0.2	0.8	0.1	1.0	0.2
OPMG_009_horn - 2	19.3	33.4	3.3	12.2	2.1	0.5	2.3	0.3	1.5	0.3	1.1	0.1	1.1	0.3
OPMG_009_horn - 3	14.4	25.7	2.4	8.3	1.7	0.4	1.6	0.3	1.4	0.4	0.9	0.1	0.9	0.2
OPMG_009_horn - 4	19.7	35.2	3.7	14.2	3.0	0.7	3.0	0.5	3.1	0.6	1.8	0.2	1.6	0.3
OPMG_009_Titian - 1	1028.0	2361.3	256.0	1055.6	229.5	49.9	231.5	34.8	220.0	42.8	122.3	15.8	102.8	14.4
OPMG_009_Titian - 2	840.8	1794.2	173.4	667.3	134.2	42.0	136.6	20.7	134.2	27.9	85.2	12.0	87.1	13.8
OPMG_009_Titian - 3	1397.6	2901.5	284.0	1071.9	205.5	68.1	202.4	30.9	202.7	41.8	130.6	18.8	136.3	20.5
OPMG_009_Titian - 4	2123.0	4711.5	475.2	1768.1	330.0	105.7	312.6	47.5	308.2	62.8	194.9	27.7	194.6	27.3
OPMG_009_Titian - 5	2265.3	4612.3	423.4	1442.3	240.7	112.1	216.3	32.9	214.7	45.2	144.5	21.7	159.8	23.8
OPMG_009_Titian - 6	1905.5	3903.6	360.8	1240.1	207.8	93.2	186.3	28.0	181.5	37.8	121.0	18.1	132.9	19.9
OPMG_009_Titian - 7	2299.1	4696.7	439.2	1518.8	252.1	104.1	227.6	33.9	219.8	46.0	146.5	21.6	159.1	23.5
OPMG_009_Titian_rim - 1	1862.7	4118.3	417.8	1580.1	302.0	95.2	289.4	44.2	288.2	59.6	183.5	26.3	185.5	26.4
OPMG_009_Titian_rim - 2	1348.4	2791.6	273.5	1033.8	199.5	65.9	198.4	30.3	198.6	41.1	127.4	18.4	133.2	20.2
OPMG_009_Titian_rim - 3	1099.2	2273.7	221.3	844.5	166.3	54.7	168.5	25.6	169.0	34.9	108.8	15.6	113.0	17.4
OPMG_009_Titian_rim - 4	805.5	1723.2	169.1	658.8	133.2	39.6	136.1	20.8	134.4	27.4	83.1	11.7	82.7	13.1
OPMG_009_Titian_rim - 5	755.1	1694.6	177.1	721.2	154.4	37.6	158.3	24.0	155.3	30.8	92.5	12.5	86.6	13.0
OPMG_009_KSP - 7	2.1	0.7	0.0	0.0	0.0	0.2	0.0	0.0	0.0	0.0	0.0	0.0	0.0	0.0
OPMG_009_KSP - 8	1.0	0.4	0.0	0.0	0.0	0.3	0.0	0.0	0.0	0.0	0.0	0.0	0.0	0.0
OPMG_009_KSP - 9	1.2	0.5	0.0	0.0	0.0	0.2	0.0	0.0	0.0	0.0	0.0	0.0	0.0	0.0
OPMG_009_KSP - 10	1.2	0.3	0.0	0.0	0.0	0.2	0.0	0.0	0.0	0.0	0.0	0.0	0.0	0.0
OPMG_009_KSP - 11	1.1	0.3	0.0	0.0	0.0	0.2	0.0	0.0	0.0	0.0	0.0	0.0	0.0	0.0
OPMG_009_KSP - 12	1.2	0.3	0.0	0.0	0.0	0.1	0.0	0.0	0.0	0.0	0.0	0.0	0.0	0.0

OPMG_009_KSP_rim - 1	2.5	0.9	0.0	0.0	0.0	0.2	0.0	0.0	0.0	0.0	0.0	0.0	0.0	0.0
OPMG_009_KSP_rim - 2	2.2	0.8	0.0	0.1	0.0	0.2	0.0	0.0	0.0	0.0	0.0	0.0	0.0	0.0
OPMG_009_KSP_rim - 3	2.3	0.7	0.0	0.0	0.0	0.2	0.0	0.0	0.0	0.0	0.0	0.0	0.0	0.0
OPMG_009_KSP_rim - 4	1.0	0.3	0.0	0.0	0.0	0.1	0.0	0.0	0.0	0.0	0.0	0.0	0.0	0.0
OPMG_009_KSP_rim - 5	1.7	0.8	0.0	0.1	0.0	0.0	0.0	0.0	0.0	0.0	0.0	0.0	0.0	0.0
OPMG_009_KSP_rim - 6	1.4	0.4	0.0	0.0	0.0	0.2	0.0	0.0	0.0	0.0	0.0	0.0	0.0	0.0
OPMG_009_KSP_rim - 7	1.9	0.6	0.0	0.1	0.0	0.1	0.0	0.0	0.0	0.0	0.0	0.0	0.0	0.0
OPMG_009_KSP_rim - 8	2.9	1.3	0.0	0.1	0.0	0.2	0.0	0.0	0.0	0.0	0.0	0.0	0.0	0.0
OPMG_009_KSP_rim - 9	1.2	0.4	0.0	0.0	0.0	0.2	0.0	0.0	0.0	0.0	0.0	0.0	0.0	0.0
OPMG_009_KSP_rim - 10	1.3	0.4	0.0	0.1	0.0	0.1	0.0	0.0	0.0	0.0	0.0	0.0	0.0	0.0
OPMG_009_horn_rining - 1	17.5	29.8	2.9	11.1	2.0	0.6	2.3	0.3	1.9	0.4	1.0	0.1	1.0	0.3
OPMG_009_horn_rining - 2	24.4	59.5	7.5	33.7	7.7	1.2	8.1	1.0	5.5	1.0	2.4	0.3	1.7	0.3
OPMG_009_horn_rining - 3	24.4	53.1	6.7	29.3	6.6	0.9	5.9	0.7	4.1	0.7	1.6	0.2	1.5	0.3
OPMG_009_horn_rining - 4	27.3	59.0	7.0	29.7	6.7	1.1	6.5	0.8	4.5	0.8	1.8	0.2	1.3	0.3
OPMG_009_horn_rining - 5	22.5	43.3	4.9	19.6	4.0	0.7	3.8	0.5	2.8	0.5	1.3	0.2	1.1	0.3
OPMG_009_horn_rining - 6	14.0	25.1	2.7	10.5	2.1	0.6	2.8	0.3	2.2	0.5	1.4	0.2	1.5	0.3
OPMG_009_horn_rining - 7	11.3	22.1	2.5	9.4	2.2	0.5	2.6	0.4	2.6	0.5	1.4	0.2	1.6	0.4
OPMG_009_horn_rining - 8	14.3	28.3	3.3	12.9	2.9	0.6	3.5	0.5	3.3	0.7	2.1	0.2	1.9	0.3
OPMG_009_horn_rining - 9	4.9	9.7	1.3	4.0	0.6	0.1	0.5	0.1	0.4	0.1	0.2	0.0	0.2	0.1
OPMG_009_horn_rining - 10	17.5	31.1	3.3	12.5	2.5	0.6	2.9	0.4	2.7	0.5	1.5	0.2	1.6	0.3
OPMG_009_horn_rining - 11	15.2	28.8	3.3	13.9	2.9	0.8	3.2	0.5	2.9	0.6	1.7	0.2	1.6	0.4
OPMG_009_horn_rining - 12	10.6	20.6	2.3	9.7	2.2	0.5	2.5	0.4	2.5	0.5	1.6	0.2	1.5	0.3
OPMG_009_horn_rining - 13	13.8	22.4	2.3	9.3	2.4	0.4	2.5	0.4	2.6	0.5	1.7	0.2	1.6	0.3
OPMG_009_horn_rining - 14	11.1	22.0	2.6	10.6	2.8	0.5	3.1	0.5	3.3	0.6	2.1	0.3	1.7	0.4
OPMG_009_horn_rining - 15	14.4	27.6	3.2	12.9	2.9	0.7	3.2	0.5	3.3	0.6	2.0	0.3	2.0	0.4
OPMG_009_horn_rining - 16	15.8	27.5	2.9	11.5	2.9	0.6	2.9	0.4	2.8	0.6	1.7	0.2	1.9	0.3
OPMG_009_horn_rining - 17	13.1	26.4	3.1	12.9	3.0	0.6	2.9	0.5	3.3	0.7	1.8	0.3	1.7	0.3
OPMG_009_horn_rining - 18	14.4	27.5	3.0	11.8	2.5	0.6	3.0	0.5	2.9	0.6	1.8	0.2	1.8	0.4
OPMG_009_horn_rining - 19	18.4	32.2	3.3	13.4	2.9	0.7	2.7	0.4	2.8	0.6	1.6	0.2	1.8	0.4

OPMG_009_horn_rining - 20	21.0	38.9	4.3	16.4	3.5	0.9	3.4	0.6	3.7	0.7	2.2	0.3	2.2	0.4
OPMG_009_horn_rining - 21	13.0	24.0	2.6	10.4	2.6	0.6	2.5	0.4	2.7	0.6	1.7	0.2	1.7	0.4
OPMG_009_BIO - 6	0.0	0.0	0.0	0.0	0.0	0.0	0.0	0.0	0.0	0.0	0.0	0.0	0.0	0.0
OPMG_009_BIO - 7	0.0	0.0	0.0	0.0	0.0	0.0	0.0	0.0	0.0	0.0	0.0	0.0	0.0	0.0
OPMG_009_BIO - 8	0.0	0.0	0.0	0.0	0.0	0.0	0.0	0.0	0.0	0.0	0.0	0.0	0.0	0.0
OPMG_009_BIO - 9	0.1	0.1	0.0	0.0	0.0	0.0	0.0	0.0	0.0	0.0	0.0	0.0	0.0	0.0
OPMG_009_BIO - 10	0.0	0.1	0.0	0.0	0.0	0.0	0.0	0.0	0.0	0.0	0.0	0.0	0.0	0.0
OPMG_009_BIO - 11	0.2	0.4	0.1	0.2	0.0	0.0	0.1	0.0	0.1	0.0	0.1	0.0	0.1	0.0
OPMG_009_BIO - 12	0.0	0.0	0.0	0.0	0.0	0.0	0.0	0.0	0.0	0.0	0.0	0.0	0.0	0.0
OPMG_009_matrix - 9	2.5	1.5	0.1	0.3	0.1	0.1	0.0	0.0	0.0	0.0	0.0	0.0	0.0	0.0
OPMG_009_matrix - 10	7.0	5.3	0.3	1.1	0.1	0.1	0.1	0.0	0.1	0.0	0.0	0.0	0.1	0.0
OPMG_009_matrix - 11	22.7	27.4	2.2	7.8	1.1	0.2	1.0	0.1	0.9	0.2	0.6	0.1	0.7	0.1
OPMG_009_matrix - 12	1.4	0.3	0.0	0.0	0.0	0.1	0.0	0.0	0.0	0.0	0.0	0.0	0.0	0.0
OPMG_009_matrix - 13	3.6	2.1	0.1	0.3	0.0	0.1	0.0	0.0	0.0	0.0	0.0	0.0	0.0	0.0
OPMG_009_matrix - 14	5.7	4.2	0.3	0.7	0.1	0.2	0.1	0.0	0.1	0.0	0.0	0.0	0.0	0.0
OPMG_009_matrix - 15	4.5	4.2	0.3	1.1	0.3	0.1	0.3	0.0	0.2	0.0	0.1	0.0	0.1	0.0
OPMG_009_Titan_ - 1	1326.4	2982.4	329.7	1369.7	297.4	61.2	294.8	43.5	271.7	52.4	149.1	18.7	117.1	15.8
OPMG_009_Titan_ - 2	1043.7	2220.0	225.4	903.2	190.5	47.1	196.1	29.6	188.3	37.8	114.2	15.1	101.4	15.2
OPMG_009_Titan_ - 3	838.0	1777.2	172.9	677.3	142.1	41.8	147.5	22.7	148.2	30.8	95.6	13.2	94.6	14.8
OPMG_009_Titan_ - 4	780.4	1410.3	120.3	426.1	80.0	40.7	80.9	12.3	82.1	17.3	56.1	8.3	62.4	10.3
OPMG_009_Titan_ - 5	1024.1	1600.9	121.3	382.6	62.1	45.6	59.7	9.0	59.7	12.9	43.3	6.7	52.3	9.2
OPMG_009_horn - 5	21.3	42.4	5.0	22.2	5.6	1.1	6.7	1.1	7.7	1.7	5.8	0.8	5.5	0.8
OPMG_009_horn - 6	31.2	76.4	9.9	42.7	10.1	1.8	10.8	1.6	10.7	2.2	6.3	0.8	5.3	0.8
OPMG_009_BIO - 13	0.0	0.0	0.0	0.0	0.0	0.0	0.0	0.0	0.0	0.0	0.0	0.0	0.0	0.0
OPMG_009_BIO - 14	0.0	0.0	0.0	0.0	0.0	0.0	0.0	0.0	0.0	0.0	0.0	0.0	0.0	0.0
OPMG_009_BIO - 15	0.0	0.0	0.0	0.0	0.0	0.0	0.0	0.0	0.0	0.0	0.0	0.0	0.0	0.0
OPMG_009_BIO - 16	0.0	0.0	0.0	0.0	0.0	0.0	0.0	0.0	0.0	0.0	0.0	0.0	0.0	0.0
OPMG_009_BIO - 17	0.1	0.1	0.0	0.0	0.0	0.0	0.0	0.0	0.0	0.0	0.0	0.0	0.0	0.0
OPMG_009_BIO - 18	0.0	0.0	0.0	0.0	0.0	0.0	0.0	0.0	0.0	0.0	0.0	0.0	0.0	0.0

OPMG_009_BIO - 19	0.0	0.0	0.0	0.0	0.0	0.0	0.0	0.0	0.0	0.0	0.0	0.0	0.0	0.0
OPMG_009_BIO - 20	0.0	0.0	0.0	0.0	0.0	0.0	0.0	0.0	0.0	0.0	0.0	0.0	0.0	0.0
OPMG_009_KSP - 13	2.1	0.7	0.0	0.1	0.0	0.2	0.0	0.0	0.0	0.0	0.0	0.0	0.0	0.0
OPMG_009_KSP - 14	7.7	6.3	0.4	1.2	0.2	0.3	0.1	0.0	0.1	0.0	0.1	0.0	0.1	0.0
OPMG_009_KSP - 15	1.9	0.6	0.0	0.0	0.0	0.5	0.0	0.0	0.0	0.0	0.0	0.0	0.0	0.0
OPMG_009_KSP - 16	40.6	52.1	4.0	11.7	1.3	0.8	1.0	0.1	0.7	0.1	0.2	0.0	0.1	0.0
OPMG_009_KSP - 17	1.5	1.6	0.1	0.4	0.1	0.7	0.1	0.0	0.1	0.0	0.1	0.0	0.1	0.0
OPMG_009_KSP_rim - 11	2.8	1.2	0.0	0.0	0.0	0.2	0.0	0.0	0.0	0.0	0.0	0.0	0.0	0.0
OPMG_009_KSP_rim - 12	3.1	1.8	0.1	0.4	0.0	0.2	0.1	0.0	0.0	0.0	0.0	0.0	0.0	0.0
OPMG_009_KSP_rim - 13	1.8	1.1	0.1	0.2	0.0	0.2	0.0	0.0	0.1	0.0	0.1	0.0	0.1	0.0
OPMG_009_KSP_rim - 14	1.1	0.5	0.0	0.1	0.0	0.1	0.0	0.0	0.0	0.0	0.0	0.0	0.0	0.0
OPMG_009_KSP_rim - 15	1.3	0.4	0.0	0.0	0.0	0.2	0.0	0.0	0.0	0.0	0.0	0.0	0.0	0.0
OPMG_009_KSP_rim - 16	1.1	0.7	0.0	0.1	0.0	0.3	0.0	0.0	0.0	0.0	0.0	0.0	0.0	0.0
OPMG_002_titan - 1	6107.2	18535.0	2035.8	7094.3	1220.1	184.0	1101.0	189.8	1336.5	286.4	908.2	122.3	745.3	84.4
OPMG_002_titan - 2	6225.6	18988.6	2099.1	7410.5	1217.2	176.0	1048.7	162.6	1060.3	221.6	688.1	94.6	590.3	71.9
OPMG_002_titan - 3	6141.8	19472.9	2216.1	7995.7	1341.6	182.4	1133.2	173.5	1121.3	230.6	710.0	96.6	604.7	73.4
OPMG_002_titan - 4	5738.2	18341.4	2108.7	7652.8	1376.6	190.0	1243.6	206.9	1415.3	299.8	937.3	127.3	789.3	91.9
OPMG_002_titan - 5	5760.2	18567.3	2229.0	8489.8	1675.8	230.7	1511.4	243.6	1560.1	309.8	909.4	116.3	701.1	80.2
OPMG_002_titan - 6	8271.5	14039.7	1132.1	3639.4	501.3	63.8	447.1	56.7	350.0	73.0	228.1	30.4	211.9	37.4
OPMG_002_titan - 7	6256.5	13322.6	1199.8	4159.9	607.4	93.1	547.8	70.0	412.7	86.3	263.5	34.1	232.3	40.0
OPMG_002_titan - 8	7978.9	16712.7	1550.9	5434.4	810.0	119.2	673.2	87.5	515.2	103.5	302.4	38.1	253.0	42.6
OPMG_002_mank - 1	1024.3	2410.7	297.0	1108.8	203.3	24.8	159.5	21.6	127.4	22.9	56.9	5.9	34.4	4.2
OPMG_002_mank - 2	81.9	278.5	45.3	222.2	60.6	4.9	64.0	10.0	61.7	11.3	29.5	3.4	19.5	3.0
OPMG_002_mank - 3	5.5	11.1	1.3	5.1	0.8	0.2	0.7	0.1	0.5	0.1	0.4	0.0	0.5	0.0
OPMG_002_mank - 4	9.8	19.2	2.1	7.5	1.3	0.2	1.1	0.2	0.8	0.2	0.5	0.1	0.6	0.1
OPMG_002_mank - 5	7.0	11.6	1.9	7.9	1.5	0.2	1.2	0.2	0.9	0.1	0.4	0.0	0.2	0.0
OPMG_002_KSP - 1	9.1	11.2	0.9	2.9	0.3	0.1	0.2	0.0	0.1	0.0	0.1	0.0	0.1	0.0
OPMG_002_KSP - 2	5.0	2.1	0.1	0.1	0.0	1.1	0.0	0.0	0.0	0.0	0.0	0.0	0.0	0.0
OPMG_002_KSP - 3	3.2	1.0	0.0	0.0	0.0	0.6	0.0	0.0	0.0	0.0	0.0	0.0	0.0	0.0

OPMG_002_KSP - 4	5.0	2.5	0.1	0.5	0.1	0.5	0.1	0.0	0.1	0.0	0.0	0.0	0.1	0.0
OPMG_002_KSP - 5	451.3	794.0	71.0	226.4	30.3	4.7	21.0	2.8	17.0	3.3	8.6	0.9	4.8	0.6
OPMG_002_KSP - 6	6.0	3.1	0.1	0.3	0.1	0.4	0.0	0.0	0.0	0.0	0.0	0.0	0.1	0.0
OPMG_002_BIO - 1	1.1	2.8	0.4	1.9	0.3	0.1	0.2	0.0	0.1	0.0	0.1	0.0	0.1	0.0
OPMG_002_BIO - 2	1.3	3.2	0.4	1.7	0.3	0.0	0.2	0.0	0.1	0.0	0.1	0.0	0.1	0.0
OPMG_002_BIO - 3	3.3	8.6	1.1	4.5	0.7	0.1	0.6	0.1	0.3	0.1	0.1	0.0	0.1	0.0
OPMG_002_BIO - 4	0.9	2.9	0.4	1.8	0.3	0.1	0.2	0.0	0.1	0.0	0.1	0.0	0.1	0.0
OPMG_002_BIO - 5	0.8	2.2	0.3	1.3	0.2	0.0	0.1	0.0	0.1	0.0	0.0	0.0	0.0	0.0
OPMG_002_BIO - 6	5024.4	12691.0	1425.1	4987.1	880.3	139.2	775.5	120.7	775.2	154.3	465.6	64.3	431.6	57.4
OPMG_002_BIO - 7	0.1	0.4	0.1	0.2	0.1	0.0	0.0	0.0	0.1	0.0	0.0	0.0	0.0	0.0
OPMG_002_idk - 1	0.7	1.7	0.3	1.1	0.2	0.0	0.2	0.0	0.1	0.0	0.1	0.0	0.0	0.0
OPMG_002_idk - 2	0.7	1.5	0.2	0.9	0.1	0.0	0.1	0.0	0.1	0.0	0.0	0.0	0.0	0.0
OPMG_002_idk - 3	0.9	2.0	0.2	1.0	0.1	0.0	0.1	0.0	0.1	0.0	0.1	0.0	0.0	0.0
OPMG_002_idk - 4	0.7	1.5	0.2	0.9	0.2	0.0	0.1	0.0	0.1	0.0	0.0	0.0	0.0	0.0
OPMG_002_idk - 5	4.1	9.0	1.2	5.0	0.8	0.1	0.7	0.1	0.4	0.1	0.2	0.0	0.1	0.0
OPMG_002_idk - 6	0.0	0.0	0.0	0.0	0.0	0.0	0.0	0.0	0.0	0.0	0.0	0.0	0.0	0.0
OPMG_002_idk - 7	0.5	1.0	0.1	0.6	0.1	0.0	0.1	0.0	0.0	0.0	0.0	0.0	0.0	0.0
OPMG_002_idk - 8	1.3	3.2	0.4	1.8	0.3	0.0	0.2	0.0	0.2	0.0	0.1	0.0	0.1	0.0
OPMG_002_KSP - 7	3.4	1.8	0.1	0.2	0.0	0.3	0.0	0.0	0.0	0.0	0.0	0.0	0.0	0.0
OPMG_002_KSP - 8	11.1	11.8	0.7	2.4	0.4	0.5	0.4	0.1	0.8	0.2	0.6	0.1	0.7	0.1
OPMG_002_KSP - 9	2.7	1.7	0.1	0.3	0.0	0.4	0.1	0.0	0.1	0.0	0.1	0.0	0.1	0.0
OPMG_002_KSP - 10	9.5	15.2	0.9	2.9	0.4	0.4	0.3	0.0	0.3	0.1	0.2	0.0	0.2	0.0
OPMG_002_KSP_matrix - 1	8.4	5.7	0.3	0.7	0.1	0.3	0.0	0.0	0.1	0.0	0.0	0.0	0.0	0.0
OPMG_002_KSP_matrix - 2	4.6	9.1	1.0	3.7	0.7	0.1	0.5	0.1	0.4	0.1	0.3	0.0	0.3	0.0
OPMG_002_KSP_matrix - 3	11.7	15.2	1.3	4.1	0.5	0.4	0.4	0.1	0.3	0.1	0.2	0.0	0.1	0.0
OPMG_002_KSP_matrix - 4	6.1	4.7	0.3	0.7	0.1	0.4	0.1	0.0	0.1	0.0	0.1	0.0	0.1	0.0
OPMG_002_KSP_matrix - 5	17.5	34.2	3.2	10.8	1.8	0.6	1.2	0.2	0.9	0.2	0.5	0.1	0.3	0.0
OPMG_002_funkyplag - 1	31.7	44.0	3.8	11.5	1.8	1.5	1.3	0.2	0.9	0.2	0.4	0.0	0.2	0.0
OPMG_002_funkyplag - 2	44.6	74.7	7.3	25.7	3.4	1.3	2.8	0.4	2.1	0.4	1.1	0.1	0.5	0.1

OPMG_002_funkyplag - 3	21.9	36.4	2.3	7.2	0.9	1.0	0.7	0.1	0.5	0.1	0.3	0.0	0.2	0.0
OPMG_002_funkyplag - 4	62.2	127.8	11.6	41.1	6.6	1.7	5.3	0.6	4.0	0.8	1.9	0.2	1.2	0.2
OPMG_002_funkyplag - 5	82.8	148.7	16.7	59.3	8.5	1.9	6.7	0.9	4.7	0.9	2.3	0.2	1.1	0.1
OPMG_002_Mafic mtrix - 1	4.9	9.5	1.1	4.0	0.8	0.1	0.6	0.1	0.5	0.1	0.3	0.0	0.3	0.1
OPMG_002_Mafic mtrix - 2	5.0	9.3	1.0	4.0	0.7	0.1	0.7	0.1	0.5	0.1	0.2	0.0	0.3	0.0
OPMG_002_Mafic mtrix - 3	5.0	6.4	0.6	2.4	0.6	0.3	1.1	0.3	3.3	0.9	4.1	0.5	4.1	0.7
OPMG_002_Mafic mtrix - 4	5.0	9.3	1.0	3.8	0.7	0.2	0.6	0.1	0.5	0.1	0.3	0.0	0.3	0.0
OPMG_002_Mafic mtrix - 5	4.7	9.1	1.0	3.8	0.7	0.1	0.5	0.1	0.4	0.1	0.3	0.0	0.3	0.0
OPMG_002_Mafic mtrix - 6	4.8	9.5	1.1	4.1	0.8	0.1	0.6	0.1	0.5	0.1	0.3	0.0	0.3	0.0
OPMG_002_Mafic mtrix - 7	89.7	248.9	29.1	113.0	22.6	3.5	19.3	2.6	15.5	2.9	7.8	0.9	5.9	1.0
OPMG_002_Mafic mtrix - 8	30.8	45.9	3.7	11.7	1.5	0.4	1.3	0.2	0.9	0.2	0.6	0.1	0.6	0.1
OPMG_002_Mafic mtrix - 9	6.9	9.7	0.9	2.8	0.4	0.2	0.3	0.0	0.3	0.1	0.2	0.0	0.2	0.0
OPMG_002_Mafic mtrix - 10	10.5	12.1	0.9	2.6	0.3	0.2	0.2	0.0	0.2	0.0	0.1	0.0	0.1	0.0
OPMG_002_Mafic mtrix - 11	6.9	8.2	0.8	2.5	0.4	0.2	0.3	0.1	0.3	0.1	0.1	0.0	0.2	0.0
OPMG_002_horn - 1	39.2	91.4	10.0	36.0	6.2	1.1	5.7	0.8	4.6	0.8	2.3	0.3	2.1	0.5
OPMG_002_horn - 2	71.1	157.1	16.0	54.5	8.3	1.5	6.9	0.9	5.2	1.0	2.8	0.4	2.7	0.6
OPMG_002_horn - 3	5.1	9.9	1.1	3.8	0.6	0.1	0.5	0.1	0.4	0.1	0.2	0.0	0.2	0.0
OPMG_002_horn - 4	39.4	89.3	9.2	31.9	5.1	1.0	4.3	0.5	3.3	0.7	1.9	0.2	2.0	0.5
OPMG_002_horn - 5	48.6	118.9	13.4	50.8	7.7	1.2	6.2	0.8	4.4	0.9	2.5	0.3	2.3	0.5
OPMG_002_horn - 6	56.4	155.2	20.9	84.7	17.0	2.0	14.9	1.7	8.8	1.4	3.7	0.5	2.9	0.7
OPMG_002_horn - 7	30.5	75.9	8.7	33.5	5.5	1.0	5.5	0.8	4.7	0.8	2.4	0.3	2.4	0.6
OPMG_002_horn - 8	17.9	42.4	4.6	16.0	2.3	0.6	2.0	0.2	1.6	0.3	1.1	0.1	1.3	0.3
OPMG_002_horn - 9	52.6	143.8	17.5	71.1	13.3	2.0	11.0	1.3	6.7	1.1	2.8	0.3	2.5	0.6
OPMG_002_horn - 10	293.6	693.0	72.8	248.2	41.4	9.5	36.5	5.6	35.4	7.2	23.9	3.4	23.5	3.4
OPMG_002_horn - 11	39.0	99.4	12.5	49.5	12.5	2.3	13.6	2.8	22.7	5.6	20.9	3.3	24.1	4.2
OPMG_002_plag - 1	4.6	8.8	1.0	3.6	0.7	0.1	0.4	0.1	0.4	0.1	0.2	0.0	0.3	0.0
OPMG_002_plag - 2	4.9	9.2	1.1	3.9	0.7	0.1	0.6	0.1	0.5	0.1	0.3	0.0	0.3	0.0
OPMG_002_plag - 3	3.5	3.8	0.3	1.1	0.2	0.1	0.2	0.0	0.2	0.0	0.1	0.0	0.1	0.0
OPMG_002_plag - 4	3212.4	7735.3	795.3	2944.2	547.2	107.9	509.8	77.5	502.6	102.6	319.6	44.8	311.4	44.9

OPMG_002_plag - 5	10.1	6.2	0.4	0.6	0.1	0.2	0.1	0.0	0.0	0.0	0.0	0.0	0.0	0.0
OPMG_002_plag - 6	7.0	7.1	0.5	1.5	0.3	0.2	0.2	0.0	0.2	0.0	0.1	0.0	0.1	0.0
OPMG_002_BIO - 8	0.4	0.9	0.1	0.4	0.1	0.0	0.1	0.0	0.1	0.0	0.1	0.0	0.0	0.0
OPMG_002_BIO - 9	0.0	0.1	0.0	0.0	0.0	0.0	0.0	0.0	0.0	0.0	0.0	0.0	0.0	0.0
OPMG_002_BIO - 10	0.0	0.0	0.0	0.0	0.0	0.0	0.0	0.0	0.0	0.0	0.0	0.0	0.0	0.0
OPMG_002_BIO - 11	0.1	0.3	0.0	0.1	0.0	0.0	0.1	0.0	0.0	0.0	0.0	0.0	0.0	0.0
OPMG_006B_KSP - 1	84.9	97.1	8.0	21.4	3.3	1.0	2.6	0.4	2.3	0.4	1.1	0.1	0.8	0.1
OPMG_006B_KSP - 2	8.0	4.1	0.2	0.3	0.0	0.5	0.0	0.0	0.0	0.0	0.0	0.0	0.0	0.0
OPMG_006B_KSP - 3	8.9	5.8	0.3	0.6	0.1	0.5	0.1	0.0	0.1	0.0	0.1	0.0	0.1	0.0
OPMG_006B_KSP - 4	2.9	2.0	0.1	0.1	0.0	0.4	0.1	0.0	0.1	0.0	0.1	0.0	0.1	0.0
OPMG_006B_KSP - 5	5.0	4.4	0.3	0.6	0.1	0.5	0.1	0.0	0.3	0.1	0.2	0.0	0.4	0.1
OPMG_006B_KSP - 6	9.0	11.3	0.9	2.2	0.3	0.4	0.3	0.0	0.4	0.1	0.3	0.0	0.4	0.1
OPMG_006B_KSP - 7	3.4	1.6	0.1	0.2	0.0	0.5	0.0	0.0	0.0	0.0	0.1	0.0	0.1	0.0
OPMG_006B_KSP - 8	100.1	143.7	11.8	34.7	4.6	1.0	3.8	0.6	3.3	0.7	1.9	0.2	1.5	0.2
OPMG_006B_KSP - 9	3.1	1.4	0.0	0.1	0.0	0.5	0.0	0.0	0.1	0.0	0.1	0.0	0.1	0.0
OPMG_006B_KSP - 10	42.7	76.2	7.3	24.4	4.3	1.0	3.6	0.5	2.9	0.5	1.2	0.1	0.8	0.1
OPMG_006B_KSP - 11	18.7	42.1	4.6	17.4	3.2	1.0	3.1	0.4	2.3	0.4	1.2	0.1	0.7	0.1
OPMG_006B_KSP - 12	9.1	7.0	0.4	0.8	0.1	0.5	0.1	0.0	0.1	0.0	0.0	0.0	0.0	0.0
OPMG_006B_KSP - 13	2.8	1.6	0.1	0.2	0.0	0.4	0.1	0.0	0.1	0.0	0.2	0.0	0.3	0.0
OPMG_006B_KSP - 14	5.6	4.4	0.3	0.7	0.1	0.3	0.1	0.0	0.1	0.0	0.1	0.0	0.1	0.0
OPMG_006B_KSP - 15	8.2	5.0	0.3	0.5	0.0	0.4	0.1	0.0	0.1	0.0	0.1	0.0	0.2	0.0
OPMG_006B_KSP - 16	0.9	1.5	0.1	0.2	0.1	0.2	0.0	0.0	0.1	0.0	0.1	0.0	0.2	0.0
OPMG_006B_KSP - 17	0.8	0.6	0.0	0.1	0.0	0.2	0.0	0.0	0.1	0.0	0.1	0.0	0.2	0.0
OPMG_006B_KSP - 18	1.3	0.8	0.0	0.1	0.0	0.4	0.0	0.0	0.0	0.0	0.0	0.0	0.1	0.0
OPMG_006B_KSP - 19	1.8	0.8	0.0	0.1	0.0	0.4	0.0	0.0	0.0	0.0	0.0	0.0	0.0	0.0
OPMG_006B_KSP - 20	1.2	0.9	0.1	0.1	0.0	0.2	0.1	0.0	0.2	0.1	0.3	0.0	0.4	0.1
OPMG_006B_KSP - 21	5.3	2.8	0.1	0.2	0.0	0.5	0.0	0.0	0.0	0.0	0.0	0.0	0.0	0.0
OPMG_006B_KSP - 22	4.3	8.5	0.9	3.5	0.5	0.1	0.5	0.1	0.3	0.1	0.3	0.0	0.2	0.0
OPMG_006B_KSP - 23	3.0	1.9	0.1	0.3	0.0	0.2	0.1	0.0	0.2	0.0	0.1	0.0	0.2	0.0

OPMG_006B_KSP - 24	5.1	2.3	0.1	0.1	0.0	0.4	0.0	0.0	0.0	0.0	0.0	0.0	0.0	0.0
OPMG_006B_KSP - 25	4.7	8.8	1.0	3.6	0.5	0.1	0.5	0.1	0.4	0.1	0.3	0.0	0.3	0.0
OPMG_006B_KSP - 26	4.6	5.4	0.5	1.7	0.2	0.3	0.2	0.0	0.4	0.1	0.2	0.0	0.3	0.0
OPMG_006B_KSP - 27	3.5	4.3	0.4	1.2	0.2	0.2	0.3	0.0	0.2	0.1	0.2	0.0	0.2	0.0
OPMG_006B_KSP - 28	14.1	30.1	0.1	0.3	0.0	0.4	0.0	0.0	0.1	0.0	0.0	0.0	0.0	0.0
OPMG_006B_KSP - 29	7.4	7.5	0.5	1.6	0.3	0.3	0.2	0.1	0.3	0.1	0.3	0.0	0.3	0.0
OPMG_006B_KSP - 30	40.0	58.3	4.9	15.1	2.0	0.7	1.6	0.2	1.3	0.2	0.7	0.1	0.4	0.1
OPMG_006B_BIO - 1	5.1	4.0	0.3	0.9	0.2	0.4	0.2	0.0	0.2	0.0	0.2	0.0	0.2	0.0
OPMG_006B_BIO - 2	64.9	115.0	4.2	13.1	2.0	0.7	1.6	0.2	1.4	0.3	0.8	0.1	0.5	0.1
OPMG_006B_BIO - 3	43.2	62.5	5.0	15.1	2.8	0.7	2.8	0.5	3.6	0.8	2.5	0.3	1.9	0.3
OPMG_006B_BIO - 4	3.7	3.8	0.2	0.6	0.1	0.3	0.1	0.0	0.1	0.0	0.1	0.0	0.1	0.0
OPMG_006B_BIO - 5	9.5	13.7	1.0	3.4	0.8	0.5	0.6	0.1	0.5	0.1	0.3	0.0	0.1	0.0
OPMG_006B_BIO - 6	15.2	10.1	0.4	0.8	0.1	0.5	0.1	0.0	0.2	0.0	0.2	0.0	0.2	0.0
OPMG_006B_KSP - 31	2.4	1.7	0.1	0.3	0.0	0.3	0.0	0.0	0.0	0.0	0.1	0.0	0.1	0.0
OPMG_006B_KSP - 32	22.2	23.8	1.5	3.5	0.4	0.4	0.4	0.0	0.4	0.1	0.2	0.0	0.1	0.0
OPMG_006B_KSP - 33	1.8	2.2	0.1	0.4	0.0	0.4	0.1	0.0	0.1	0.0	0.1	0.0	0.2	0.0
OPMG_006B_KSP - 34	3.8	4.2	0.2	0.7	0.1	0.4	0.1	0.0	0.1	0.0	0.1	0.0	0.2	0.0
OPMG_006B_KSP - 35	6.7	11.4	0.4	1.2	0.2	0.3	0.1	0.0	0.1	0.0	0.1	0.0	0.1	0.0
OPMG_006B_BIO - 7	0.1	0.1	0.0	0.0	0.0	0.0	0.0	0.0	0.0	0.0	0.0	0.0	0.0	0.0
OPMG_006B_BIO - 8	0.0	0.0	0.0	0.0	0.0	0.0	0.0	0.0	0.0	0.0	0.0	0.0	0.0	0.0
OPMG_006B_BIO - 9	0.0	0.0	0.0	0.0	0.0	0.0	0.0	0.0	0.1	0.0	0.2	0.0	0.3	0.0
OPMG_006B_Mess - 1	0.0	0.1	0.0	0.0	0.0	0.0	0.0	0.0	0.0	0.0	0.1	0.0	0.1	0.0
OPMG_006B_Mess - 2	0.1	0.3	0.0	0.1	0.0	0.0	0.1	0.0	0.3	0.1	0.5	0.1	0.7	0.1
OPMG_006B_Mess - 3	1.4	2.2	0.2	0.5	0.1	0.0	0.0	0.0	0.0	0.0	0.0	0.0	0.0	0.0
OPMG_006B_HORN - 1	0.2	0.3	0.0	0.1	0.0	0.0	0.0	0.0	0.0	0.0	0.0	0.0	0.0	0.0
OPMG_006B_HORN - 2	74.1	172.6	17.1	51.2	7.1	1.2	5.8	0.9	6.4	1.4	5.3	0.9	7.7	1.7
OPMG_006B_HORN - 3	0.1	0.2	0.0	0.1	0.0	0.0	0.0	0.0	0.0	0.0	0.0	0.0	0.0	0.0
OPMG_006B_HORN - 4	6.6	16.9	1.9	6.5	1.4	0.3	1.5	0.3	2.3	0.5	1.7	0.2	1.7	0.3
OPMG_006B_HORN - 5	0.2	0.3	0.0	0.0	0.0	0.0	0.0	0.0	0.0	0.0	0.0	0.0	0.0	0.0

OPMG_006B_HORN - 6	52.1	133.2	15.1	53.4	9.2	1.3	8.3	1.3	8.8	1.9	6.5	1.0	8.0	1.7
OPMG_006B_HORN - 7	0.0	0.0	0.0	0.0	0.0	0.0	0.0	0.0	0.0	0.0	0.0	0.0	0.0	0.0
OPMG_006B_HORN - 8	24.6	92.8	17.3	97.9	36.4	3.0	44.4	7.2	45.2	8.1	19.8	2.1	12.8	2.1
OPMG_006B_HORN - 9	30.3	116.0	21.2	117.2	42.0	3.1	51.5	8.2	51.6	8.9	21.6	2.3	13.2	2.1
OPMG_006B_HORN - 10	35.2	120.0	21.0	113.1	40.4	2.9	50.8	8.0	48.6	8.4	18.9	1.9	11.0	2.0
OPMG_006B_HORN - 11	30.9	87.7	11.3	51.7	15.9	1.7	18.7	3.0	19.8	3.7	10.1	1.2	8.8	1.7
OPMG_006B_HORN - 12	140.6	246.8	22.6	78.6	13.7	1.7	14.2	1.9	12.2	2.5	7.7	0.9	6.2	1.1
OPMG_006B_HORN - 13	4930.3	15596.4	1959.6	7425.6	1247.8	183.4	1092.3	169.7	1105.6	223.5	692.5	95.7	627.4	79.6
OPMG_006B_HORN - 14	21.1	76.5	13.5	73.7	25.1	2.1	29.4	4.7	31.0	6.0	17.4	2.3	16.9	3.6
OPMG_006B_HORN - 15	48.9	138.8	20.1	96.3	31.8	2.8	40.7	6.5	41.2	7.5	18.5	2.0	12.1	2.2
OPMG_006B_KSP - 36	0.5	0.8	0.1	0.2	0.1	0.1	0.1	0.0	0.1	0.0	0.1	0.0	0.1	0.0
OPMG_006B_KSP - 37	1.8	0.9	0.0	0.1	0.0	0.2	0.0	0.0	0.1	0.0	0.1	0.0	0.1	0.0
OPMG_006B_KSP - 38	2.5	1.7	0.1	0.3	0.0	0.4	0.1	0.0	0.1	0.0	0.1	0.0	0.2	0.0
OPMG_006B_KSP - 39	3.8	3.8	0.2	0.7	0.1	0.4	0.1	0.0	0.1	0.0	0.1	0.0	0.2	0.0
OPMG_006B_KSP - 40	13.2	18.8	1.3	4.0	0.6	0.4	0.9	0.1	0.7	0.2	0.6	0.1	0.7	0.1
OPMG_006B_KSP - 41	1.4	1.1	0.1	0.2	0.0	0.3	0.1	0.0	0.1	0.0	0.2	0.0	0.2	0.0
OPMG_006B_KSP - 42	3.4	4.2	0.2	0.7	0.1	0.2	0.2	0.0	0.4	0.1	0.4	0.1	0.5	0.1
OPMG_006B_KSP - 43	53.0	89.8	8.0	24.9	3.9	0.8	3.1	0.4	2.8	0.5	1.4	0.2	1.1	0.2
OPMG_006B_Messplag - 1	5.0	10.0	1.0	4.0	0.7	0.1	0.6	0.1	0.5	0.1	0.3	0.0	0.2	0.0
OPMG_006B_Messplag - 2	5.4	10.0	1.1	3.8	0.8	0.1	0.6	0.1	0.5	0.1	0.3	0.0	0.3	0.0
OPMG_006B_Messplag - 3	6.0	10.9	1.2	4.5	0.8	0.2	0.7	0.1	0.7	0.1	0.5	0.1	0.4	0.1
OPMG_006B_Messplag - 4	13.2	8.8	0.3	0.6	0.1	0.5	0.1	0.0	0.0	0.0	0.0	0.0	0.0	0.0
OPMG_006B_Messplag - 5	5.6	7.8	0.3	0.8	0.1	0.5	0.1	0.0	0.1	0.0	0.0	0.0	0.0	0.0
OPMG_016_horn - 1	37.9	88.9	10.1	39.0	7.2	1.1	6.5	0.9	4.7	0.8	2.4	0.3	3.1	0.8
OPMG_016_horn - 2	3384.7	9263.3	1114.2	4427.3	895.8	128.9	767.2	108.1	647.0	118.4	328.9	41.7	267.2	33.4
OPMG_016_horn - 3	4328.5	6398.9	458.9	1484.5	198.8	26.3	177.4	19.9	112.2	22.5	65.0	8.4	60.6	10.9
OPMG_016_horn - 4	55.4	112.1	11.5	42.0	7.6	1.2	6.7	0.8	4.9	0.9	2.6	0.4	3.4	0.8
OPMG_016_horn - 5	6473.9	9449.2	679.9	2196.4	293.3	38.2	267.5	30.4	172.7	34.7	102.2	12.7	90.2	15.7
OPMG_016_horn - 6	359.8	973.9	120.4	482.9	97.2	14.7	82.8	11.7	70.0	13.0	37.2	4.8	32.0	4.4

OPMG_016_horn - 7	38.6	89.3	10.1	38.3	7.2	1.1	6.3	0.8	4.6	0.9	2.7	0.4	3.3	0.8
OPMG_016_horn - 8	137.5	362.5	43.5	172.1	34.2	5.8	30.0	4.1	24.8	4.6	13.4	1.8	12.8	2.0
OPMG_016_horn - 9	38.0	88.8	10.0	38.7	7.3	1.0	6.5	0.8	4.5	0.9	2.4	0.4	3.0	0.8
OPMG_016_horn - 10	49.1	119.8	14.5	59.2	11.8	1.7	10.6	1.4	7.9	1.4	3.7	0.4	3.4	0.9
OPMG_016_horn - 11	5359.6	7767.2	583.7	1926.4	268.5	34.5	231.6	26.8	146.5	28.4	80.5	10.0	65.8	10.8
OPMG_016_horn - 12	4083.8	6083.3	448.4	1478.6	201.0	27.2	182.7	20.7	117.7	23.4	68.8	8.8	63.9	11.6
OPMG_016_horn - 13	5.3	2.6	0.1	0.2	0.0	0.2	0.0	0.0	0.0	0.0	0.0	0.0	0.0	0.0
OPMG_016_horn - 14	527.0	1364.4	147.2	569.4	108.6	17.0	92.6	12.9	76.9	14.5	40.8	5.3	35.2	4.9
OPMG_016_horn - 15	27.8	68.2	7.8	29.6	5.6	0.9	5.2	0.7	4.2	0.8	2.6	0.4	3.3	0.8
OPMG_016_horn - 16	35.6	82.0	9.3	35.4	6.7	1.0	6.2	0.7	4.5	0.8	2.4	0.3	3.0	0.8
OPMG_016_horn - 17	34.0	79.8	9.0	34.4	6.3	0.9	5.5	0.7	4.1	0.8	2.3	0.3	3.1	0.8
OPMG_016_horn - 18	34.9	79.0	8.7	33.0	6.3	1.0	5.7	0.8	5.0	1.0	3.3	0.4	3.8	0.9
OPMG_016_horn - 19	6.8	3.6	0.1	0.3	0.0	0.2	0.0	0.0	0.0	0.0	0.0	0.0	0.0	0.0
OPMG_016_horn - 20	46.9	111.9	13.2	52.2	10.1	1.4	8.9	1.1	6.4	1.2	3.2	0.4	3.5	0.8
OPMG_016_horn - 21	34.1	80.3	9.2	35.0	6.3	0.9	5.9	0.7	4.2	0.8	2.3	0.3	3.1	0.8
OPMG_016_horn - 22	9.4	15.0	1.6	5.3	0.9	0.2	0.8	0.1	0.5	0.1	0.2	0.0	0.4	0.0
OPMG_016_horn - 23	5.3	3.7	0.3	0.8	0.1	0.2	0.2	0.0	0.2	0.1	0.2	0.0	0.2	0.0
OPMG_016_horn - 24	29.5	49.4	3.7	10.8	1.5	0.3	1.1	0.1	0.8	0.2	0.4	0.1	0.5	0.1
OPMG_016_horn - 25	34.4	57.4	4.6	13.6	2.1	0.4	1.5	0.2	1.1	0.2	0.6	0.1	0.5	0.1
OPMG_016_horn - 26	28.7	50.3	4.0	11.8	1.8	0.4	1.2	0.1	0.8	0.2	0.5	0.1	0.5	0.1
OPMG_016_matrix - 1	5.9	11.1	1.2	4.4	0.7	0.2	0.6	0.1	0.5	0.1	0.4	0.0	0.4	0.1
OPMG_016_matrix - 2	78.0	216.3	28.0	131.0	25.8	4.6	20.2	2.8	16.7	3.0	7.9	1.0	6.6	0.8
OPMG_016_matrix - 3	9.4	16.0	1.6	5.6	0.9	0.2	0.8	0.1	0.7	0.1	0.4	0.1	0.4	0.1
OPMG_016_matrix - 4	4.7	9.2	1.1	3.7	0.6	0.1	0.5	0.1	0.4	0.1	0.3	0.0	0.3	0.0
OPMG_016_matrix - 5	7.7	13.8	1.4	5.0	0.9	0.2	0.8	0.1	1.1	0.2	1.0	0.1	1.1	0.1
OPMG_016_BIO - 1	0.0	0.0	0.0	0.0	0.0	0.0	0.0	0.0	0.0	0.0	0.0	0.0	0.0	0.0
OPMG_016_BIO - 2	0.0	0.0	0.0	0.0	0.0	0.0	0.0	0.0	0.0	0.0	0.0	0.0	0.0	0.0
OPMG_016_BIO - 3	0.0	0.0	0.0	0.0	0.0	0.0	0.0	0.0	0.0	0.0	0.0	0.0	0.0	0.0
OPMG_016_BIO - 4	0.0	0.0	0.0	0.0	0.0	0.0	0.0	0.0	0.0	0.0	0.0	0.0	0.0	0.0

OPMG_016_BIO - 5	0.0	0.0	0.0	0.0	0.0	0.0	0.0	0.0	0.0	0.0	0.0	0.0	0.0	0.0
OPMG_016_BIO - 6	0.0	0.0	0.0	0.0	0.0	0.0	0.0	0.0	0.0	0.0	0.0	0.0	0.0	0.0
OPMG_016_BIO - 7	0.0	0.0	0.0	0.0	0.0	0.0	0.0	0.0	0.0	0.0	0.0	0.0	0.0	0.0
OPMG_016_FELDS - 1	2.8	1.9	0.1	0.2	0.0	0.0	0.1	0.0	0.1	0.0	0.1	0.0	0.1	0.0
OPMG_016_FELDS - 2	444.5	1003.5	105.8	368.3	61.4	15.6	49.6	7.3	48.1	9.9	32.7	4.7	35.2	5.3
OPMG_016_FELDS - 3	30.1	29.0	1.9	5.4	0.6	0.3	0.6	0.1	0.4	0.1	0.3	0.0	0.2	0.0
OPMG_016_FELDS - 4	29.3	63.8	6.6	21.8	4.3	1.1	3.6	0.5	2.7	0.6	1.5	0.2	0.9	0.1
OPMG_016_FELDS - 5	11.8	8.0	0.4	0.9	0.1	0.2	0.1	0.0	0.1	0.0	0.1	0.0	0.1	0.0
OPMG_016_FELDS - 6	329.5	876.6	105.8	417.2	78.2	15.1	63.6	8.7	51.2	9.7	27.3	3.4	23.8	3.2
OPMG_016_FELDS - 7	216.5	398.6	36.7	118.4	17.9	5.5	13.9	1.9	12.0	2.4	7.1	1.0	7.4	1.2
OPMG_016_FELDS - 8	1.6	1.5	0.1	0.4	0.1	0.1	0.4	0.1	1.3	0.4	1.6	0.2	1.6	0.2
OPMG_016_FELDS - 9	1.9	1.3	0.1	0.2	0.0	0.0	0.0	0.0	0.0	0.0	0.0	0.0	0.0	0.0
OPMG_016_FELDS - 10	10.2	6.6	0.3	0.7	0.1	0.2	0.1	0.0	0.1	0.0	0.1	0.0	0.1	0.0
OPMG_016_FELDS - 11	9.2	15.7	1.3	4.2	0.7	0.2	0.8	0.1	1.0	0.3	0.9	0.1	1.2	0.3
OPMG_016_Anorthite - 1	83.9	340.7	61.6	324.5	95.7	7.4	101.1	15.5	95.4	17.3	44.3	4.7	25.8	3.5
OPMG_016_Anorthite - 2	83.7	226.0	26.5	97.8	19.9	2.7	19.9	3.4	24.3	5.2	16.4	2.0	12.1	2.0
OPMG_016_Anorthite - 3	61.1	210.5	34.2	167.6	43.6	3.4	45.4	6.4	35.9	6.1	13.7	1.3	7.9	1.5
OPMG_016_Anorthite - 4	52.9	177.9	26.7	123.1	30.1	2.9	30.1	4.5	27.2	5.1	13.5	1.6	11.6	2.5
OPMG_016_Anorthite - 5	72.5	171.9	17.5	58.0	9.8	1.7	9.5	1.5	10.6	2.4	8.3	1.3	10.4	2.1
OPMG_016_Anorthite - 6	87.0	352.4	63.6	339.0	101.1	7.5	109.2	17.3	108.8	20.2	51.9	5.5	29.5	3.9
OPMG_016_magnetite - 1	46.3	52.0	4.8	14.7	1.9	0.3	1.6	0.2	1.0	0.2	0.9	0.1	0.8	0.2
OPMG_016_magnetite - 2	85.3	142.7	14.9	49.0	7.9	1.1	5.9	0.8	4.9	1.0	3.1	0.4	2.8	0.5
OPMG_016_magnetite - 3	0.0	0.1	0.0	0.0	0.0	0.0	0.0	0.0	0.0	0.0	0.0	0.0	0.0	0.0
OPMG_016_magnetite - 4	107.3	148.4	12.8	34.6	3.4	0.5	2.4	0.2	1.1	0.2	0.6	0.1	0.6	0.1
OPMG_016_magnetite - 5	0.0	0.0	0.0	0.0	0.0	0.0	0.0	0.0	0.0	0.0	0.0	0.0	0.0	0.0
OPMG_016_magnetite - 6	0.0	0.1	0.0	0.1	0.0	0.0	0.0	0.0	0.0	0.0	0.0	0.0	0.0	0.0
OPMG_016_magnetite - 7	0.3	0.4	0.1	0.4	0.1	0.0	0.1	0.0	0.3	0.1	0.3	0.0	0.3	0.0
OPMG_016_magnetite - 8	0.0	0.0	0.0	0.0	0.0	0.0	0.0	0.0	0.0	0.0	0.0	0.0	0.0	0.0
OPMG_016_magnetite - 9	0.0	0.0	0.0	0.0	0.0	0.0	0.0	0.0	0.0	0.0	0.0	0.0	0.0	0.0

OPMG_016_magnetite - 10	0.1	0.1	0.0	0.1	0.0	0.0	0.0	0.0	0.0	0.0	0.0	0.0	0.0	0.0
OPMG_016_magnetite - 11	0.0	0.0	0.0	0.0	0.0	0.0	0.0	0.0	0.0	0.0	0.0	0.0	0.0	0.0
OPMG_016_KSP - 1	6.3	7.3	0.6	2.1	0.2	0.4	0.2	0.0	0.2	0.1	0.2	0.0	0.4	0.1
OPMG_016_KSP - 2	4.8	3.2	0.2	0.4	0.0	0.4	0.0	0.0	0.1	0.0	0.1	0.0	0.2	0.0
OPMG_016_KSP - 3	1.3	0.5	0.0	0.0	0.0	0.3	0.0	0.0	0.0	0.0	0.0	0.0	0.1	0.0
OPMG_016_KSP - 4	3.6	1.0	0.0	0.0	0.0	0.4	0.0	0.0	0.0	0.0	0.0	0.0	0.0	0.0
OPMG_016_KSP - 5	6.0	2.9	0.1	0.1	0.0	0.5	0.0	0.0	0.0	0.0	0.0	0.0	0.0	0.0
OPMG_016_KSP - 6	5.7	2.2	0.1	0.0	0.0	0.7	0.0	0.0	0.0	0.0	0.0	0.0	0.0	0.0
OPMG_016_KSP - 7	3.3	1.2	0.1	0.1	0.0	0.6	0.0	0.0	0.1	0.0	0.1	0.0	0.1	0.0
OPMG_016_titan - 1	541.0	2373.3	387.6	1702.2	542.9	77.4	687.9	136.7	1036.3	238.1	819.9	119.1	805.3	103.4
OPMG_016_titan - 2	5940.0	18695.1	2018.1	7047.0	1224.5	142.9	1075.1	172.7	1157.8	246.5	806.7	115.4	774.2	101.0
OPMG_016_titan - 3	5332.1	17591.9	1862.9	6048.0	970.1	84.9	871.9	151.8	1098.7	252.1	881.1	131.8	902.9	115.5
OPMG_016_titan - 4	5741.2	19891.2	2256.3	7807.8	1385.4	100.2	1313.6	243.6	1798.7	405.8	1357.8	190.9	1194.7	140.2
OPMG_016_titan - 5	5579.0	19553.6	2234.4	7677.6	1359.0	97.5	1293.0	238.0	1761.6	399.8	1336.3	186.7	1181.8	137.6
OPMG_016_titan - 6	7267.6	23523.4	2680.9	9167.0	1598.0	118.4	1493.1	270.0	1968.9	443.9	1465.1	203.3	1277.3	150.0
OPMG_016_titan - 7	5527.2	17050.8	1720.8	5517.0	859.9	86.4	757.1	129.1	923.7	212.5	740.6	110.9	773.9	98.6
OPMG_016_titan - 8	5159.2	15875.5	1772.9	6566.9	1196.0	150.4	1009.4	152.6	965.0	192.2	592.0	81.3	540.3	69.2
OPMG_016_titan - 9	6305.1	16530.2	1560.0	5024.6	777.6	135.7	671.2	102.6	681.3	145.0	489.6	73.8	544.4	78.1
OPMG_016_titan - 10	2842.4	8523.2	867.9	3055.8	654.6	128.9	667.8	111.5	751.3	159.1	517.3	74.8	528.2	70.1
OPMG_016_titan - 11	6515.8	17346.6	1666.4	5432.8	846.6	139.5	728.2	110.7	731.2	156.4	519.7	78.7	572.5	81.4
OPMG_016_matix - 1	2.2	1.2	0.0	0.1	0.0	0.1	0.0	0.0	0.1	0.0	0.1	0.0	0.1	0.0
OPMG_016_matix - 2	3.7	2.0	0.1	0.3	0.1	0.2	0.2	0.1	0.6	0.2	0.6	0.1	0.8	0.1
OPMG_016_matix - 3	10.6	5.7	0.2	0.3	0.0	0.2	0.0	0.0	0.1	0.0	0.1	0.0	0.1	0.0
OPMG_016_matix - 4	7.3	8.3	0.6	2.0	0.2	0.2	0.1	0.0	0.2	0.0	0.1	0.0	0.0	0.0
OPMG_016_matix - 5	12.8	16.8	1.2	3.5	0.4	0.3	0.3	0.0	0.2	0.0	0.1	0.0	0.1	0.0
OPMG_016_matix - 6	55.6	79.4	5.9	17.8	2.2	0.5	1.6	0.2	1.2	0.3	0.8	0.1	0.8	0.2
OPMG_016_matix - 7	6.5	3.3	0.1	0.2	0.0	0.1	0.0	0.0	0.0	0.0	0.0	0.0	0.0	0.0
OPMG_016_matix - 8	3.4	3.2	0.3	0.9	0.1	0.1	0.1	0.0	0.2	0.0	0.0	0.0	0.1	0.0
OPMG_016_matix - 9	3.0	2.8	0.1	0.4	0.1	0.1	0.0	0.0	0.1	0.0	0.1	0.0	0.2	0.0

OPMG_016_matix - 10	2.2	1.4	0.1	0.2	0.0	0.1	0.0	0.0	0.1	0.0	0.1	0.0	0.1	0.0
OPMG_016_matix - 11	4.8	7.1	0.7	2.6	0.4	0.1	0.4	0.1	0.4	0.1	0.2	0.0	0.2	0.0
OPMG_016_matix - 12	116.1	158.4	9.3	27.0	3.1	0.8	2.5	0.4	2.3	0.6	2.0	0.3	2.1	0.4
OPMG_016_horn - 27	107.5	318.9	45.4	196.8	42.1	5.1	36.5	4.8	25.0	3.8	6.9	0.5	2.6	0.6
OPMG_016_horn - 28	95.8	238.1	29.3	123.5	23.6	3.3	21.1	2.5	13.0	2.1	4.7	0.4	2.9	0.6
OPMG_016_horn - 29	46.9	98.7	11.6	44.8	7.7	1.1	6.5	0.8	4.2	0.7	1.9	0.3	2.3	0.5
OPMG_016_mag - 1	1.6	4.7	0.1	0.3	0.1	0.0	0.1	0.0	0.4	0.1	0.5	0.1	0.6	0.1
OPMG_016_mag - 2	0.8	1.6	0.2	1.0	0.3	0.1	0.3	0.1	0.9	0.2	1.0	0.2	1.2	0.2
OPMG_016_horn - 30	179.8	237.0	18.2	56.7	7.6	1.7	7.0	0.9	5.6	1.2	3.8	0.5	3.9	0.8
OPMG_016_horn - 31	47.5	92.0	9.3	33.9	5.8	1.0	5.3	0.6	3.6	0.7	2.2	0.3	2.6	0.6
OPMG_016_horn - 32	94.1	273.9	39.0	165.6	35.8	5.1	31.7	4.1	21.3	3.2	6.0	0.5	2.7	0.5
OPMG_016_horn - 33	152.5	285.9	32.1	122.4	21.0	3.1	17.9	2.0	9.7	1.7	4.0	0.4	2.9	0.6
OPMG_016_horn - 34	4.8	9.5	1.1	4.1	0.7	0.1	0.5	0.1	0.4	0.1	0.3	0.1	0.3	0.0
OPMG_016_horn - 35	54.8	82.7	7.3	24.6	3.5	0.8	2.8	0.3	2.0	0.4	1.3	0.2	1.6	0.4
OPMG_016_horn - 36	81.3	169.2	19.4	74.1	13.8	2.3	11.2	1.3	6.5	1.0	2.3	0.3	2.0	0.4
OPMG_016_horn - 37	132.1	292.0	35.6	130.5	25.1	4.1	20.7	2.4	11.6	1.8	3.2	0.4	2.2	0.5
OPMG_016_horn - 38	18.4	33.1	3.0	10.3	1.7	0.4	1.7	0.2	1.6	0.4	1.3	0.2	1.5	0.3
OPMG_016_horn - 39	2810.8	3232.6	195.2	558.1	66.8	15.0	60.1	6.8	36.5	7.3	20.2	2.5	17.3	3.4
OPMG_016_horn - 40	1320.2	1524.5	94.2	270.4	32.1	7.5	29.2	3.3	17.8	3.6	10.0	1.2	8.7	1.7
OPMG_016_BIO - 8	21.4	23.6	1.4	4.0	0.4	0.1	0.4	0.0	0.3	0.1	0.2	0.0	0.2	0.0
OPMG_016_BIO - 9	8.1	9.4	0.6	1.8	0.2	0.1	0.2	0.0	0.1	0.0	0.1	0.0	0.1	0.0
OPMG_016_BIO - 10	101.5	110.9	6.9	18.9	2.2	0.6	1.9	0.2	1.1	0.2	0.7	0.1	0.7	0.2
OPMG_016_BIO - 11	55.4	61.4	3.8	10.6	1.3	0.3	1.0	0.1	0.6	0.1	0.4	0.0	0.4	0.1
OPMG_016_plag - 1	111.4	116.8	7.3	19.9	2.5	0.7	2.1	0.3	1.9	0.4	1.5	0.2	1.6	0.3
OPMG_016_plag - 2	33.0	33.7	2.2	6.3	0.8	0.3	0.8	0.1	0.8	0.2	0.7	0.1	0.8	0.1
OPMG_016_plag - 3	67.7	91.8	7.1	24.8	7.0	2.2	10.5	2.5	23.9	6.7	27.3	4.5	32.4	5.2
OPMG_016_plag - 4	48.1	55.8	4.0	11.6	2.1	0.7	2.6	0.6	4.7	1.4	4.9	0.8	5.4	0.8
OPMG_016_plag - 5	6.4	5.0	0.4	1.4	0.5	0.2	0.8	0.2	2.0	0.5	2.1	0.3	2.5	0.4
OPMG_016_plag - 6	1628.7	3288.9	287.1	1009.4	164.3	39.0	144.2	20.0	122.7	24.7	73.4	9.8	67.3	10.0

OPMG_016_plag - 7	50.4	53.5	3.3	9.2	1.2	0.4	1.1	0.1	0.9	0.2	0.8	0.1	0.8	0.1
OPMG_016_plag - 8	1386.8	2706.8	233.2	803.1	134.3	41.2	117.5	16.7	104.7	20.7	62.8	8.5	59.3	8.9
OPMG_016_mag - 3	881.0	1420.3	106.0	278.4	26.3	4.2	19.9	2.0	10.4	2.2	6.9	0.9	6.9	1.4
OPMG_016_mag - 4	4.6	6.2	0.5	1.3	0.1	0.0	0.1	0.0	0.1	0.0	0.0	0.0	0.1	0.0
OPMG_016_mag - 5	3.1	3.4	0.3	0.8	0.1	0.0	0.1	0.0	0.0	0.0	0.0	0.0	0.0	0.0
OPMG_016_mag - 6	4.2	4.6	0.4	1.0	0.1	0.0	0.1	0.0	0.1	0.0	0.1	0.0	0.1	0.0
OPMG_016_mag - 7	86.7	101.2	8.4	22.5	2.2	0.4	1.3	0.1	0.8	0.2	0.7	0.1	0.8	0.2
OPMG_016_mag - 8	29.4	38.3	3.1	8.2	0.9	0.2	0.5	0.1	0.3	0.1	0.2	0.0	0.3	0.1
OPMG_016_plag - 9	40.4	46.7	3.4	10.4	1.1	1.7	0.6	0.1	0.4	0.1	0.2	0.0	0.2	0.0
OPMG_016_plag - 10	17.6	12.3	0.6	1.0	0.0	1.2	0.0	0.0	0.0	0.0	0.0	0.0	0.0	0.0
OPMG_016_plag - 11	19.0	13.2	0.6	1.0	0.0	0.9	0.0	0.0	0.0	0.0	0.0	0.0	0.0	0.0
OPMG_016_plag - 12	32.9	37.5	2.8	7.8	0.9	0.6	0.7	0.1	0.5	0.1	0.2	0.0	0.1	0.0
OPMG_016_plag - 13	5.7	4.5	0.3	0.9	0.1	0.4	0.1	0.0	0.1	0.0	0.1	0.0	0.1	0.0
OPMG_016_plag - 14	3.4	2.6	0.1	0.3	0.0	0.3	0.0	0.0	0.0	0.0	0.0	0.0	0.0	0.0
OPMG_016_mag - 9	53.1	59.7	5.2	14.1	1.7	0.3	1.5	0.2	0.9	0.2	0.6	0.1	0.6	0.1
OPMG_016_mag - 10	0.9	2.8	0.3	0.8	0.2	0.0	0.2	0.1	0.5	0.1	0.6	0.1	0.9	0.2
OPMG_016_mag - 11	6433.0	18499.6	2103.1	7086.8	1092.4	160.3	945.9	150.1	999.9	212.7	692.6	100.0	682.5	89.8

Appendix D
Table of Ni, Cu and Zn in rock forming minerals from LA-ICP-MS

Analysis	60Ni	65Cu	66Zn
OPMG_009_Anorthite - 1	6.070394	1.169858	37.17643
OPMG_009_Anorthite - 2	2.8052	0.851404	16.68085
OPMG_009_Anorthite - 3	5.857599	31.32161	141.6936
OPMG_009_Anorthite - 4	109.4973	33.26491	943.557
OPMG_009_Anorthite - 5	1.618199	0.575125	9.870727
OPMG_009_Anorthite - 6	1.129168	0.822641	8.603652
OPMG_009_Anorthite - 7	0.562692	-0.03102	4.186552
OPMG_009_Anorthite - 8	59.11136	10.88988	561.3907
OPMG_009_Anorthite - 9	0.769809	0.035835	4.980307
OPMG_009_Anorthite - 10	1.533154	0.168439	15.81842
OPMG_009_Anorthite - 11	7.549029	2.998193	74.25065
OPMG_009_Anorthite_rim - 1	37.76502	34.35109	279.2506
OPMG_009_Anorthite_rim - 2	4.953848	15.51569	44.24296
OPMG_009_Anorthite_rim - 3	1.830884	0.983122	22.61629
OPMG_009_Anorthite_rim - 4	4.483853	1.214524	44.85076
OPMG_009_Anorthite_rim - 5	0.899474	0.435644	11.09262
OPMG_009_Anorthite_rim - 6	0.758287	0.447717	12.73993
OPMG_009_Anorthite_rim - 7	5.963854	9.328759	55.89959
OPMG_009_Anorthite_rim - 8	4.006711	0.23826	28.07581
OPMG_009_Anorthite_rim - 9	0.733005	0.205005	18.56927
OPMG_009_Titan - 1	0.149646	1.057354	2.310369
OPMG_009_Titan - 2	0.06912	1.077857	1.694688
OPMG_009_Titan - 3	0.191691	6.984792	2.818536
OPMG_009_Titan - 4	0.034698	1.176438	2.219086
OPMG_009_Titan - 5	0.123045	1.736867	2.030081
OPMG_009_Titan - 6	0.383965	3.85682	2.64399
OPMG_009_Titan - 7	0.171271	5.205424	2.256845
OPMG_009_Titan - 8	0.088211	0.97271	1.866016
OPMG_009_Titan - 9	0.066572	1.014039	1.945036
OPMG_009_Titan - 10	0.080505	1.017711	1.892724
OPMG_009_Titan - 11	0.09104	1.355493	3.121643
OPMG_009_Titan - 12	0.377109	3.422583	2.276451
OPMG_009_Titan - 13	0.048731	1.240355	2.098919
OPMG_009_Titan - 14	3.267046	6.668437	5.445981
OPMG_009_KSP - 1	0.792653	13.48111	16.90037
OPMG_009_KSP - 2	0.319251	5.291536	12.42234
OPMG_009_KSP - 3	0.388201	1.709634	14.27639
OPMG_009_KSP - 4	0.350548	5.119137	48.30738
OPMG_009_KSP - 5	0.156256	1.642517	7.563196
OPMG_009_KSP - 6	0.111166	0.560108	5.219992
OPMG_009_KSPrim - 1	-0.00603	0.472413	12.44073
OPMG_009_KSPrim - 2	0.864091	3.563883	27.68775

OPMG_009_KSPrim - 3	0.388235	3.357559	2.119533
OPMG_009_KSPrim - 4	8.043752	39.67735	25.18637
OPMG_009_KSPrim - 5	0.197255	1.211544	2.120874
OPMG_009_KSPrim - 6	0.013735	0.988638	0.93415
OPMG_009_KSPrim - 7	0.282663	2.34919	3.506118
OPMG_009_BIO - 1	0.345572	4.784126	1.818907
OPMG_009_BIO - 2	0.24386	4.979557	1.774803
OPMG_009_BIO - 3	0.326006	4.823042	1.324615
OPMG_009_BIO - 4	0.373724	4.951818	1.005179
OPMG_009_BIO - 5	0.266496	5.04612	1.45464
OPMG_009_matrix - 1	45.01131	57.39658	113.2174
OPMG_009_matrix - 2	10.62069	29.86858	39.40177
OPMG_009_matrix - 3	122.4397	168.8926	870.2992
OPMG_009_matrix - 4	91.57378	142.8726	674.841
OPMG_009_matrix - 5	12.52524	55.21478	58.26008
OPMG_009_matrix - 6	64.1701	68.4495	456.8808
OPMG_009_matrix - 7	7.861042	21.67015	34.98468
OPMG_009_matrix - 8	0.095309	0.018881	4.402697
OPMG_009_horn - 1	58.60253	0.867601	721.2161
OPMG_009_horn - 2	57.99003	0.986204	721.0663
OPMG_009_horn - 3	119.946	190.585	689.7013
OPMG_009_horn - 4	55.20775	1.735382	703.0818
OPMG_009_Titian - 1	0.079089	0.817208	1.903471
OPMG_009_Titian - 2	0.044305	0.926035	2.132034
OPMG_009_Titian - 3	0.055304	0.885797	2.069258
OPMG_009_Titian - 4	0.121413	0.961253	2.236014
OPMG_009_Titian - 5	0.071075	0.942032	2.180145
OPMG_009_Titian - 6	0.026821	0.892213	1.872709
OPMG_009_Titian - 7	0.361173	2.57563	5.385072
OPMG_009_Titian_rim - 1	0.030861	0.974239	2.140367
OPMG_009_Titian_rim - 2	0.054228	1.329783	4.811471
OPMG_009_Titian_rim - 3	0.006495	1.00127	1.748238
OPMG_009_Titian_rim - 4	0.066193	1.381937	2.519309
OPMG_009_Titian_rim - 5	0.06099	1.177103	2.190025
OPMG_009_KSP - 7	0.097504	0.452828	0.862217
OPMG_009_KSP - 8	0.159414	0.387167	0.955309
OPMG_009_KSP - 9	2.388865	3.789978	28.7705
OPMG_009_KSP - 10	0.062406	0.250199	0.671847
OPMG_009_KSP - 11	0.140454	0.895114	2.33078
OPMG_009_KSP - 12	0.092327	0.279064	0.447675
OPMG_009_KSP_rim - 1	0.094776	0.386819	0.764263
OPMG_009_KSP_rim - 2	-0.01828	0.43024	2.480764
OPMG_009_KSP_rim - 3	0.100987	0.523974	6.272402
OPMG_009_KSP_rim - 4	0.05749	0.321449	0.857995
OPMG_009_KSP_rim - 5	0.448417	0.268859	7.743408

OPMG_009_KSP_rim - 6	0.024739	0.239704	0.536993
OPMG_009_KSP_rim - 7	0.055122	0.625305	7.966034
OPMG_009_KSP_rim - 8	0.370352	0.912812	5.594815
OPMG_009_KSP_rim - 9	0.737172	2.489309	12.64882
OPMG_009_KSP_rim - 10	4.503678	6.934584	54.217
OPMG_009_horn_rining - 1	61.71506	0.801151	776.2925
OPMG_009_horn_rining - 2	62.79768	1.534033	752.1448
OPMG_009_horn_rining - 3	56.98505	1.122748	716.7821
OPMG_009_horn_rining - 4	56.27629	0.47555	759.1553
OPMG_009_horn_rining - 5	63.96707	2.297918	790.4546
OPMG_009_horn_rining - 6	61.22578	0.630011	728.5562
OPMG_009_horn_rining - 7	59.22323	0.717973	707.3061
OPMG_009_horn_rining - 8	57.54637	0.528562	695.6605
OPMG_009_horn_rining - 9	0.194537	5.886668	2.591263
OPMG_009_horn_rining - 10	57.63935	0.95355	727.1371
OPMG_009_horn_rining - 11	56.20035	0.532664	736.1573
OPMG_009_horn_rining - 12	63.24407	1.755597	782.6385
OPMG_009_horn_rining - 13	49.88314	0.736603	689.0804
OPMG_009_horn_rining - 14	57.86969	0.646451	816.2563
OPMG_009_horn_rining - 15	57.5571	0.966093	640.0763
OPMG_009_horn_rining - 16	59.84529	3.723072	656.5306
OPMG_009_horn_rining - 17	57.7853	1.103505	626.8943
OPMG_009_horn_rining - 18	60.55412	1.658866	636.3344
OPMG_009_horn_rining - 19	59.12987	0.497539	645.5962
OPMG_009_horn_rining - 20	62.33504	4.266094	750.9929
OPMG_009_horn_rining - 21	60.75914	0.604726	517.8565
OPMG_009_BIO - 6	99.68539	5.456923	871.1931
OPMG_009_BIO - 7	97.96141	3.082451	845.8731
OPMG_009_BIO - 8	100.6523	4.769424	859.2364
OPMG_009_BIO - 9	101.4381	6.957085	854.1178
OPMG_009_BIO - 10	100.1035	4.421382	807.2086
OPMG_009_BIO - 11	103.371	4.31778	849.5404
OPMG_009_BIO - 12	100.4203	5.467997	850.2902
OPMG_009_matrix - 9	0.859802	0.441549	15.6556
OPMG_009_matrix - 10	0.202473	0.076472	5.683538
OPMG_009_matrix - 11	0.948059	0.308334	20.29867
OPMG_009_matrix - 12	0.04511	0.442065	1.596427
OPMG_009_matrix - 13	0.029532	0.16069	6.772891
OPMG_009_matrix - 14	0.630996	0.555767	13.23292
OPMG_009_matrix - 15	9.186616	3.461823	112.7384
OPMG_009_Titan_ - 1	0.117517	0.91065	2.16576
OPMG_009_Titan_ - 2	0.048037	1.116922	2.283332
OPMG_009_Titan_ - 3	0.051688	0.878882	1.920306
OPMG_009_Titan_ - 4	0.214278	1.226327	3.470738
OPMG_009_Titan_ - 5	0.030171	0.856856	2.115901

OPMG_009_horn - 5	55.27816	0.526206	675.0591
OPMG_009_horn - 6	57.02439	2.512494	676.5316
OPMG_009_BIO - 13	82.57877	3.730511	925.2738
OPMG_009_BIO - 14	82.23972	10.25869	969.2275
OPMG_009_BIO - 15	86.72432	3.498915	931.3528
OPMG_009_BIO - 16	84.61354	2.658428	945.4309
OPMG_009_BIO - 17	82.39675	10.63644	1155.674
OPMG_009_BIO - 18	82.27684	4.525588	958.7984
OPMG_009_BIO - 19	86.88615	3.424521	935.7527
OPMG_009_BIO - 20	92.70877	4.076207	925.0929
OPMG_009_KSP - 13	0.055291	0.592412	22.09507
OPMG_009_KSP - 14	0.52004	0.273016	23.94089
OPMG_009_KSP - 15	0.074858	0.636803	17.18809
OPMG_009_KSP - 16	0.309035	0.766401	19.08414
OPMG_009_KSP - 17	1.362878	0.589733	22.66181
OPMG_009_KSP_rim - 11	-0.08776	0.325903	1.99734
OPMG_009_KSP_rim - 12	0.228705	0.945877	17.02009
OPMG_009_KSP_rim - 13	0.253093	0.50468	71.4683
OPMG_009_KSP_rim - 14	0.001857	0.445104	24.4308
OPMG_009_KSP_rim - 15	0.182288	0.389404	13.45352
OPMG_009_KSP_rim - 16	0.162424	1.004146	26.83654
OPMG_002_titan - 1	0.17973	3.746755	19.45574
OPMG_002_titan - 2	-0.0019	1.189677	4.935784
OPMG_002_titan - 3	-0.03373	0.887884	4.375718
OPMG_002_titan - 4	0.178363	2.909571	13.06278
OPMG_002_titan - 5	0.48823	7.181937	39.26909
OPMG_002_titan - 6	0.020012	0.299787	0.20132
OPMG_002_titan - 7	3.005302	32.13615	166.3927
OPMG_002_titan - 8	0.615822	2.242707	10.20857
OPMG_002_mank - 1	14.63994	43.99612	516.7423
OPMG_002_mank - 2	21.13462	5.42414	694.5474
OPMG_002_mank - 3	0.773116	6.30984	8.793232
OPMG_002_mank - 4	0.491288	4.794463	3.179957
OPMG_002_mank - 5	30.68872	8.319767	1073.328
OPMG_002_KSP - 1	0.067874	1.0087	30.3752
OPMG_002_KSP - 2	0.062662	0.271833	3.238597
OPMG_002_KSP - 3	0.015474	0.396444	3.37255
OPMG_002_KSP - 4	0.221441	0.702137	5.705577
OPMG_002_KSP - 5	0.190017	2.092803	24.15609
OPMG_002_KSP - 6	0.305253	1.649294	132.7964
OPMG_002_BIO - 1	26.69849	3.422412	1147.684
OPMG_002_BIO - 2	24.43793	8.504745	996.4424
OPMG_002_BIO - 3	25.94422	6.680588	1146.622
OPMG_002_BIO - 4	23.89604	6.133016	1125.839
OPMG_002_BIO - 5	25.49261	3.500585	1145.285

OPMG_002_BIO - 6	1.29115	55.60173	57.87732
OPMG_002_BIO - 7	14.28975	0.181045	100.3039
OPMG_002_idk - 1	25.07963	6.379596	1249.28
OPMG_002_idk - 2	23.75311	2.028586	1171.085
OPMG_002_idk - 3	24.02285	8.355585	1214.394
OPMG_002_idk - 4	24.19277	2.73386	1242.299
OPMG_002_idk - 5	24.51938	6.334021	1272.956
OPMG_002_idk - 6	13.46183	0.161899	136.0862
OPMG_002_idk - 7	24.00674	3.393953	1101.453
OPMG_002_idk - 8	24.13824	3.775706	1245.994
OPMG_002_KSP - 7	0.152222	1.606724	15.66131
OPMG_002_KSP - 8	0.139215	1.500321	18.11133
OPMG_002_KSP - 9	0.108636	1.750317	76.93034
OPMG_002_KSP - 10	-0.01251	1.484189	18.37583
OPMG_002_KSP_matrix - 1	0.245568	9.182084	16.15695
OPMG_002_KSP_matrix - 2	0.260816	3.734586	2.56643
OPMG_002_KSP_matrix - 3	0.097548	2.228773	21.89025
OPMG_002_KSP_matrix - 4	0.210808	1.64875	9.927134
OPMG_002_KSP_matrix - 5	0.761264	20.86991	138.3325
OPMG_002_funkyplag - 1	0.307279	9.12073	15.56391
OPMG_002_funkyplag - 2	0.714186	21.79032	40.96826
OPMG_002_funkyplag - 3	0.116547	2.681795	16.24907
OPMG_002_funkyplag - 4	0.859207	25.90838	48.52315
OPMG_002_funkyplag - 5	1.064567	35.51731	69.59694
OPMG_002_Mafic mtrix - 1	0.289674	3.596231	1.938802
OPMG_002_Mafic mtrix - 2	0.286604	3.790321	1.843338
OPMG_002_Mafic mtrix - 3	0.223385	7.238437	36.31899
OPMG_002_Mafic mtrix - 4	0.290423	3.569918	1.899373
OPMG_002_Mafic mtrix - 5	0.260898	3.820583	3.772963
OPMG_002_Mafic mtrix - 6	3.750355	7.32713	90.01111
OPMG_002_Mafic mtrix - 7	26.09162	210.0722	849.4428
OPMG_002_Mafic mtrix - 8	0.269072	5.635823	15.01394
OPMG_002_Mafic mtrix - 9	0.318587	5.955138	17.7216
OPMG_002_Mafic mtrix - 10	0.2198	3.509726	14.20925
OPMG_002_Mafic mtrix - 11	0.374799	5.438526	11.96385
OPMG_002_horn - 1	19.88253	18.97061	744.3775
OPMG_002_horn - 2	23.02424	70.08358	802.8708
OPMG_002_horn - 3	0.458154	4.152467	1.647946
OPMG_002_horn - 4	23.77216	51.00074	941.3127
OPMG_002_horn - 5	22.92651	34.52479	840.1554
OPMG_002_horn - 6	22.02146	22.83602	778.7387
OPMG_002_horn - 7	19.31148	12.19224	740.8701
OPMG_002_horn - 8	21.6988	0.563461	737.9169
OPMG_002_horn - 9	25.17322	74.8311	870.6935
OPMG_002_horn - 10	23.78038	48.96142	798.7364

OPMG_002_horn - 11	20.56556	16.40103	715.4609
OPMG_002_plag - 1	0.245716	3.485269	2.244987
OPMG_002_plag - 2	0.298608	3.624671	2.356354
OPMG_002_plag - 3	0.303316	10.0178	25.85156
OPMG_002_plag - 4	0.069153	1.070798	3.651572
OPMG_002_plag - 5	-0.09272	1.921917	7.832043
OPMG_002_plag - 6	0.406417	15.17555	22.73424
OPMG_002_BIO - 8	37.67997	17.17051	1187.73
OPMG_002_BIO - 9	37.37324	3.712666	1152.909
OPMG_002_BIO - 10	37.06824	2.20092	1100.614
OPMG_002_BIO - 11	65.72616	25.3275	1070.397
OPMG_006B_KSP - 1	0.084679	0.833619	19.39169
OPMG_006B_KSP - 2	-0.02362	0.450273	12.23591
OPMG_006B_KSP - 3	0.011431	0.13638	9.581643
OPMG_006B_KSP - 4	0.153005	0.33489	9.335587
OPMG_006B_KSP - 5	0.093899	0.764309	31.12628
OPMG_006B_KSP - 6	0.076833	0.463464	15.33085
OPMG_006B_KSP - 7	-0.00177	0.522965	13.72816
OPMG_006B_KSP - 8	-0.09467	1.544042	12.56536
OPMG_006B_KSP - 9	0.051951	0.700671	46.26089
OPMG_006B_KSP - 10	0.263246	5.05556	87.96577
OPMG_006B_KSP - 11	0.023605	1.437524	14.56793
OPMG_006B_KSP - 12	-0.01475	0.051001	125.9168
OPMG_006B_KSP - 13	0.054594	5.148099	33.46546
OPMG_006B_KSP - 14	0.407408	1.18908	28.93049
OPMG_006B_KSP - 15	0.400967	1.295563	94.20694
OPMG_006B_KSP - 16	0.199344	0.835188	80.5164
OPMG_006B_KSP - 17	0.054894	0.564773	38.03558
OPMG_006B_KSP - 18	-0.02727	0.371488	24.75684
OPMG_006B_KSP - 19	0.22894	0.23923	3.890664
OPMG_006B_KSP - 20	0.515615	0.929414	50.13482
OPMG_006B_KSP - 21	0.090369	0.1799	12.01629
OPMG_006B_KSP - 22	0.223832	3.644911	9.489506
OPMG_006B_KSP - 23	0.214361	1.058769	19.70385
OPMG_006B_KSP - 24	-0.05569	0.07275	6.530697
OPMG_006B_KSP - 25	0.26877	3.682242	2.717315
OPMG_006B_KSP - 26	0.351617	3.02604	15.0969
OPMG_006B_KSP - 27	0.342307	1.020782	16.07396
OPMG_006B_KSP - 28	0.075855	0.605145	13.29857
OPMG_006B_KSP - 29	0.03676	0.925919	21.03121
OPMG_006B_KSP - 30	0.085228	0.879571	31.2428
OPMG_006B_BIO - 1	0.20191	2.550683	15.94113
OPMG_006B_BIO - 2	0.24766	2.520417	17.74964
OPMG_006B_BIO - 3	0.334365	1.547094	13.67507
OPMG_006B_BIO - 4	0.240529	1.341245	48.30801

OPMG_006B_BIO - 5	0.136225	3.681724	30.59426
OPMG_006B_BIO - 6	0.780701	6.131788	136.9409
OPMG_006B_KSP - 31	0.178372	5.231866	16.4606
OPMG_006B_KSP - 32	0.141275	0.32933	5.979493
OPMG_006B_KSP - 33	0.050433	0.911119	12.50141
OPMG_006B_KSP - 34	0.192551	3.369502	28.66465
OPMG_006B_KSP - 35	0.15933	1.191226	30.99676
OPMG_006B_BIO - 7	37.85736	1.178945	1258.917
OPMG_006B_BIO - 8	37.70662	0.795098	1242.146
OPMG_006B_BIO - 9	37.57652	1.026914	1267.822
OPMG_006B_Mess - 1	24.94294	5.855269	1563.11
OPMG_006B_Mess - 2	24.70096	25.23765	1418.111
OPMG_006B_Mess - 3	24.71027	7.909796	1647.215
OPMG_006B_HORN - 1	30.01131	10.83452	1442.401
OPMG_006B_HORN - 2	18.97483	0.608173	926.6191
OPMG_006B_HORN - 3	27.59587	10.42122	1405.588
OPMG_006B_HORN - 4	29.40022	15.58573	1342.21
OPMG_006B_HORN - 5	31.17136	3.657629	1459.86
OPMG_006B_HORN - 6	19.37476	11.78243	993.1468
OPMG_006B_HORN - 7	25.83052	3.793382	1275.304
OPMG_006B_HORN - 8	10.7729	1.344627	826.8381
OPMG_006B_HORN - 9	61.26288	301.7826	817.6345
OPMG_006B_HORN - 10	18.00983	11.38707	882.3433
OPMG_006B_HORN - 11	19.49848	20.67649	909.7535
OPMG_006B_HORN - 12	32.14822	3.585071	1227.479
OPMG_006B_HORN - 13	3.112063	22.88835	223.3719
OPMG_006B_HORN - 14	20.13395	15.66377	1192.524
OPMG_006B_HORN - 15	18.44465	20.02505	877.661
OPMG_006B_KSP - 36	0.076035	0.636858	21.58078
OPMG_006B_KSP - 37	0.069016	4.639358	15.71772
OPMG_006B_KSP - 38	0.051038	0.728092	14.18174
OPMG_006B_KSP - 39	0.042224	0.425061	26.91752
OPMG_006B_KSP - 40	0.0775	0.914212	21.09858
OPMG_006B_KSP - 41	0.746559	0.915208	59.85753
OPMG_006B_KSP - 42	0.325241	1.104549	36.71411
OPMG_006B_KSP - 43	0.274002	1.815021	29.45051
OPMG_006B_Messplag - 1	0.307584	3.968719	2.496502
OPMG_006B_Messplag - 2	0.262485	4.465415	3.132895
OPMG_006B_Messplag - 3	0.402893	4.268119	10.27534
OPMG_006B_Messplag - 4	0.44479	2.579997	21.48383
OPMG_006B_Messplag - 5	0.159185	2.272745	10.06363
OPMG_016_horn - 1	30.71816	2.944855	826.3342
OPMG_016_horn - 2	1.865178	5.682021	54.12106
OPMG_016_horn - 3	0.170226	0.573793	3.844692
OPMG_016_horn - 4	31.77888	13.35308	891.9744

OPMG_016_horn - 5	0.039537	0.37652	1.453241
OPMG_016_horn - 6	29.24357	9.524912	767.3207
OPMG_016_horn - 7	29.15965	2.686982	833.2266
OPMG_016_horn - 8	30.36643	27.8882	800.6616
OPMG_016_horn - 9	31.10035	2.577624	837.5569
OPMG_016_horn - 10	29.03123	0.487038	856.2866
OPMG_016_horn - 11	0.005364	0.071168	0.693823
OPMG_016_horn - 12	11.30927	40.12282	242.1356
OPMG_016_horn - 13	0.138169	0.353538	7.72392
OPMG_016_horn - 14	29.01671	5.795016	780.6254
OPMG_016_horn - 15	29.62614	4.957458	887.385
OPMG_016_horn - 16	33.1438	39.17126	940.9372
OPMG_016_horn - 17	28.11192	1.937925	834.9326
OPMG_016_horn - 18	28.24085	3.448785	870.1971
OPMG_016_horn - 19	0.197799	1.708698	12.64715
OPMG_016_horn - 20	28.96148	2.898018	783.2734
OPMG_016_horn - 21	28.92067	2.645588	824.63
OPMG_016_horn - 22	0.22642	4.15374	3.587532
OPMG_016_horn - 23	1.320216	16.42956	33.56339
OPMG_016_horn - 24	0.172643	4.80778	3.809175
OPMG_016_horn - 25	0.230948	5.327103	6.961832
OPMG_016_horn - 26	0.283876	4.52982	4.703797
OPMG_016_matrix - 1	0.228013	4.503124	3.908211
OPMG_016_matrix - 2	0.404124	5.218711	6.495719
OPMG_016_matrix - 3	0.202575	4.752545	5.637681
OPMG_016_matrix - 4	0.299877	4.126074	2.460781
OPMG_016_matrix - 5	0.352915	4.552098	5.578721
OPMG_016_BIO - 1	47.66943	6.665223	1181.666
OPMG_016_BIO - 2	47.73731	6.612339	1202.174
OPMG_016_BIO - 3	47.1637	13.92974	1177.694
OPMG_016_BIO - 4	47.02863	5.472771	1197.631
OPMG_016_BIO - 5	47.91187	2.365004	1186.16
OPMG_016_BIO - 6	48.33951	6.170896	1181.747
OPMG_016_BIO - 7	48.11464	4.878379	1190.9
OPMG_016_FELDS - 1	0.334413	3.78822	64.55516
OPMG_016_FELDS - 2	3.43045	13.96491	179.2798
OPMG_016_FELDS - 3	0.369751	1.868644	63.85974
OPMG_016_FELDS - 4	0.65545	9.945483	40.08438
OPMG_016_FELDS - 5	2.420098	20.99913	75.92078
OPMG_016_FELDS - 6	0.285324	2.920525	59.57493
OPMG_016_FELDS - 7	1.787114	7.015326	90.76874
OPMG_016_FELDS - 8	0.42032	6.357971	83.39163
OPMG_016_FELDS - 9	1.994489	33.66683	104.5551
OPMG_016_FELDS - 10	2.657049	55.49001	251.3737
OPMG_016_FELDS - 11	0.347304	5.93687	51.7335

OPMG_016_Anorthite - 1	9.096354	1.241811	1052.261
OPMG_016_Anorthite - 2	11.87232	1.218937	1131.502
OPMG_016_Anorthite - 3	11.87257	2.599791	1169.392
OPMG_016_Anorthite - 4	10.48709	1.579766	982.137
OPMG_016_Anorthite - 5	9.685853	2.024486	1057.474
OPMG_016_Anorthite - 6	13.21956	4.034309	1008.783
OPMG_016_magnetite - 1	10.90265	4.415868	333.0759
OPMG_016_magnetite - 2	9.696594	1.132839	128.0984
OPMG_016_magnetite - 3	11.0161	0.254209	151.5773
OPMG_016_magnetite - 4	12.47329	0.172838	237.7905
OPMG_016_magnetite - 5	13.03309	0.247632	130.8229
OPMG_016_magnetite - 6	13.07345	0.332454	142.3053
OPMG_016_magnetite - 7	25.7704	0.414107	159.3472
OPMG_016_magnetite - 8	25.53473	0.099704	165.2864
OPMG_016_magnetite - 9	29.39974	0.05787	125.521
OPMG_016_magnetite - 10	32.89044	0.108395	111.237
OPMG_016_magnetite - 11	24.56053	1.465401	119.7396
OPMG_016_KSP - 1	0.25526	13.34416	83.29977
OPMG_016_KSP - 2	0.226456	2.896692	9.736043
OPMG_016_KSP - 3	0.0475	0.725486	18.76881
OPMG_016_KSP - 4	0.117024	0.199859	1.194697
OPMG_016_KSP - 5	0.101527	0.24588	2.698803
OPMG_016_KSP - 6	-0.01007	0.342774	1.177464
OPMG_016_KSP - 7	0.082193	1.718633	7.533726
OPMG_016_titan - 1	0.833152	11.22854	41.90488
OPMG_016_titan - 2	0.01826	1.145468	3.751347
OPMG_016_titan - 3	0.160543	0.830526	5.357737
OPMG_016_titan - 4	0.286966	1.009883	8.325312
OPMG_016_titan - 5	0.093391	0.671665	8.445036
OPMG_016_titan - 6	0.152759	0.720886	7.623903
OPMG_016_titan - 7	8.292258	16.20463	67.11001
OPMG_016_titan - 8	8.976806	5.665894	22.42505
OPMG_016_titan - 9	0.46657	4.625952	18.1192
OPMG_016_titan - 10	268.2326	15.64448	46.26483
OPMG_016_titan - 11	0.030524	1.020141	4.34428
OPMG_016_matix - 1	1.56174	30.04336	79.6821
OPMG_016_matix - 2	0.379601	8.52249	21.08578
OPMG_016_matix - 3	0.010135	0.277724	8.073252
OPMG_016_matix - 4	0.154376	0.740037	11.9255
OPMG_016_matix - 5	-0.09661	0.009429	6.537142
OPMG_016_matix - 6	0.193767	2.263901	11.89724
OPMG_016_matix - 7	0.176876	0.500795	14.15153
OPMG_016_matix - 8	8.022049	28.48964	184.4195
OPMG_016_matix - 9	8.374147	13.96658	516.0028
OPMG_016_matix - 10	0.40571	4.367502	75.55224

OPMG_016_matix - 11	0.371637	3.745977	9.738517
OPMG_016_matix - 12	0.23257	3.963482	72.36384
OPMG_016_horn - 27	21.62446	57.61248	1395.636
OPMG_016_horn - 28	19.82846	11.40009	963.7617
OPMG_016_horn - 29	25.75033	57.33834	1962.155
OPMG_016_mag - 1	20.20843	6.467844	80.89247
OPMG_016_mag - 2	23.51637	19.57052	535.0762
OPMG_016_horn - 30	31.61095	99.18781	3195.715
OPMG_016_horn - 31	36.20085	119.8961	2505.622
OPMG_016_horn - 32	38.52376	249.7171	2475.743
OPMG_016_horn - 33	40.45968	82.05293	2272.605
OPMG_016_horn - 34	0.413816	4.855506	2.449159
OPMG_016_horn - 35	27.61786	103.8587	2139.347
OPMG_016_horn - 36	21.56063	37.37981	1060.647
OPMG_016_horn - 37	44.91042	467.4418	1294.612
OPMG_016_horn - 38	24.73545	48.665	1409.327
OPMG_016_horn - 39	16.39412	96.48254	1389.078
OPMG_016_horn - 40	23.14446	36.30255	1029.719
OPMG_016_BIO - 8	32.93285	10.18396	1567.078
OPMG_016_BIO - 9	30.97357	3.741355	1515.129
OPMG_016_BIO - 10	33.82198	37.38739	1561.914
OPMG_016_BIO - 11	32.69896	1.93131	1529.327
OPMG_016_plag - 1	0.139456	1.957095	21.46088
OPMG_016_plag - 2	2.0735	5.208582	105.2106
OPMG_016_plag - 3	44.5576	96.58543	940.7319
OPMG_016_plag - 4	14.6093	63.78394	667.1152
OPMG_016_plag - 5	2.209418	5.895429	200.2877
OPMG_016_plag - 6	0.729311	8.659487	60.92618
OPMG_016_plag - 7	2.128283	7.282117	28.58795
OPMG_016_plag - 8	0.231805	7.551675	37.87613
OPMG_016_mag - 3	19.13481	0.338929	110.8794
OPMG_016_mag - 4	20.03868	0.033746	76.87442
OPMG_016_mag - 5	22.76169	0.328753	82.84742
OPMG_016_mag - 6	23.26761	0.042971	69.86665
OPMG_016_mag - 7	92.73087	160.4299	284.3266
OPMG_016_mag - 8	21.75283	0.056157	81.08846
OPMG_016_plag - 9	0.925891	25.63484	51.68943
OPMG_016_plag - 10	0.144691	2.173702	18.41612
OPMG_016_plag - 11	0.30696	2.789553	38.15157
OPMG_016_plag - 12	0.157162	2.955582	27.32732
OPMG_016_plag - 13	-0.03646	1.577841	11.42621
OPMG_016_plag - 14	0.055012	1.457769	17.34202
OPMG_016_mag - 9	12.44192	0.110222	93.42935
OPMG_016_mag - 10	1.573657	1.527861	1963.583
OPMG_016_mag - 11	2.374943	10.38255	55.84346

LA-ICP-MS of Sulphides showing Co, Ni, Cu and Zn

Analysis	59Co	60Ni	65Cu	66Zn
OPMG_009 - 1	1775.163	2987.045	0.328392	1.574275
OPMG_009 - 2	9107.894	15.1005	0.048643	0.798833
OPMG_009 - 3	10384.52	16.54415	0.04945	0.842576
OPMG_009 - 4	12867.92	155.662	230.9294	12.53379
OPMG_009 - 5	12099.25	18.54584	0.072717	0.813109
OPMG_009 - 6	12734.88	22.98583	0.31669	0.614144
OPMG_009 - 7	554.5581	129.3802	3.800695	1.096538
OPMG_009 - 8	10.51357	2999.087	649.3081	1239.442
OPMG_009 - 9	0.368822	2874.096	10.66335	1.113991
OPMG_009 - 10	0.524988	1918.586	52.10618	5.546829
OPMG_009 - 11	399.2024	575.8184	69.5546	30.32027
OPMG_009 - 12	392.3131	374.2499	0.231499	0.649889
OPMG_009 - 13	178.1313	127.7573	17.40008	119.7257
OPMG_009 - 14	1384.237	93.29945	0.303391	0.734075
OPMG_009 - 15	572.1916	152.9317	0.568754	0.980748
OPMG_009 - 16	9818.87	53.74816	0.505216	0.96983
OPMG_009 - 17	8701.576	49.23131	0.393932	0.844408
OPMG_009 - 18	11820.55	44.87733	0.692486	0.93471
OPMG_009 - 19	12187.64	38.32025	0.281437	0.755137
OPMG_009 - 20	11609.2	112.1679	49.11482	529.7146
OPMG_009 - 21	14.68839	20.65834	7.209001	30.00976
OPMG_009 - 22	5235.91	46.43966	-0.02945	0.578597
OPMG_009 - 23	3925.538	92.85299	0.135753	0.763744
OPMG_009 - 24	3372.108	97.88527	0.081293	0.75342
OPMG_009 - 25	7120.76	60.57101	-0.12642	0.81643
OPMG_009 - 26	1826.8	96.75229	0.572876	0.791792
OPMG_009 - 27	1435.961	79.46073	0.26452	0.812421
OPMG_009 - 28	718.1025	105.1357	0.259617	0.649575
OPMG_009 - 29	9.196598	251.5746	0.240947	0.715392
OPMG_009 - 30	17.83826	1880.734	0.014742	0.797633
OPMG_009 - 31	31.17405	1772.893	0.283825	0.757271
OPMG_009 - 32	26.43647	1420.048	0.052697	0.767345
OPMG_009 - 33	44.43857	670.0571	0.465457	0.681346
OPMG_009 - 34	48.06348	138.2028	14.50782	4.274749
OPMG_009 - 35	347.2173	86.23666	0.233951	0.855796
OPMG_009 - 36	9.592573	119.7942	0.169427	0.707811
OPMG_009 - 37	14.62798	195.6999	0.237079	1.025888
OPMG_009 - 38	27.74968	769.3352	0.242392	0.863786
OPMG_009 - 39	108.9277	493.811	0.202222	0.918666
OPMG_009 - 40	7.968636	229.3333	0.16535	0.861097
OPMG_009 - 41	11.91172	488.3819	-0.03345	0.679446
OPMG_009 - 42	0.12356	11379.05	4.909733	1.302067
OPMG_009 - 43	0.091532	11204.97	3.241738	3.800046

OPMG_009 - 44	0.08365	13383.2	0.993275	1.562824
OPMG_009 - 45	0.050089	33270.71	23.87201	1.851836
OPMG_009 - 46	0.045682	9862.756	3.144374	1.259098
OPMG_009 - 47	0.396869	5711.812	1.288404	1.260168
OPMG_009 - 48	1.751906	4549.288	558.2751	20.69652
OPMG_009 - 49	17.23755	5218.869	27.09636	5.315288
OPMG_009 - 50	14.01166	4965.937	2.943795	1.14497
OPMG_009 - 51	12.43647	4286.441	15.06098	2.984367
OPMG_009 - 52	9.822609	964.5545	138.861	23.36702
OPMG_009 - 53	122.6243	375.7814	681.0155	5333.86
OPMG_009 - 54	121.5669	358.8114	13.20204	12060.33
OPMG_009 - 55	12.89401	15.8409	50.38584	94.03564
OPMG_009 - 56	16.96298	25.31577	15.82277	137.9499
OPMG_009 - 57	12975.92	21.98851	73.77124	143.6002
OPMG_002 - 1	598.1413	278.2174	10.55494	20.95024
OPMG_002 - 2	1538.692	203.5217	0.703904	1.185711
OPMG_002 - 3	875.1545	32.35263	5.715339	10.54379
OPMG_002 - 4	851.7052	54.61999	55.12342	81.00393
OPMG_002 - 5	864.2716	46.69337	0.77399	1.191453
OPMG_002 - 6	980.4837	32.94915	4.263174	14.44526
OPMG_002 - 7	1065.41	160.67	1.630874	1.951745
OPMG_002 - 8	716.5395	186.6254	1.255654	1.408837
OPMG_002 - 9	420.018	214.1484	2.058937	2.019755
OPMG_002 - 10	333.9505	66.8563	1.868922	2.002297
OPMG_002 - 11	432.1263	73.02498	1.103566	2.007794
OPMG_002 - 12	395.5867	65.20945	0.746368	1.643002
OPMG_002 - 13	861.4846	93.42432	1.151963	1.601626
OPMG_002 - 14	1862.923	241.9911	0.563172	1.107891
OPMG_002 - 15	3840.902	380.2194	0.456227	1.136644
OPMG_002 - 16	1271.257	123.4798	0.709122	1.329905
OPMG_002 - 17	2222.039	355.7826	0.851823	1.130279
OPMG_002 - 18	1162.805	79.63934	0.634141	1.229036
OPMG_002 - 19	581.1196	67.85039	1.12044	1.74857
OPMG_002 - 20	2707.167	61.38276	4.571254	22.31202
OPMG_002 - 21	10039.3	139.3933	2.887453	12.82372
OPMG_002 - 22	159.3844	225.6842	4.685016	0.957443
OPMG_002 - 23	411.1488	389.0439	102.4074	6.55559
OPMG_002 - 24	450.726	201.15	701.0654	49.81719
OPMG_002 - 25	1455.473	1395.343	6.254938	6.060295
OPMG_002 - 26	103.9205	279.1947	17.67217	15.83577
OPMG_002 - 27	353.7953	900.4292	1456.981	100.9293
OPMG_002 - 28	1015.972	531.9864	34.57132	41.54946
OPMG_002 - 29	790.1474	121.677	0.924145	1.288778
OPMG_002 - 30	2834.754	651.3634	6777.043	26872.66
OPMG_002 - 31	17.2493	151.8808	8155.165	57.64539

OPMG_002 - 32	227.1055	55.86236	2.168823	2.47351
OPMG_002 - 33	11888.4	16.36325	1.553174	2.508088
OPMG_002 - 34	141.7908	154.9213	0.891139	1.143079
OPMG_002 - 35	1154.02	1195.863	1.578256	1.266424
OPMG_002 - 36	2161.568	504.1344	2.042222	1.243661
OPMG_002 - 37	2749.254	605.749	1083.688	53.15027
OPMG_002 - 38	1777.993	581.787	0.650114	1.045693
OPMG_002 - 39	298.517	248.7005	47.38015	82.59284
OPMG_002 - 40	259.8136	136.8284	1.414222	1.273811
OPMG_002 - 41	281.1649	519.6447	4436.576	80.55071
OPMG_002 - 42	211.3616	359.7365	9668.319	63.09662
OPMG_006c - 1	771.912	540.2173	3455.286	370.7231
OPMG_006c - 2	420.7571	207.8402	1241.614	38.25649
OPMG_006c - 3	288.8923	734.2841	48921.05	180.3439
OPMG_006c - 4	501.2858	1463.205	2783.677	30.39489
OPMG_006c - 5	361.1836	254.3101	10.53167	3.198859
OPMG_006c - 6	904.4356	404.9641	1.757727	8.837229
OPMG_006c - 7	237.1896	89.30295	26587.21	200.3611
OPMG_006c - 8	358.9678	282.425	392.5761	12.71104
OPMG_006c - 9	129.2044	119.2953	2.296594	42.23241
OPMG_006c - 10	1848.554	118.4969	17.40099	101.6442
OPMG_006c - 11	1101.339	75.03141	1838.816	18.96693
OPMG_006c - 12	1311.439	101.9502	217.4889	6.835064
OPMG_006c - 13	196.1402	480.3306	2041.373	45.11986
OPMG_006c - 14	301.0453	157.3176	55.21183	12.81648
OPMG_006c - 15	2403.886	210.3813	4.040315	62.02335
OPMG_016 - 1	2385.909	18.22703	0.779639	1.094107
OPMG_016 - 2	2504.636	17.21215	1.506203	1.312724
OPMG_016 - 3	2021.408	20.35429	0.464948	1.175834
OPMG_016 - 4	1010.881	121.9453	1.097498	1.387457
OPMG_016 - 5	1021.996	781.1879	0.724872	1.132341
OPMG_016 - 6	1347.592	151.6829	1.057158	1.341705
OPMG_016 - 7	1810.368	46.06596	1.305162	1.2928
OPMG_016 - 8	246.9926	255.9639	0.9883	1.159991
OPMG_016 - 9	506.773	495.0322	2.350566	3.724803
OPMG_016 - 10	283.5789	192.8826	0.933422	1.237969
OPMG_016 - 11	220.5168	200.8897	1.441954	1.643143
OPMG_016 - 12	2717.465	17.4802	0.878034	1.330896
OPMG_016 - 13	3010.403	18.85956	1.856461	1.480063

OPMG_016 - 14	3083.54	17.86626	1.09213	1.485735
OPMG_016 - 15	1273.154	54.77978	2.133816	1.587606
OPMG_016 - 16	752.7413	238.8874	0.199032	1.200476
OPMG_016 - 17	775.7276	193.3203	1.736157	1.620039
OPMG_016 - 18	1061.059	190.1602	0.835263	1.346821
OPMG_016 - 19	1235.238	177.4799	7.454272	12.71693
OPMG_016 - 20	2010.438	141.6704	1.737981	1.418559
OPMG_016 - 21	3091.756	161.1934	1.707218	1.77353
OPMG_016 - 22	2491.823	117.7565	1.135563	1.500297
OPMG_016 - 23	7832.901	84.37894	0.858668	1.351772
OPMG_016 - 24	4189.303	135.4834	1.392745	1.629421
OPMG_016 - 25	382.871	42.84286	56.31666	64.99551
OPMG_016 - 26	269.5285	198.3587	84941.13	19483.58
OPMG_016 - 27	1829.22	17.86811	3.205297	1.751891
OPMG_016 - 28	226.9587	145.9311	1.033155	1.278714
OPMG_016 - 29	295.6312	151.5833	1.115695	1.693865
OPMG_016 - 30	299.3407	216.6561	0.97178	1.35138
OPMG_016 - 31	634.3446	158.9549	0.299104	1.201949
OPMG_016 - 32	620.0112	149.5068	0.969435	1.278759
OPMG_016 - 33	870.1026	179.3355	1.105839	1.280035
OPMG_016 - 34	1115.376	636.4598	3.42891	1.776507
OPMG_016 - 35	971.9866	143.9642	1.032368	1.17053
OPMG_016 - 36	4939.719	224.4062	1.630707	1.826699
OPMG_016 - 37	23189.62	549.2344	8.245283	10.62805
OPMG_016 - 38	2122.208	1292.395	1396.223	130.8656
OPMG_016 - 39	556.8112	87.98956	13.05506	50.04728
OPMG_016 - 40	366.7094	129.9776	3.106278	1.884882
OPMG_016 - 41	319.7673	236.9213	14886.91	83.90158
OPMG_016 - 42	170.1289	120.6938	27.74478	39.49342
OPMG_016 - 43	2600.973	41.9738	2.469145	1.58022
OPMG_016 - 44	167.267	325.0039	30.82373	12.39703
OPMG_016 - 45	4607.444	19.63456	16.22103	1.576465
OPMG_016 - 46	2170.178	20.41383	3.062266	6.615608
OPMG_016 - 47	376.3473	521.4113	449.0639	9.503176
OPMG_016 - 48	198.8562	317.9281	48.90515	3.038014
OPMG_016 - 49	1395.217	1534.566	8.579865	2.407009
OPMG_016 - 50	1362.186	1512.982	2.921254	4.547129
OPMG_016 - 51	2290.935	2408.83	3377.791	140.826
OPMG_016 - 52	109.8278	849.3269	0.949551	1.385409
OPMG_016 - 53	236.5017	665.9994	28.78737	22.30437
OPMG_016 - 54	126.9817	711.4389	1465.06	5.834683
OPMG_016 - 55	679.2671	535.7482	36.70833	3.503599
OPMG_016 - 56	3578.378	46.20829	0.382217	0.971337
OPMG_016 - 57	3207.249	22.5724	1.876727	19.22924
OPMG_016 - 58	13540.3	16.55414	0.451212	1.140605

OPMG_016 - 59	5766.451	103.0824	50.97022	308.5057
OPMG_016 - 60	7866.16	128.5064	144.6926	188.9046
OPMG_016 - 61	4762.671	52.06781	190.4117	19.27713
OPMG_016 - 62	2011.804	993.7033	13.33726	65.68661
OPMG_016 - 63	9.287216	269.0885	783.8028	4.47668
OPMG_016 - 64	16.62089	656.7636	694.022	162.3662
OPMG_016 - 65	8.827926	318.3715	629.3854	1.29997
OPMG_016 - 66	2473.168	794.5564	2.300638	10.86661
OPMG_016 - 67	1843.168	759.2549	19.84986	70.27048
OPMG_016 - 68	51.79033	268.6937	166.5387	20.79183
OPMG_016 - 69	196.9803	483.0636	7980.438	44.49186
OPMG_016 - 70	193.0701	263.4844	197.8991	141.9718
OPMG_016 - 71	822.5341	498.2907	6473.755	85.01807
OPMG_016 - 72	1588.173	65.42115	63.23178	1.872008
OPMG_016 - 73	775.0282	382.9591	2.568825	6.287589
OPMG_016 - 74	4093.197	21.61858	43.82066	135.3754
OPMG_016 - 75	32.3651	429.4284	0.848333	1.257377
OPMG_016 - 76	602.0002	76.97355	684.1966	32.21382
OPMG_016 - 77	72.45656	380.6301	19.10844	83.2239
OPMG_016 - 78	7517.554	48.82815	107.1027	8.756395
OPMG_016 - 79	569.5803	37.83298	0.219075	1.034866
OPMG_016 - 80	36.19077	75.81193	11.74872	43.73699
OPMG_016 - 81	3354.525	47.90196	3.508837	31.22806
OPMG_016 - 82	4759.795	83.18191	18.58073	2.399864
OPMG_016 - 83	175.7285	212.1161	1.239075	1.258732
OPMG_016 - 84	359.2252	280.7602	7363.531	80.42952
OPMG_016 - 85	351.8774	98.45069	0.15965	1.10217
OPMG_016 - 86	329.6753	207.1922	984.5999	78.48804
OPMG_016 - 87	64.48178	710.9161	1526.888	148.7101